Cyanostyrene Based Photoluminescent Materials: Design, Synthesis and Photophysical Studies

Thesis Submitted to the University of Calicut for the Award of

DOCTOR OF PHILOSOPHY IN CHEMISTRY

By

Ramya N K

Under the supervision of

Dr. Reji Thomas

DEPARTMENT OF CHEMISTRY

FAROOK COLLEGE (AUTONOMOUS), KOZHIKODE

KERALA, INDIA – 673632

DECEMBER 2023

Declaration

I hereby declare that the thesis entitled **Cyanostyrene Based Photoluminescent Materials: Design, Synthesis and Photophysical Studies** is a bonafide record of the original work carried out by me under the supervision of Dr. Reji Thomas, Assistant Professor, Department of Chemistry, Farook College (Autonomous), Kozhikode, Kerala for the award of the degree of Doctor of Philosophy in Chemistry under the faculty of sciences, University of Calicut, Kerala. The content of the thesis has not been submitted to any other institute or university for the award of any degree or diploma, except where due acknowledgement has been made in the text.

Farook College

13.05.2024

Ramya N. K.

Certificate

This is to certify that the work embodied in the thesis entitled '**Cyanostyrene Based Photoluminescent Materials: Design, Synthesis and Photophysical Studies**' submitted by **Ramya N K** to the University of Calicut for the award of degree of Doctor of Philosophy in Chemistry under the Faculty of Sciences, is an authentic record of precise research work carried out at the Department of Chemistry, Farook College (Autonomous), Kozhikode under my supervision and guidance. The contents of the thesis have been checked for plagiarism using the software iTHENTICATE and the similarity index falls under the criteria laid by the University of Calicut. I further certify that the contents of the thesis have not been submitted elsewhere for any degree or diploma. I also certify that the corrections/suggestions recommended by the adjudicators have been incorporated in the thesis.

Farook College

13.05.2024

Dr. Reji Thomas

Dr. Reji Thomas
Assistant Professor
Department of Chemistry
Farook College (Autonomous)
Farook College P.O.
Kozhikode - 673 632

Acknowledgement

Even though this journey is an individual endeavor, I couldn't have navigated this path without the invaluable suggestions, encouragement, love, and kindness generously shared by many wonderful people. Yet, this is an attempt to thank them all; I apologize if I missed mentioning anyone.

First and foremost, I would like to express my deepest gratitude to my research supervisor Dr. Reji Thomas, Assistant Professor, Department of Chemistry, Farook College for guidance, support, and invaluable insights throughout the course of my research. His guidance, coupled with his wealth of research experience, played a pivotal role in the successful completion of this thesis.

I am also indebted to the RAC committee members Prof. Abdul Mujeeb, Prof. Mohamed Shahin Thayyil and Prof. N K Renuka for their thoughtful critique and suggestions throughout the process.

I take this opportunity to thank the current and former principals of Farook College Calicut, Dr. K A Ayisha Swapna, Dr. K M Naseer and Prof. E P Imbichikoya, for their support in the completion of this work. I extend my sincere gratitude to both the current and former heads of the Department of Chemistry, Dr. Kavitha A P, Dr. P E M Abdul Rasheed and Dr. Abdul Rahim, , for their support in the completion of my research work.

I sincerely thank all the teaching and non-teaching staff of the Department of Chemistry, Farook College, Kozhikode for their support.

Special thanks to Dr. Retheesh Krishnan, Government College for Women, Thiruvananthapuram, and Dr. Manoj Mathews, St. Josephs College, Devagiri for their collaboration along with insightful comments and recommendations. I also express my thanks to Dr. Kumaradhas P, Periyar University, Selam for providing Single Crystal X-ray diffraction analysis facility. I extend my thanks to Dr. Jatish Kumar, IISER ,Tirupati for quantum yield measurement facility. I would like to express my deepest gratitude to Ms. Divya S Mohanakumari, Research Scholar, Government College for Women, Thiruvananthapuram for her support in carrying out various photophysical studies including low temperature photophysical measurements, and valuable suggestions on my research work. I also thank Suganya Suresh and Hemalatha Balasubramaniam, Periyar University, Selam for helping me in

carrying out a Single crystal X-ray diffraction analysis. I thank Dr. Anju K Sasidharan for her support and valuable suggestions.

I express my gratitude to Dr. Yahya A I and Dr. Rajiv S. Menon, current and former heads of the Department of Chemistry at the University of Calicut, for their support in expanding the experimental facilities. Special thanks to Dr. Fazalurahman K for assisting me in conducting the fluorescence lifetime analysis. Additionally, I extend my appreciation to research scholars, Department of Chemistry, University of Calicut, especially Mr Deepak Joshy, Ms Arifa K V, and Ms Nimisha, for their invaluable support in conducting various photophysical studies. I would also like to express my gratitude to the office staff of Farook College, Kozhikode, for their assistance and support.

I extend my heartfelt appreciation to Mr Diljith V, NIT Calicut, for his selfless support.

I thank UGC, Government of India, for financial assistance as a research fellowship.

I thank Ms Athira P for her academic and personal support in the successful completion of my research work. I express my gratitude to Sumayya teacher and Yelena for welcoming me into their circle of privacy during a critical period in my research.

I would like to convey my heartfelt gratitude to Thufail, Farhan, Hadiya, Ramya, Nizamuddin, and Rajeena for creating a warm and supportive atmosphere. I cherished every moment spent together and truly appreciated the personal support extended by each of them. I also thank Rajitha, Shanavas sir, Deepa teacher, and Rajagopalan sir for the good moments we shared.

I thank all the project students who worked in our lab especially Ms. Shafna, Ms. Rafida Ms. Sahla, Ms. Fathima, Mr. Gokul, Mr. Sanal, Mr. Jaleel, and Mr. Rohith. I express my gratitude to Sachu and Rasanth for providing not only fun and support but also deeper insights that proved to be stabilizing during a challenging and traumatic period in my research. I extend my heartfelt thanks to Johnson Sir for the unwavering support, love, and care that he provided throughout the research journey. I express my gratitude to my teachers, Suresh sir and Pradeep sir, for serving as inspirations in my academic journey.

Above all, I express profound gratitude to my family for their love, support, sincere encouragement, and inspiration throughout my life. My parents, serving as my pillars of strength, have been with me through thick and thin. Their unconditional support has been a constant source of motivation, enabling me to successfully navigate through the challenges of this research journey. I extend my gratitude to my little ones, Ishaan and Rayaan, acknowledging that we have sacrificed numerous precious moments due to the demands of my research. I extend my heartfelt thanks to my sister Soumya for her

unconditional support. Thanks to Praveen, Parvathi, Neerav and Nainika for the good moments we had. Additionally, I am grateful to my in-laws, especially my mother-in-law, for their support in various ways. Thanks to my grandparents for their love and support.

I am forever indebted to my husband, for his unconditional support during the highs and lows of the entire Ph.D. process, and for the sacrifices he has made to prioritize my work in our lives.

Ramya N K

Abstract

Solid-state luminescent materials based on π-conjugated molecules attracted enormous research interest due to their wide range of applications. Most of the luminophores that are highly luminescent in the solutions showed poor emission in the solid state due to aggregation caused quenching and limits their practical applications. Design and synthesis of solid-state photoluminescence materials with switchable emission behaviour is therefore a promising area of research in materials science. However, there are several designs and design parameters were put forward to achieve solid-state emissive materials with high quantum efficiency and stimuli-responsive behaviour, a detailed study exploring the combined effect of molecular structure and solid state packing is necessary to understand the exact mechanism behind enhanced solid-state photoluminescence. Here this investigation pertains to design and synthesis of cyanostyrylbenzene and cyanostyrylthiophene derivatives with enhanced luminescence properties along with stimuli-responsive emission. The research tries to understand the aggregation-induced emission and the stimuli-responsive emission properties supported by molecular structure and packing parameters derived from single crystal and powder X-ray diffraction. Apart from the stimuli-responsive emission switching, the study examined the low-temperature photophysical behaviour of some cyanostyrylbenzene derivatives to understand the role of restricted intramolecular motions on luminescence lifetime. All the cyanostyrene derivatives synthesized have excellent photophysical properties and the molecular designs can largely contribute to various optoelectronic applications.

സംഗ്രഹം

ഓർഗാനിക് സംയോജിത തന്മാത്രകളെ അടിസ്ഥാനമാക്കിയുള്ള ഖരാവസ്ഥയിൽ പ്രകാശദീപ്തി കാണിക്കുന്ന വസ്തുക്കൾ അവയുടെ വിപുലമായ ഉപയോഗങ്ങൾ കാരണം ഗവേഷണം താത്പര്യം അർഹിക്കുന്നു. ലായനികളിൽ വളരെയധികം പ്രകാശദീപ്തി കാണിക്കുന്ന മിക്ക സംയോജിത തന്മാത്രകളും ഖരാവസ്ഥയിൽ പ്രകാശദീപ്തി കാണിക്കുന്നില്ല .ഇതിനുകാരണം ഖരാവസ്ഥയിൽ തന്മാത്രകൾ അടുത്ത് ക്രമീകരിക്കപ്പെടുന്നത് മൂലം പ്രകാശദീപ്തി ഇല്ലാതായിത്തീരുന്നതാണ്. ഇത് പരിഹരിക്കാൻ തന്മാത്രകളുടെയും അഗ്ഗ്രഗേറ്റുകളുടേയും കൃത്യമായ രൂപകൽപ്പനയും സമന്വയവും ആവശ്യമാണ്. ആയതിനാൽ ഖരാവസ്ഥയിൽ പ്രകാശ ദീപ്തി കാണിക്കുന്നതും പ്രകാശ ദീപ്തിയിൽ മാറ്റം വരുന്നതുമായ വസ്തുക്കളുടെ രൂപകല്പനയും സമന്വയവും മെറ്റീരിയൽ സയൻസിലെ ഗവേഷണത്തിന്റെ ഒരു സുപ്രധാന മേഖലയാണ്. ഖരാവസ്ഥയിൽ ഉയർന്ന ക്വാണ്ടം യിൽഡും ഉത്തേജക-പ്രതികരണ സ്വഭാവവുമുള്ള പ്രകാശദീപ്തി കാണിക്കുന്ന വസ്തുക്കൾ ഉണ്ടാക്കിയെടുക്കുന്നതിന് നിരവധി ഡിസൈനുകളും ഡിസൈൻ ചെയ്യുമ്പോൾ പരിഗണിക്കേണ്ടതായ ഘടകങ്ങളും മുന്നോട്ട് വച്ചിട്ടുണ്ട്. മെച്ചപ്പെട്ട പ്രകാശദീപ്തിയുള്ള വസ്തുക്കൾ രൂപകല്പനചെയ്യുന്നതിന് തന്മാത്രാ ഘടനയുടെയും ഖരാവസ്ഥയിലുള്ള തന്മാത്രകളുടെ ക്രമീകരണവും സമയോചിതമായി പര്യവേക്ഷണം ചെയ്യുന്ന വിശദമായ പഠനം ആവശ്യമാണ്. ഇവിടെ പരാമർശിക്കുന്ന ഗവേഷണം ഉത്തേജക-പ്രതികരണീയമായ ഉദ്വമനത്തോടൊപ്പം മെച്ചപ്പെട്ട പ്രകാശദീപ്തിയുള്ള സയനോസ്റ്റെൽബെൻസീൻ, സയനോസ്റ്റെറിൽത്തിയോഫെൻ എന്നിവയുടെ ഡെറിവേറ്റീവുകളുടെ രൂപകല്പനയും സംശ്ലേഷണവുമായി ബന്ധപ്പെട്ടിരിക്കുന്നു. ഈ ഗവേഷണം സിംഗിൾ ക്രിസ്റ്റൽ എക്സ്-റേ ഡിഫ്രാക്ഷൻ, പൗഡർ എക്സ്-റേ ഡിഫ്രാക്ഷൻ എന്നിവയിൽ നിന്ന് ഉരുത്തിരിഞ്ഞ തന്മാത്രാ ഘടനയും ഖരാവസ്ഥയിലുള്ള തന്മാത്രകളുടെ ക്രമീകരണത്തിന്റെയും അടിസ്ഥാനത്തിൽ അഗ്രഗേഷൻ-ഇൻഡ്യൂസ്ഡ് എമിഷൻ, ഉത്തേജക-പ്രതികരണപരമായ എമിഷൻ എന്നീ പ്രതിഭാസങ്ങളെ മനസ്സിലാക്കാൻ ശ്രമിക്കുന്നു. ഈ പഠനങ്ങൾക്ക് പുറമെ

പ്രകാശദീപ്തിയുടെ ആയുസ്സിൽ നിയന്ത്രിത തന്മാത്രാ ചലനങ്ങളുടെ പങ്ക് മനസിലാക്കാൻ ചില സയനോസ്റ്റെൽബെൻസീൻ ഡെറിവേറ്റീവുകളുടെ താഴ്ന്ന-താപനില ഫോട്ടോഫിസിക്കൽ സ്വഭാവവും പഠനവിധേയമാക്കി.പുതിയതായി നിർമ്മിച്ച സയനോസ്റ്റൈറെൻ ഡെറിവേറ്റീവുകൾക്ക് മികച്ച ഫോട്ടോഫിസിക്കൽ ഗുണങ്ങളുള്ളവയാണ്. കൂടാതെ, ഈ തന്മാത്രാ നിർമിതികൾ വിവിധ ഒപ്റ്റോഇലക്ട്രോണിക് ആപ്ലിക്കേഷനുകൾക്ക് വൻതോതിൽ സംഭാവന ചെയ്യാൻ കഴിവുള്ളവയുമാണ്.

Table of Contents

List of Abbreviations

NMR	Nuclear Magnetic Resonance
XRD	X-ray diffraction
TCSPC	Time-Correlated Single Photon Counting System
DMF	Dimethylformamide
DCM	Dichloromethane
HRMS	High-Resolution Mass Spectroscopy
DSC	Differential Scanning Calorimetry
THF	Tetrahydrofuran
PXRD	Powder X-ray Diffraction
AIE	Aggregation Induced Emission
AIEE	Aggregation Induced Enhanced Emission
UV	Ultraviolet
2-MeTHF	2-Methyl Tetrahydrofuran
CT	Charge Transfer
CCDC	Cambridge Crystallographic Data Centre
POM	Polarized Optical Microscope
LC	Liquid Crystal
TPE	Tetraphenylethene

Preface

The thesis pertains to the synthesis, photophysical studies and structure property correlations of some assemblies of cyano styrene derivatives. The molecules based on π-conjugated systems are well known for their optoelectronic properties and various other material applications. The major class of molecules so far explored includes the oligomers and polymers of phenylenevinylenes, phenyleneethynylenes, phenylenes and derivatives of other polyaromatic hydrocarbons. Although there are several derivatives of π- conjugated molecules with strong solution state emission were reported, the molecules showing strong solid state emission were limited due to aggregation caused quenching. The aggregation induced quenching limits their application that calls for strong solidstate emission. The major reason behind the aggregation induced quenching is the planar structure of the molecules, where the planar shaped molecules generally show a tendency to aggregate as stacks with π-π interactions resulting in luminescence quenching. So, the planar conjugated molecules, especially those systems with disc like structures are not good candidates to explore the solid state emission. The major strategies to obtain unquenched emission in the solid state include the introduction of twist in π-backbone or functionalization with non-conjugated bulky groups. The first molecule which is not emissive in the dilute solution and highly emissive in the solid phase was reported by Tang and co-workers. Following the strong solid state emission in 1-methyl-1,2,3,4,5-pentaphenylsilole several silole derivatives with strong solid state emission were synthesized by the same group and found the unquenched solid state emission is originating from a phenomenon called aggregation induced emission as result of restricted intramolecular motion. Following this observation various research groups

were synthesized various twisted molecules based on different chromophores like cyanostyrenes, phenylenevinylenes, pyrene etc.

Among various π-conjugated solid state emitters, cyanostyryl derivatives received paramount interest attributed to the aggregation induced emission and multistimuli responsive behaviour. Several researchers explored the emission characteristics of these classes of molecules carrying different functional groups under the influence of various stimuli. Although there are several reports on solid state emission properties of cyanostyrene based molecules, there are limited investigations that relate the structural origin of solid state emission and its modulation. Therefore, a detailed investigation involving synthesis, property studies and structure property correlation supported by detailed structural data is relevant.

The general introduction to solid-state emissive π-conjugated materials and their design strategies is the content of **Chapter 1**. The first part of the introduction gives a brief overview of the relevant investigations in the field of aggregation induced emission in various classes of π-conjugated molecules.

Chapter 2 Discusses the instrumental details and experimental methods adopted for various spectroscopic and diffraction studies.

Chapter 3 Explains the synthesis, photophysical properties and structure property correlation of alkyloxy substituted dicyanodistyrylbenzene based positional isomers. The synthesis of three octyloxy substituted positional isomers of dicyanodistyryl benzene derivatives namely **CSO**, **CSM** and **CSP** was carried out to explore the role of positional isomerism and stimuli responsive emission of the molecules in the solid state. All three isomers are very less emissive in the solution phase and showed aggregation induced enhanced emission in the solid state. Among the three isomers the *ortho*

isomer **CSO** showed stimuli responsive blue shifted emission in the solid state. The switching of emission from greenish yellow to cyan while grinding is attributed to the change in aggregate structure from J-aggregate to X-aggregate indicated by the single crystal and powder X-ray diffraction studies and analysis of also literature data. The *meta* isomer, **CSM**, also demonstrated an aggregation induced emission in the solid state, however, this molecule was insensitive to any kind of stimuli owing to the various intermolecular interactions present in the crystalline state. The *para* isomer, **CSP** also showed aggregation induced enhanced emission in the solid state and the system is responsive to multiple stimuli such as mechanical stress, heat and solvent vapours. The molecule showed tricolour emission in the solid state which is rare among π-conjugated molecules. The origin of stimuli responsive emission in **CSP** was studied using analysis of spectroscopic and single crystal and powder X-ray diffraction data. The observed tricolour emission in **CSP** is attributed to the formation of different crystalline phases under the influence of various stimuli.

Chapter 4 discusses the ultralong lifetime in low temperatures (77K) and the enhanced emission efficiency of *ortho* alkyloxy substituted dicyanodistyrylbenzene derivatives. The synthesis and detailed structural characterisation of five different alkyl chain variants of dicyanodistyrylbenzenes were carried out to explore the luminescence properties in the solid state. Among various positional isomers of cyanostyryl systems the *para*-alkyloxy derivatives of dicyanodistyrylbenzenes with linear structure, received greater attention due to their AIE properties and switchable emission. The linear structure of the para isomer gives rise to sliding movement on applied stress and thereby switchable emission. It can be envisaged that the molecule with *ortho* substitution having a nonlinear structure may limit the sliding motion, thereby resulting in the twisting of π-

back bone with rigid molecular packing. The twisted molecular systems are found to show higher emission efficiency. Here all five alkyloxy derivatives from ethyl to decyl showed enhanced quantum yield. All the compounds showed very faint fluorescence emission in the corresponding 2-methyl-THF at room temperature a redshifted spectrum was obtained at 77 K attributed to the restricted intramolecular rotation. The spectra recorded at 77 K with a delay of 0.5 ms showed a redshifted emission with an ultralong lifetime indicating phosphorescence in the molecules. The good-quality single crystals of all compounds were obtained from various solvents and a detailed structure-property correlation study was carried out. The study showed that, apart from twist in the π-back bone, the parameters such as $\pi - \pi$ overlap, interplanar distance etc play crucial role in determining the higher quantum yield of the dicyanodistyrylbenzene derivatives.

The content of the **Chapter 5** is AIEE, stimuli responsive emission and liquid crystalline behaviour of two cholesterol appended heterocyclic cyanostyrene derivatives**,** where the hetrocyclic group constitute the thiophene units with connectivity at 2- (**CS-1**) and 3- (**CS-2**) respectively. Both newly synthesized compounds showed aggregation induced emission which is proved by the intensity enhancement on increasing the water fraction in dilute THF solutions of the compounds. Among the molecules explored, **CS-2** showed thermochromism and mechanochromism with a methanol vapour induced phase reversal while the molecule **CS-1**, showed thermochromic emission switching. The DSC thermogram of both **CS-1** and **CS-2** indicated the formation of chiral nematic (N*) phase confirmed by the polarized optical microscopy studies. Both the compounds on cooling resulted in a glassy chiral nematic phase, while the compound **CS-1** showed slow transformation to a crystal phase on standing at room temperature.

The thesis concludes with a summary of the findings of the investigations discussed in the various chapters. The compounds and molecular designs discussed in this thesis leave ample scope for future exploration of various optical properties and device applications.

Chapter 1

Introduction

1.1 *Abstract*

Aggregation induced emissive (AIE) materials are an important class of compounds because of their various solid-state optoelectronic applications. These materials are non-emissive or weakly emissive in solutions but highly emissive on aggregation. The main reason for the enhanced emission in the solid state of these materials is the regulation of the supramolecular interactions to avoid emission quenching in the aggregated state. The major interest behind the AIE systems lies in the fact that some of these classes are known for their stimuli responsive emission switching in the solid state such as heat, mechanical stress, solvent vapours, electric field etc. The stimuli-responsive behaviour of π conjugated systems can be utilised in various devices such as switches, sensors, data storage, security devices etc. The emission switching in these types of materials is achieved by controlling the weak interactions and packing in the solid state. The molecular structure and the packing mode play a decisive role in making stimuli-responsive solid-state emissive materials. Therefore, the suitable structural modification of luminogens can result in stimuli responsive materials capable of subtle emission tuning. This chapter gives a brief overview of the AIE and stimuli-responsive materials with special importance to the design and structural aspects.

1.2 Aggregation Induced Emission (AIE) and Aggregation Induced Enhanced Emission (AIEE) in π-Conjugated Molecules

Molecular systems that are luminescent in the solid state play a crucial role in material science and technology since they are the major counterparts of optoelectronic devices, sensors, switches etc.[1-6] The initial days of solid state lighting technology were mainly based on solid state emitters of inorganic origin and in recent days there are several technologies based on organic materials were evolved.[7-11] The interest in organic materials as candidates for various optoelectronic applications pertains to the easiness of synthesis and processability along with high reproducibility and device efficiency.[12,13] Although there are several reports on organic luminescent materials exploring properties in dilute solutions, the reports on highly emissive solid state luminescent material are limited due to the luminescence quenching in the solid state.[14-17] In the organic luminescent materials, the mechanism behind the luminescent behaviour in the dilute solutions and the solid state were distinct. Highly planar structures exhibited strong luminescence in solutions due to extensive conjugation, however, these systems were found non-luminescent in the solid state. Several researchers made efforts towards the design of solid state emitters based on organic conjugated molecules with unquenched luminescence. Although a strategy based on the substitution of bulky groups on conjugated π-systems was explored as a tool to prevent molecular packing induced quenching, these efforts were not successful. The main cause of aggregation caused quenching in conventional luminophores is the planar structure of the luminophores where the planar π-systems give rise to closely packed π-π stacked assemblies resulting in luminescence quenching.[18,19] The highly emissive planar molecules like perylenebisimide

with large π-system assemble in a disc like arrangement in the solid state which results in the formation of excimers and exciplex having decreased quantum efficiency.[20] Here in these molecular systems, the gradual increase in concentration leads to simultaneous emission quenching, and it is known that the increases in concentration result in various types of aggregates of the luminophore in the solution. The aggregates formed at a high concentration of the luminophore result in luminescence quenching known as aggregation caused quenching (ACQ), where this phenomenon is quite detrimental in the making of solid-state luminescent materials out of π-conjugated molecules.[21-25] One of the ACQ systems with a perylene core is shown in Figure 1.1. As obvious from the figure, an increased water fraction causes emission quenching due to the formation of aggregates in the concentrated solutions. Thus to make solid state emissive systems, the aggregation should work constructively by stabilizing the excited states. Many strategies were proposed to design and synthesize highly emissive molecular systems in the solid state. As already discussed, non-planar architectures are expected to show better emission in solid state by reducing the quenching in the aggregated state. The non-planar structures reduce the cofacial π-π stacking interaction in the solid state thereby reducing the emission quenching of the luminophores. So the formation of nonplanar or twisted systems is the main focus in the development of solid state luminescent materials. One of the major challenges in designing twisted molecular systems with strong solid state emissions is the maintenance of conjugation despite the twisted geometry. Consequently, several researchers succeeded in synthesising molecules with high emission in solid states by incorporating twists in the π-system.[26-31]

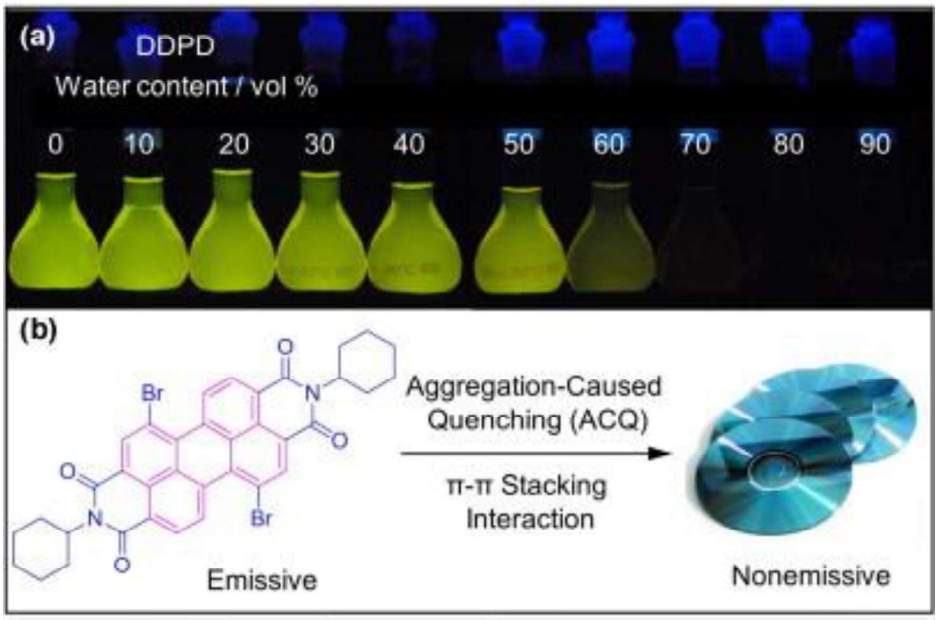

Figure 1.1: (a) Fluorescence images illustrating aggregation caused quenching (ACQ) effect (N, N-dicyclohexyl-1,7-dibromo-3,4,9,10-perylenetetracarboxylic diimide (DDPD). (b) Disk-shaped DDPD molecules non-fluorescent aggregates because of strong π–π stacking interaction in the aggregated state. (Reproduced with permission from reference 20, Copyright RSC 2011)

It is quite interesting to note that the making of highly luminescent materials is possible from molecular systems which are non-luminescent in the solution phase. This phenomenon is a milestone in the development of organic optoelectronic materials, known as aggregation induced emission (AIE).[32-40] In AIE systems, aggregation works constructively to enhance the luminescence efficiency (Figure 1.2). There are several reports on molecular systems with AIE showing higher luminescence efficiency despite poor or non-emissive solution phases. Tang and co-workers first demonstrated the AIE emission in silole derivatives, *viz*. 1-methyl-1,2,3,4,5-pentaphenylsilole, with highly conjugated π-system.[41] In this report the molecule showed a

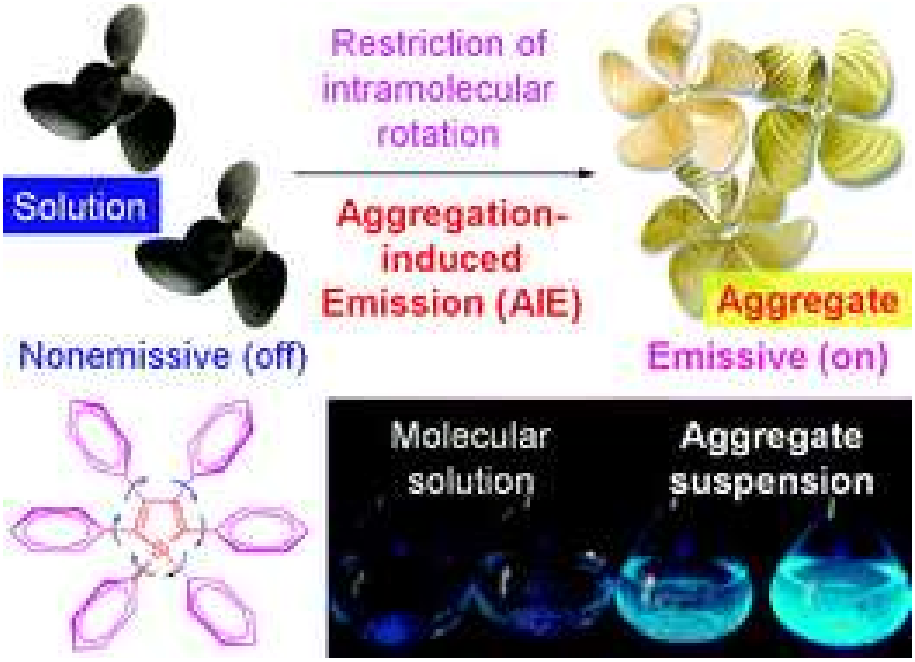

Figure 1.2: An illustration showing the non-planar propeller-shaped AIEgen Hexaphenyl silole and its AIE behaviour in an aggregated state. (Reproduced with permission from reference 48, Copyright RSC 2009)

diminished emission on TLC with a wet spot and turned bright on drying with an emission enhancement. The study also demonstrated a 333 times emission enhancement in large aggregates formed in ethanol-water mixture. Following this study, several silole derivatives were synthesized and explored for aggregation induced emission (AIE).[42-46,] The studies by Tang and co-workers proposed the mechanism of the aggregation induced emission observed in the silole derivatives arising from the restricted intramolecular rotation (RIR) on aggregation.[47, 48] According to the RIR hypothesis most of the conjugated systems execute intramolecular rotations in the solution state, where the higher level of

molecular rotations consumes the excited state energy of the molecules resulting in the decay of the molecules from the excited state by quick non-radiative decay processes. Conversely, the higher intermolecular interactions in the solid-state lead to the restriction of the intramolecular rotation to a large extent which blocks the non-radiative decay pathways and gives rise to solid state emission enhancement. In addition, the aggregate formation blocks the intramolecular vibrations resulting in aggregation induced enhanced emission (AIEE) behaviour of organic luminophores. Hence both restricted intramolecular rotation (RIR) and restricted intramolecular vibration (RIV) contribute collectively to AIE in the π-conjugated molecular assemblies.[47-50] The two phenomena, RIR and RIV are collectively termed restricted intramolecular motion (RIM) and assigned as the mechanism of aggregation induced emission. Since the RIM process is found to be the major cause of aggregation induced emission, the rigidity of the aggregated structure also played a quite important role in the AIEE process.[51, 52] Therefore, the molecular systems showing twisted structures and those capable of forming rigid aggregates are quite important in making highly efficient solid state luminescent materials. The photoluminescence behaviour of molecules in the solid state is also highly dependent on the nature of the aggregate formed. According to Kasha and co-workers,[53,54] the emission properties of the molecules are dependent on the coupling of molecular transition dipoles in aggregated state. The parallel arrangement of transition dipoles results in the formation of H-aggregates. The H-aggregate formation normally results in blue-shifted luminescence with reduced quantum yield. A slipped stack arrangement of molecular transition dipoles in the aggregate results in the formation of J-aggregate which in turn results in red-shifted photoluminescence with increased quantum

yield. A cross stacking of dipole results in the formation of an X-aggregate with strong fluorescence characteristics. Hence RIM and the type of the aggregate formed decide the overall behaviour of photoluminescent materials.

Aggregation-induced emission is the basic phenomenon behind various solid-state photophysical properties like room temperature phosphorescence (**RTP**),[55] aggregation induced delayed fluorescence (**AIDF**),[56] crystallization-induced emission (**CIE**),[57] clusterization-triggered emission (**CTE**),[58] mechanoluminescence (**ML**),[59] circularly polarized luminescence (**CPL**)[60] etc (Figure 1.3). The nature of aggregates formed determines the type of luminescence emission found in solid state luminogens, for example, a rigid aggregate formation is preferred in the case of an RTP material conversely a loosely packed aggregate is favourable in the case of stimulai responsive systems.

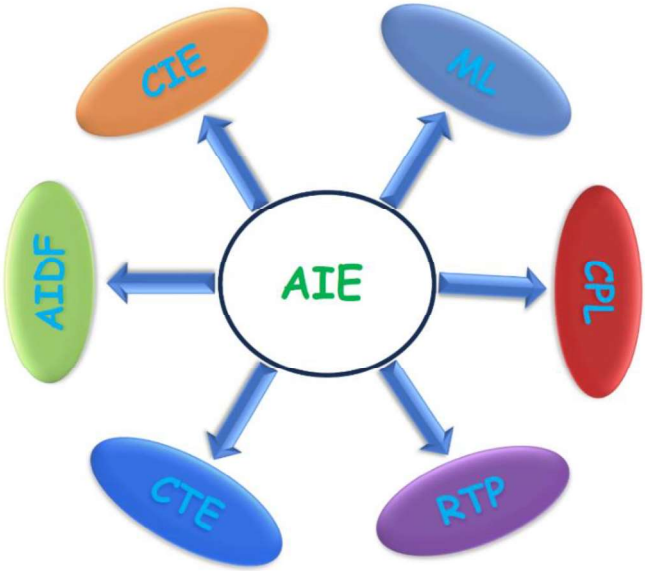

Figure 1.3: Various optical properties evolved by aggregation of organic luminophores.

Following the studies on silole derivatives by Tang and co-workers, many research groups synthesized different molecular systems showing AIE in the aggregated state.[61-63] Several π- conjugated molecules were extensively studied for aggregation induced emission. Derivatives of tetraphenylethene, phenyleneethynylene phenylenevinylene, cyanostilbene and pyrene were some examples of π-conjugated molecules that are explored for AIE behaviour.[64-68] The tetraphenylethene (TPE) derivatives serve as one of the best examples of an aggregation induced emissive systems. In the solution phase, the intramolecular rotation of phenyl rings causes higher non-radiative decay pathways and hence emission quenching.[69] The restriction of the rotation of the aryl rotors is responsible for the AIE observed in the solid state of these molecules. Tang and co-workers synthesized three TPE derivatives showing bluish-green fluorescence with a very high quantum yield.[69] The emission behaviour of these TPE derivatives can be tuned by incorporating strong electron withdrawing groups like CN by replacing the free phenyl rings of the TPE derivative. For these cyano substituted ones, better aggregation induced emission enhancement was observed. A report on *E* and *Z* isomers of ureidopyrimidinone functionalized TPE demonstrated the morphology dependent AIE behaviour where the crystalline isomer showed a blueshifted emission compared to their amorphous phases.[70] Li and co-workers reported the synthesis of a TPE derivative in which tetraphenylethene groups were connected with carbazole or spiropyran moieties, where these systems demonstrated aggregation induced emission behaviour.[71] Another tetraphenylethene derivative showing AIEE property and a high quantum yield of 97.7 % was synthesized by Cao and co-workers (Figure 1.4).[72] Highly

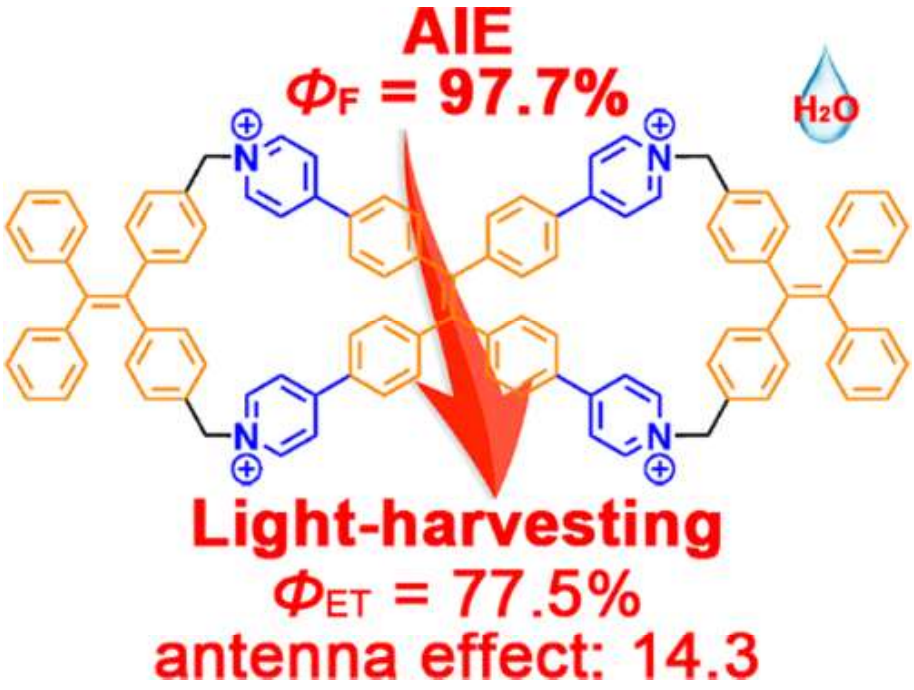

Figure 1.4: Aggregation induced emission in TPE derivatives. (Reproduced with permission from reference 72, Copyright 2019 American Chemical Society)

emissive pyrene-based systems were also synthesized by various research groups. A study by Misra and co-workers demonstrated a novel AIEE system with fluorescent emission enhancement on chelation (see Figure 1.5).[73] Phenylenevinylenes were also enlisted as a better chromophore for designing molecular systems with AIEE behaviour. Phenylenevinylene based AIEE system having highly emissive aggregated phase were synthesized by Swager and co-workers.[74] Apart from the above mentioned compounds various other π-conjugated systems were also explored for their AIEE properties. Among various AIEE systems explored, cyanostilbene derivatives received greater attention due to the easiness of structure modification and emission tuning. In addition, the cyanostilbene systems are relevant owing to the easy

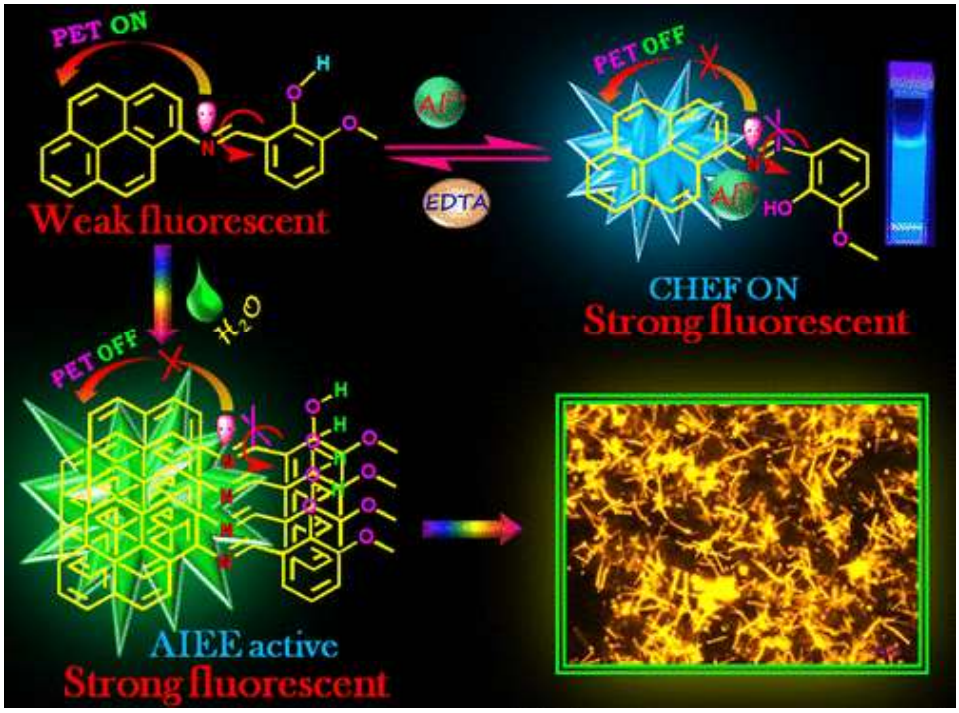

Figure 1.5: Image of a strongly fluorescent pyrene scaffold (Reproduced with permission from reference 73, Copyright 2016 American Chemical Society)

incorporation of the various substituents into the core structure of cyanostilbene by using simple synthetic procedures.

1.21 Aggregation induced emission in cyanostilbene / cyanostyrene based systems

Stilbenes are the class of molecules with the possibility for versatile chemical and photophysical properties such as fluorescence, phosphorescence, *cis-trans* isomerization, intermolecular reactions like [2+2] cycloaddition etc.[75] Stilbene has been explored for many years as a model compound for its luminescent properties.[76] Since stilbene is a molecule having lower emission efficiency and

also spans a shorter spectral range, to improve the luminescent properties of the molecule various structural modifications are necessary.[77] The investigations for obtaining promising luminescent materials with subtle emission tuning led to the development of several novel classes of stilbene derivatives. The cyanostilbenes are one of the most intelligent modifications of the stilbenes ever made in the literature. Cyanostilbenes with the basic conjugated stilbene skeleton in which the CN group is covalently attached to the *para* position of the aromatic ring is known as the 4-cyanostilbenes (Figure 1.6). The presence of the CN group in the structure broadens the emission range considerably making the emission in the visible region.[78] The tuning of luminescence in cyanostilbene requires proper functionalization of the luminophore, while the lack of suitable substitution positions in aryl units limits the needful structural modification of

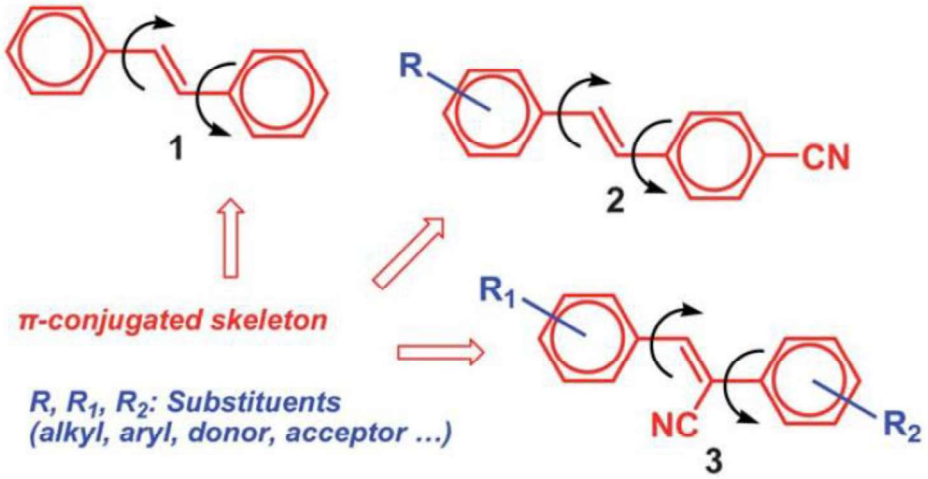

Figure 1.6: Chemical structures of (1) stilbene. (2) 4-cyanostilbene and (3) α-cyanostilbene. The arrows represent the intramolecular rotation of the aromatic group (Reproduced with permission from reference 78, Copyright RSC 2013)

4-cyanostilbene.[78] Further research on suitable modification of stilbene moiety resulted in the development of α-cyanostilbene in which the -CN group was attached to the α-position of the ethylenic bond, where this structure gives scope for the easy functionalization to bring about versatile emission behaviour in the solid state.[79-83] The steric interaction between the CN group and the phenyl ring in α-cyanostilbene makes the molecule twisted and this twist in the molecular structure reduces the π-π stacking which in turn results in decreased emission quenching. In 2004 Park and co-workers synthesized an AIE active α-cyanostilbene derivative, 1-cyano-trans-1,2-bis-(3′,5′-bis-trifluoromethyl-biphenyl)ethylene (CN-TFMBE), where this molecule showed a high gelation efficiency with emission enhancement on gelation.[84] The luminescence intensity of the compound showed an increase of 150 times by gelation in comparison to a dilute solution in dichloromethane. The reason behind this phenomenon is the presence of bulky and polar CN groups enhances the formation of a J-type aggregate which is unfavourable for an exciplex formation and also results in the formation of emissive aggregates. The AIE/AIEE effect in the cyanostilbene based system can be verified by recording emission spectra in solutions containing varying fractions of poor solvents. If the molecule shows aggregation induced emission there will be an increase in the emission intensity in solutions containing increased fractions of poor solvents. Here in this expriment, as the fraction of poor solvent increases, molecules tend to aggregate with increased emission intensity. In most of the cases, there will be a redshift in the emission on increasing the aggregate size, where this observation is also considered as an indication of aggregation induced emission.[85]

One of the recent reports on V-shaped cyanostilbene amide substituted with a tertiary butyl group in its structure showed the influence of molecular geometry and conformation in the AIEE effect.[86] The V-shaped conformation

of the molecule helps in self-assembling by incorporating various intermolecular interactions. The molecule was nonemissive in chloroform solution while it showed gelling on standing with enhanced emission. A report by Kanvah and coworkers on cyanostilbene derivatives containing dimethyl aniline, diphenylaniline and carbazole demonstrated the aggregation induced emission enhancement by adding different fractions of water to the dilute solutions of the molecules in dioxane.[87] The molecule, which is less emissive in dilute solutions showed emission enhancement with increased water fraction in the solution as a result of the aggregation of molecules in poor solvent like water. Alkyl chain substituted cyanostyrylbenzene derivatives also showed aggregation induced emission behaviour. Various alkyl chain substituted symmetric and non-symmetric systems were studied by the different research groups. Park and co-workers explored a symmetric akyloxy substituted dicyanodistyrylbenzene in two different works and both cases, the molecules showed aggregation induced emission.[88] Hence the aggregation induced emission is a constructive mechanism to produce highly efficient solid state luminescent materials.

The literature on cyanostilbene derivatives demonstrated that aggregation has a pivotal role in their photoluminescence efficiency. A comprehensive analysis that probes the structural and mechanistic aspects that contribute to the solid state luminescent quantum yield can help in the design of highly efficient cyanostyrene derivatives. The comparison of emission quantum yield in π-systems showed a sharp enhancement as a result of aggregate formation mainly from twisted chromophores such as cyanostilbenes. In one of their studies, Chen and co-workers synthesized a star-shaped cyanostilbenes having very low quantum yields in the solution phase due to torsionally induced deactivation, while the same molecule showed a quantum yield enhancement in the solid state owing to effective

blocking of nonradiative decay pathways on aggrgation.[89] Various factors deciding the increased solid state luminescent quantum yields in *para* substituted dicyanodistyrylbenzene systems were thoroughly studied by various research groups.[88] In the case of cyanostyrylbenzene systems, the solution phase showed very low quantum yield due to enhanced nonradiative decay pathways operating in the molecules in the solutions.[90] The detailed analysis of divers reports on cyanostyrene systems showed that various electronic and steric factors largely contributes to the enission in the solid state and inactivate the possibilities for nonradiative decay. It is already known that cyanostilbenes with twisted chromophoric structure has a prominent role in observed AIE behaviour. Therefore, the derivatives of cyanostilbenes were good candidates for making systems with enhanced luminescence and quantum yield in solid state.

As already discussed, the RIM process is the key mechanism of the aggregation induced emission.[47-50] By restricting the intermolecular motions in twisted architectures, it is possible to achieve the triplet state in organic luminogens by preventing the non-radiative decay pathways. There are previous reports in which the photoluminescence lifetime increased by restricting molecular motions by various methods such as using viscous media or low temperature media.[91] Consequently, it is possible to achieve the phosphorescence emission at low temperatures by freezing the molecular motions. Another interesting part of the AIE systems is related to their stimuli responsive emission behaviour. Various chromophoric systems showing AIE mechanisms are also vulnerable to various stimuli. The explorations on stimuli responsive materials are quite important in the area of material research.

1.3 Stimuli responsive emission in organic chromophores

Nature has its responsive mechanism to different stimuli, and it always inspires the quest for the development of smart materials with tailor made properties. The opening of seedlings, the closing of mimosa leaves on touching etc. are examples of nature's response to different stimuli, where all these responses are due to some sensitive structures present in these systems. The key factor behind this stimulus responsive behavior in natural systems is the regulation of some weak interactions present in the system. The stimuli can be physical or chemical in nature. The various physical stimuli include stress, heat, magnetic fields etc. while, p^H, different chemical species like oxidizing or reducing agents serve as chemical stimuli. Inspired by nature, different types of stimuli responsive smart materials were synthesized by researchers worldwide, where a fine control over this response was achieved by managing the different weak nonbonding interactions. Molecular systems were able to switch between two stable conformations according to the applied stimuli, and in some cases, even multi-stable switching was also achieved. The sensitivity obtained on different external stimuli is due to the physical or chemical changes that occur in response to a particular stimulus. The stimuli responsive materials relevant in various applications such as switchable optoelectronic materials, sensors, targeted drug delivery, robotics etc.[92-98]

In general, the stimuli responsive switches are either molecular or supramolecular. In molecular switches, the stimuli response is achieved by the structural modification under applied stimuli whereas the supramolecular switching is achieved by the modulation of intermolecular interactions and molecular packing. Molecular systems containing photoisomerizable units can

act as molecular switches since they can be switched between the two stable isomeric states.[99] The assemblies of conjugated molecules such as phenylenevinylene, phenyleneethynylene, phenylene and cyanostilbenes backbone showed switching of optoelectronic properties originating from two stable supramolecular states. The difference in intermolecular interactions in two supramolecular states bring about modification in the conformation of the functional motif and electronic coupling between adjacent molecules in the assembly.[100-104]

The last two decades witnessed a tremendous interest in π-conjugated luminophores attributed to their applications in various fields. Theoretical and experimental studies have shown that molecular packing has a significant role in determining the luminescence efficiencies and emission switching in the solid state.[105, 106] The ability of the self assembly of π- systems to modify their structure via subtle tuning of their primary structure and intermolecular interactions gives the scope for achieving tunable optoelectronic properties. Various explorations to understand the mechanism behind the stimuli responsive emission behaviour of π-conjugated molecules in the solid state demonstrated the role of aggregate structure in determining their emission properties. Researchers around the globe explored the change in various photophysical properties such as absorption, reflection, emission etc. in response to multiple stimuli. Among various responses explored so far, the stimuli response in the form of photoluminescence emissions such as fluorescence and phosphorescence received greater interest owing to their potential applications. The stimuli responsive emission from the organic self-assemblies is due to the switching between different aggregate structures in response to the applied stimuli. The change in aggregate structure can be evidenced as either crystal to crystal transition or crystal to amorphous transition and vice versa. In one of the recent works, Park and co-workers

explored the multistimuli responsive tricolour emission because of crystal to amorphous phase transition.[88] The stimuli responsive phase change brings about the modification of aggregation pattern and thereby emission switching. An investigation by Xu et al. demonstrated the emission switching from yellow to green in a co-crystal system caused by crystal-to-crystal transition under multiple stimuli such as heat, solvent vapours, mechanical stress etc.[107] The Nature of the stimuli also has a major role in determining the emission changes in the stimuli responsive materials. In several systems, the mechanical stimuli are found to induce crystalline to an amorphous phase transition,[88] while the recovery of the crystalline phase can be achieved by a different stimulus. The stimulus such as temperature and solvent found to bring about the recovery of the crystalline phase from amorphous phases.[88] The vulnerability of aggregate structures to different stimuli depends upon the structural flexibility of the molecules and intermolecular interactions. So, the key features to be incorporated while designing stimuli responsive self-assemblies are the flexible side chains and functional groups capable of forming relatively weaker intermolecular interactions. To achieve fine tuning of the solid state emission properties under various stimuli, different classes of chromophoric systems were engineered.[108-112] Among divers π-conjugated chromophores employed to obtain stimuli responsive smart materials, the systems based on tetraphenylethene, oligophenylenevinylene, cyanostilbene, pyrenes etc. take the prime position.

1.3.1 Stimuli responsive emission in some relevant class of compounds.

Among various π-conjugated chromophores explored for stimuli responsive emission properties the tetraphenylethene (TPE) derivatives got greater attention as AIEE and stimuli responsive materials. The reports by Tang and

co-workers demonstrated the versatility of functionalized TPE systems to generate stimuli responsive materials with precise control over multiple stimuli.[113] In one of their studies, *E* and *Z* isomers of TPE derivatives were synthesized using Click synthesis, where the *E* and *Z* isomers behave quite differently on applied stimuli.[114] The *E* isomer of the compound is highly responsive to mechanical stress, while the *Z*-isomer showed a negligible shift on applied stress. The solid *E* isomer with off-white emission showed an emission switching to bluish green on grinding and the off-white emission was recovered on heating at 120 ˚C. The comparatively red shifted emission observed in the *Z*-isomer is ascribed to the amorphous solid state of the isomer. The observed insignificant emission shift in *Z*-isomer on griding can be attributed to the morphological change that had happened to the amorphous solid. In the case of *E* isomer, the substantial emission shift is due to the transition from a crystalline phase to an amorphous phase. The crystalline nature of the *E* isomer was established from the PXRD pattern. On grinding, the PXRD pattern changes from sharp diffraction peaks to somewhat broad peaks and on heating the crystalline form is regenerated as evident from the PXRD pattern. Hence here a crystalline to amorphous phase transition was explained as the reason for mechanochromism.

Bu et. al synthesized a vinylpyridine substituted TPE system showing multistimuli responsive emission switching (Figure 1.7).[115] The molecule showed emission switching to mechanical stress, hydrostatic compression and also on protonation. The single crystal X-ray diffraction studies showed that the molecule has a highly twisted conformation with a packing structure with shrinkable space which is capable of undergoing deformations under applied pressure. In a different study, Tang and coworkers[116] examined the effect of the donor (D) and acceptor group on the emission behaviour of a TPE trimer.

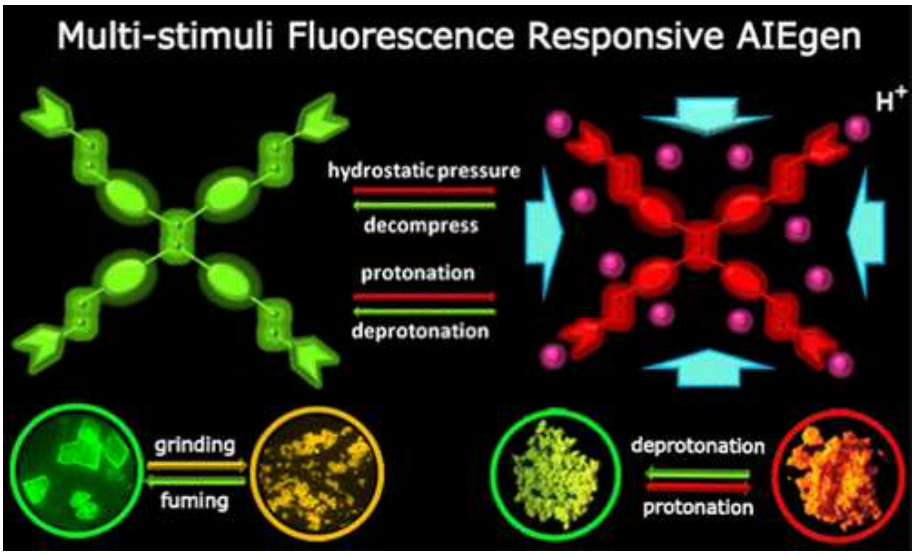

Figure 1.7: A vinyl pyridine functionalized TPE system showing multistimuli responsive emission switching. (Reproduced with permission from reference 115, Copyright 2018 American Chemical Society)

The study tried to understand the emission switching in three TPE derivatives carrying either acceptor or donor-acceptor groups and compared them with unsubstituted TPE. The mechanochromic TPE system functionalized with an acceptor unit is prepared by substituting fumaronitrile, while the N, N-diethylamino group served the role of donor. The acceptor-linked TPE synthesized as a yellow emissive powder changed the emission to an orange colour on grinding. The original yellow emission colour was regained on thermal treatment above 160 ˚C or exposure to solvent vapours such as DCM and THF. The observed piezochromic emission switching in this system was also attributed to the transition between crystalline to amorphous phases.

In 2013 Zhao et. al synthesized a pyridinium salt of TPE showing a high contrast mechanochromic emission having an emission wavelength shift

of 80 nm.[117] To understand the mechanism behind the mechanochromic emission X-ray diffraction experiments were carried out on ground samples and compared to that of unground samples. The analysis showed the crystalline to less crystalline or amorphous phase transition as evidenced by the broad peaks in PXRD. A set of organic boron complexes of TPE was synthesized by Ren and co-workers, where the complexes showed distinct mechanochromic emission behaviour on smashing and grinding.[118] The red-shifted emission on grinding was attributed to the crystalline to amorphous phase transition while the blue shifted emission observed on ultrasonic treatment and smashing was explained as the destruction of a J-type aggregate structure that was found in the crystalline form. So, in the solid state of TPE derivatives, the stimuli responsive emission was mainly a consequence of phase transitions including crystal to crystal or crystal to amorphous transition where the molecules aggregates differently bring about switchable photoluminescence. All the previously discussed molecules have an inherent mechanochromic behaviour on mechanical agitation caused by the modulation of aggregate structure as a result of the change in molecular structure. In general, the red shifted emission on mechanical agitation is due to the planarization of the π-luninogens. The planarization leads to the increase in conjugation in the π-system along with improved dipolar coupling leading to redshifted emission. The recovery of the original emission from the ground sample by other stimuli such as temperature and solvent were credited to the recovery of the crystalline phases.

Phenyleneethylene-based molecules are also explored for their solid state emissive behaviour and single molecular conductors owing to the possibility for free rotation about the triple bond which leads to different levels of planarity. The deviation from planarity can give rise to different levels of conjugation thereby resulting in different energy levels. A report by Bunz and

coworkers demonstrated the thermochromic luminescence in octyloxy substituted phenyleneethynylene polymer, where the emission switching in this polymer is achieved by switching of degree of planarity at the liquid crystalline state.[119] A similar study was conducted by Kulkarni and workers on a dimethoxy derivative of the oligo phenyleneethylene system, where this study demonstrated a cooling rate dependent control over fluorescence spectra and emission colour (Figure 1.8).[120] The investigation also explored the effect of surface morphology on emission behaviour. The cooling rate-controlled emission colour is assigned to preferential wetting of the surface on cooing and planarization. Maji and co-workers explored a multifunctional phenylene ethynylene chromophore showing mechanochromic blue shift.[121] The molecule showed strong and weak intermolecular interactions in the crystalline state and the mechanochromic modulation of these interactions leads to the stress induced switchable emission. A recent report by Sagara et al. on luminescent cyclophane that is comprised of two 9,10-bis(phenylethynyl)anthracene moieties linked through hexaethylene glycol

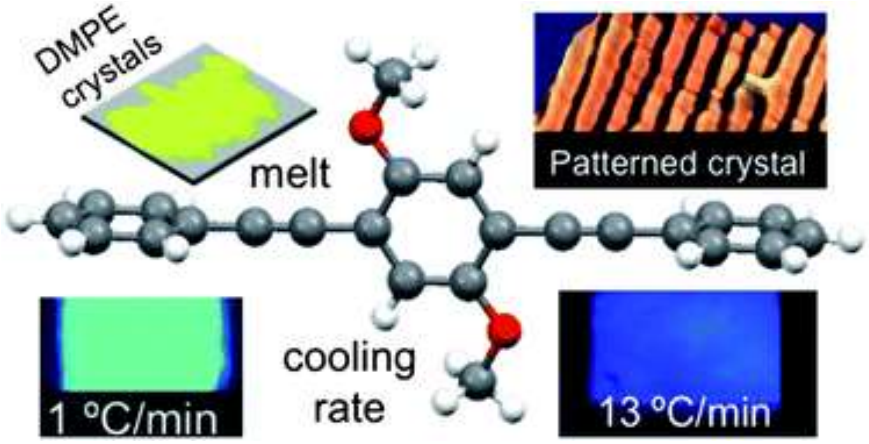

Figure 1.8: A stimuli responsive phenyleneethenylene derivative (Reproduced with permission from reference 120, Copyright RSC 2012).

units, demonstrated the mechanochromic and thermochromic emission switching caused by different molecular assembling.[122] The thermochromism in this system is achieved by crystal to liquid crystalline phase transition while the mechanochromism is attributed to shear stress induced change in molecular assembly. The study demonstrated a fine control over stimuli response by controlling the ring size of the cyclophane moiety.

1.3.2 Cyanostilbene / Cyanostyrene based Stimuli responsive systems.

In recent years cyanostyrene based π-conjugated luminophores got paramount interest owing to their highly emissive properties in the solid state, easiness in synthesis and property modifications. In general, cyanostilbenes and cyanostyrene derivatives are weakly fluorescent in solutions whereas, several members of these systems showed a highly enhanced emission in solid state with fast response to external stimuli such as temperature, pressure, nature of solvent, p^H etc. The cyanostilbene based stimuli responsive fluorescent molecules have been explored by various research groups for their emission dependence on various stimuli such as pressure, temperature, solvent, pH etc. Fan et al, synthesised cyanostilbene based multi-stimuli responsive positional isomers by varying the position of cyano groups where the study explored

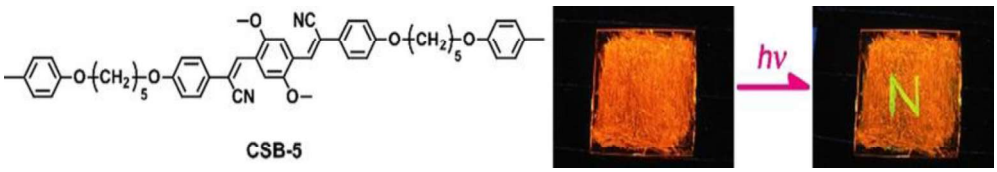

Figure 1.9: A photo-responsive cyanostyrylbenzene derivative (Reproduced with permission from reference 126, Copyright 2018 Wiley-VCH)

the relationship between structure and photoluminescence properties.[123] The report successfully demonstrated the effect of positional variation of the cyano group on luminescence behaviour by various spectroscopic and single crystal X-ray diffraction methods. A study on the donor-acceptor cyanostilbene based system by Wang et al., explored the stimuli responsive nature of the assembly.[124] The fluorescence switching in this molecule is related to the crystal-to-amorphous phase transition. This donor-acceptor system was highly responsive to P^H changes in the solvent which made the compound useful in sensor like applications. A study by Zhang et al, proposed cyanostilbene as a promising group to prepare luminescent polymers by incorporating into a polymer matrix, where this could be employed in a variety of optoelectronic applications.[125] In addition, there are several reports on cyanostilbene based gels showing AIEE and stimuli responsive behaviour.

Nakano and coworkers synthesized a biscyanostyrylbenzene derivative (CB-5) showing both photoinduced and mechanochromic reversible emission switching. This molecule showed green to orange emission switching on rubbing and recovery was observed on photoirradiation (Figure 1.9).[126] The molecule showed emission colour change on mechanical stress attributed to the crystalline to amorphous phase transition. The quite interesting observation in this system is that the rubbed films of the molecule showed emission switching from orange to green on UV exposure. This response is a result of a photochemical reaction occurring in the system. A report by Jiang and co-workers on organo gels derived from V-shaped cyanostilbene derivatives demonstrated the formation of emissive assemblies that are highly responsive to different stimuli.[127] From the various reports it is evident that the assemblies of cyanostilbene derivatives with cyanostilbene core are promising in the field of stimuli responsive smart materials owing to their highly emissive nature with vulnerability to different stimuli in

crystalline, amorphous and soft materials such as gels. Recently symmetrically substituted cyanostilbene core systems with alkyl and alkoxy groups of different chain lengths were synthesized[88, 128] by different research groups and the first attempt in this direction was by Park and co-worker on methyl substituted symmetric cyanostilbene derivative.[128] The study demonstrated the emission enhancement attributed to the formation of J-aggregate and planarization of the π system. A butoxy derivative of the dicyanodistyrylbenzene was also reported by Park et al, where this compound showed the formation of highly emissive aggregates along with multistimuli responsive emission.[88b] The study also explored the structure-property relationship correlating the observed emission property to the structure and molecular packing derived from single crystal X-ray diffraction. In recent work, Park and co-workers reported a tricolour emission from a dodecyloxy derivative and demonstrated the multistimuli responsive emission switching assigned to crystal to crystal and crystal to amorphous phase transition.[88a] Although the effectiveness in the tuning of optoelectronic properties of the cyanostilbene core systems lies in the selection of substituents, the exact relationship between the molecular structure and stimuli responsive behaviour

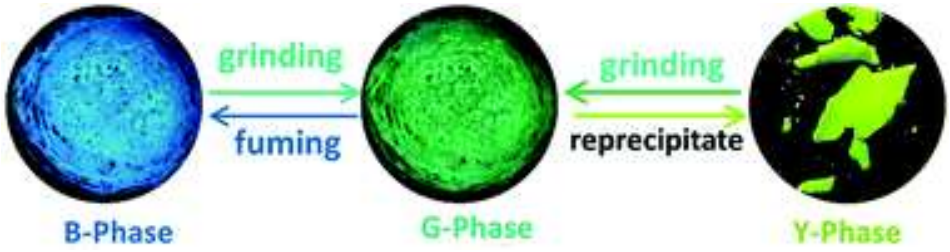

Figure 1.10: A Mult stimuli-responsive cyanostyrylbenzene-based system (Reproduced with permission from reference 130, Copyright RSC 2021).

of substituted cyanostilbene systems remains unclear. Xu et al.[129] attribute the stimuli responsive emission in cyanostilbene derivatives to the probability of a crystalline to amorphous phase transition, while Park and coworkers suggest the formation of two energetically stable emissive phases and they further assign the observed mechnofluorochromism in cyanostilbene derivatives to low-energy shear sliding between the molecular layers.[84] Zhang and co-workers synthesized a tricolour emissive luminophore based on cyanostilbene showing multistimuli responsive emission in solid state (Figure 1.10).[130] The crystalline powder of the compound showed blue emission (B-phase) which on grinding resulted in green emissive G-phase. The yellow emissive Y-phase was obtained by the reprecipitation of the G-phase and reversible switching was observed on griding. The formation of Y-phases is ascribed to the arrangement of the chiral molecule with specific handedness, while the formation of the G-phase is assigned to crystalline to amorphous transition. A report on the assembly of triphenylamine appended dicyanodistyrylbenzene system showed mechanofluorochromism along with electrochromism. The molecule comprised a donor-acceptor system, where the dicyanodistyryl and triphenylamine act as acceptor and donor moieties respectively. The PXRD pattern of the ground powder indicated the low crystallinity of the sample and represented the pattern obtained for the amorphous sample. Similar to the previously discussed example, the observed mechanochromism also originated from a phase transition from a less crystalline to a purely amorphous form.

The major attractions of the cyanostyrene based compounds are the easiness of synthesis and structure tunability. Various researchers could easily attain stimuli responsive optoelectronic properties in cyanostilbene derivatives by suitably modifying the cyanostyrene core with flexible groups. It is also possible to attain twisted/non-planar structures from the cyanostyrene core by

suitable substitution. The cyanostyrene based systems with the capability for luminescence switching that can be achieved by subtle modification of the structure always attracted enormous research interest.

1.4 Design strategies of AIEE systems and understanding the structural origin of photoluminescence behaviour.

The discussions on various literature on AIEE and stimuli responsive systems, the photoluminescence emission behaviour and the stimuli responsive switching behaviour of organic luminogens were highly dependent on various structural factors. As already discussed, luminogens having specific structural requirements are preferred for developing AIEE systems. Aggregation induced emissive systems were mainly developed from twisted chromophores. In the solid, the aggregate formation must happen in such a way that the luminescence behaviour should be enhanced. Therefore, to make a general design principle of AIEE systems it is quite important to study the aggregate structure of the luminophores under investigation. Single crystal X-ray diffraction studies might help to investigate the aggregated structure of the luminophores. The aggregate forming nature of various chromophores can be well understood from X-ray diffraction studies. In the designing step of an AIEE system, it is better to choose a twisted chromophore or make a twisted system by suitably substituting planar molecules. Structural rigidity is another criterion in the formation of systems having high emission efficiency. Making cross-linked structures or fixing the chromophores in a rigid matrix, crystallization etc are mainly used in the formation of efficient solid state emissive materials. The restriction of intermolecular motion in various cases including stilbenes systems results in the triplet emission.[131] Therefore

selecting a twisted luminophore and rigidifying the aggregate structure using various methods are important in the making of systems having high emission efficiency and longer lifetimes.

The emission switching observed in the organic luminophores also depends on the structural modification that happened during the application of particular stimuli, crystal to crystal or crystal to amorphous phase transitions are reported as the reason for stimuli responsive emission switching. It is important to know what kind of structural transformations happen to a system during the application of stimuli. The crystal to amorphous phase transitions may be clearly understood from the powder X-ray diffraction patterns obtained for the respective phase. The nature of the diffraction pattern indicates the nature of the phase transition. Various polymorphic forms also showed differences in the emission behaviour. Here the diffraction studies, especially the single crystal X-ray diffraction method are quite useful for understanding the structural change of the polymorphic forms and also the pattern of aggregate forms in each case. The main focus of this thesis is to probe the structural aspects contributing to the AIE and stimuli responsive emission in cyanostyrene based photoluminescent molecules.

1.5 References

1. Ostroverkhova, *Chem. Rev.,* 2016, **116**, 13279–13412.
2. N. A. Kukhta and M. R. Bryce, *Mater. Horiz*., 2021, **8**, 33–55.
3. M. Shimizu and T. Hiyama, *Chem. Asian J.*, 2010, **5**, 1516–1531.
4. P. Gayathri, M. Pannipara, A. G. Al-Sehemi and S. P. Anthony, *New J. Chem.*, 2020, **44**, 8680–8696.
5. S. Ito, C. Nishimoto and S. Nagai, *Cryst. Eng. Comm*., 2019, **21**, 5699–5706.
6. Y. Jiang, Y.-Y. Liu, X. Liu, H. Lin, K. Gao, W.-Y. Lai and W. Huang, *Chem. Soc. Rev*., 2020, **49**, 5885–5944.
7. J. E. Kwon and S. Y. Park, *Adv. Mater.*, 2011, **32**, 3615–3642.
8. H. Kaji, H. Suzuki, T. Fukushima, K. Shizu, K. Suzuki, S. Kubo, T. Komino, H. Oiwa, F. Suzuki, A. Wakamiya, Y. Murata and C. Adachi, *Nat. Commun*., 2015, **6**, 8476.
9. T. P. I. Saragi, T. Spehr, A. Siebert, T. F. Lieker and J. Salbeck, *Chem. Rev.*, 2007, **107**, 1011–1065.
10. N. Keller and T. Bein, *Chem. Soc. Rev.*, 2021, **50**, 18131845.
11. S. R. Forrest and M. E. Thompson, *Chem. Rev.*, 2007, **107**, 923925.
12. D. Li, P. Li, Y. Zhao, R. Su, Y. Guo, W. Su and T. Yu, *New J. Chem.*, 2022, **46**, 2321323224.
13. (a) B. Xu, J. He, Y. Liu, B. Xu, Q. Zhu, M. Xie, Z. Zheng, Z. Chi, W. Tian, C. Jin, F. Zhao, Y. Zhang and J. Xu*, J. Mater. Chem. C*, 2014, **2**, 3416-3428; (b) G. Qian, Z. Zhong, M. Luo, D. Yu, Z. Zhang, Z. Y. Wang and D. Ma, *Adv. Mater.*, 2009, **21**, 111116.
14. M. K. Bera, P. Pal and S. Malik, *J. Mater. Chem. C*, 2020, **8**, 788802.
15. Z. Ning, Z. Chen, Q. Zhang, Y. Yan, S. Qian, Y. Cao and H. Tian, *Adv. Funct. Mater.*, 2007, **17**, 37993807.

16. H. Nie, K. Hu, Y. Cai, Q. Peng, Z. Zhao, R. Hu, J. Chen, S.- J. Su, A. Qin and B. Z. Tang, *Mater. Chem. Front.*, 2017, **1**, 11251129.
17. X. Ma, R. Sun, J. Cheng, J. Liu, F. Gou, H. Xiang and X. Zhou*, J. Chem. Educ*., 2016, **93**, 345–350.
18. F. J. M. Hoeben, P. Jonkheijm, E. W. Meijer and A. P. H. J. Schenning, *Chem. Rev.*, 2005, **105**, 1491–1546.
19. D. G.-Rodrı´guez and A. P. H. J. Schenning, *Chem. Mater.*, 2011, **23**, 310–325.
20. Y. Hong, J. W. Y., Lam and B. Z. Tang, *Chem. Soc. Rev.*, 2011, **40**, 5361-5388.
21. W. Z. Yuan, P. Lu, S. Chen J. W. Y. Lam, Z. Wang, Y. Liu, H. S. Kwok, Y. Ma and B. Z. Tang, *Adv. Mater.*, 2010, **22**, 2159–2163.
22. F. Hu, S. Xu and B. Liu, *Adv. Mater.*, 2018, **30**, 1801350.
23. D. Wang and B. Z. Tang, *Acc. Chem. Res*., 2019, 52, **9**, 2559–2570.
24. Y. Huang, J. Xing, Q. Gong, L.- C. Chen, G. Liu, C. Yao, Z. Wang, H.- Li Zhang, Z. Chen and Q. Zhang , *Nat. Commun*., 2019, **10**, 169.
25. G. Qian, Z. Zhong, M. Luo, D. Yu, Z. Zhang, Z. Y. Wang and D. Ma, *Adv. Mater.*, 2009, **21**, 111116.
26. Y. Sun, Z. Lei and H. Ma*, J. Mater. Chem. C*, 2022, **10**, 14834–14867.
27. Y. Chen, J. W. Y. Lam, R. T. K. Kwok, B. Liu and B. Z. Tang, *Mater. Horiz.*, 2019, **6**, 428–433.
28. K. Kokado and K. Sada, *Angew. Chem.*, 2019, **131**, 8724–8731.
29. J. Zhang, B. Xu, J. Chen, L. Wang and W. Tian, *J. Phys. Chem. C,* 2013, **117**, 23117–23125.
30. H. Zhang, J. Liu, L. Du, C. Ma, N. L. C. Leung, Y. Niu, A. Qin, J. Sun, Q. Peng, H. H. Y. Sung, I. D. Williams, R. T. K. Kwok, J. W. Y. Lam, K. S. Wong, D. L. Phillips and B. Z. Tang, *Mater. Chem. Front.*, 2019, **3**, 1143–1150.

31. S. Xu, Y. Duan and B. Liu, *Adv. Mater*., 2020, **32**, 1903530.
32. J. Li, J. Wang, H. Li, N. Song, D. Wang and B. Z. Tang, *Chem. Soc. Rev.*, 2020*,* **49**, 1144–1172.
33. R. Hu, A. Qin and B. Z. Tang, *Prog. Polym. Sci.*, 2020, **100**, 101176.
34. H. Wang and G. Liu, *J. Mater. Chem. B*, 2018, **6**, 40294042.
35. X. Cai and B. Liu, 2020, *Angew.Chem. Int. Ed.*, **59**, 9868–9886.
36. D. Li and J. Yu, *Small*, 2016, **12**, 6478–6494.
37. W. He, T. Zhang, H. Bai, R. T. K. Kwok, J. W. Y. Lam and B. Z. Tang, *Adv. Healthcare Mater.*, 2021, **10**, 2101055.
38. T. Mondal, S. Roy, I. Mondal, M. V. Mane and S. S. Panja, *J. Photochem. Photobiol. A*, 2021, **406**, 112998.
39. R. Hu, X. Yang, A. Qin and B. Z. Tang, *Mater. Chem. Front.*, 2021, **5**, 40734088.
40. M. Zhang, W. Yang, T. Gong, W. Zhou and R. Xue, *Phys. Chem. Chem. Phys.*, 2017, **19**, 2167221682.
41. J. Luo, Z. Xie, J. W. Y. Lam, L. Cheng, H. Chen, C. Qiu, H. S. Kwok, X. Zhan, Y. Liu, D. Zhu and B. Z. Tang, *Chem.Commun.*, 2001, 1740.
42. L. Xu, Y. Li, S. Li, R. Hu, A. Qin, B. Z. Tang and B. Su, *Analyst*, 2014, **139**, 2332–2335.
43. H. Nie, B. Chen, C. Quan, J. Zhou, H. Qiu, R. Hu, S. Su, A. Qin, Z. Zhao and B. Z. Tang, *Chem. Eur. J.*, 2015, **21**, 8137–8147.
44. Z. Li, Y. Q. Dong, J. W. Y. Lam, J. Sun, A. Qin, M. Häußler, Y. P. Dong, H. H. Y. Sung, I. D. Williams, H. S. Kwok and B. Z. Tang, *Adv. Funct. Mater.*, 2009, **19**, 905–917.
45. M. H. Haque and H. Sohn, *Dyes Pigm.*, 2022, **201**, 110175.
46. X. Du and Z. Y. Wang, *Chem. Commun.*, 2011, **47**, 4276.

47. Q. Zeng, Z. Li, Y. Dong, C. Di, A. Qin, Y. Hong, L. Ji, Z. Zhu, C. K. W. Jim, G. Yu, Q. Li, Z. Li, Y. Liu, J. Qin and B. Z. Tang, *Chem. Commun.*, 2007, 70–72.
48. Y. Hong, J. W. Y. Lam and B.Z. Tang, *Chem. Commun.*, 2009, 43324353.
49. Y. Q. Dong, J. W. Y. Lam and B. Z. Tang, *J. Phys. Chem. Lett.*, 2015, **6**, 3429–3436.
50. Y. Wang, G. Zhang, M. Gao, Y. Cai, C. Zhan, Z. Zhao, D. Zhang and B. Z. Tang, *Faraday Discuss.*, 2017, **196**, 930.
51. F. Würthner, *Angew. Chem. Int. Ed.*, 2020, **59**, 1419214196.
52. X. - Y. Lou and Y. - W. Yang, *Adv. Opt. Mate.,* 2018, **6**, 1800668.
53. M. Kasha, H. R. Rawls and M. A. Bayoumi, *Pure Appl. Chem.*, 1965, **11,** 371392.
54. M. Kasha. *Radiat. Res.*, 1963, **20**, 5570.
55. W. Zhao, Z. He and B. Z. Tang, *Nat. Rev. Mater.*, 2020, **5**, 869–885.
56. H. Tsujimoto, D. - Gwang Ha, G.Markopoulos, H. S. Chae, M. A. Baldo and T. M. Swager, *J. Am. Chem. Soc.*, 2017, **139**, 4894–4900.
57. C. Zheng, Q. Zang, H. Nie, W. Huang, Z. Zhao, A. Qin O, R. Hu and B. Z. Tang, *Mater. Chem. Front.*, 2018, **2**, 180188.
58. X. Chen, T. Yang, J. Lei, X. Liu, Z. Zhao, Z. Xue, W. Li, Y. Zhang and W. Z. Yuan, *J. Phys. Chem. B*, 2020, **124**, 8928–8936.
59. L. Tu, Y. Xie and Z. Li, *J. Phys. Chem. Lett.*, 2022, **13**, 5605–5617.
60. A. Nitti and D. Pasini, *Adv. Mater.,* 2020, **32**, 1908021.
61. X. Feng, C. Qi, H - T. Feng. Z. Zhao. H. H. Y. Sung, I. D. Williams, R. T. K. Kwok, J. W. Y. Lam. A. Qin and B. Z. Tang*, Chem. Sci.*, 2018, **9**, 5679-5687.
62. M. Paramasivam and S. Kanvah, *J. Phys. Chem. C*, 2016, **120**, 10757–10769.

63. M. M. Islam, Z. Hu, Q. Wang, C. Redshaw and X. Feng, *Mater. Chem. Front*., 2019, **3**, 762781.
64. Y. Mise, K. Imato, T. Ogi, N. Tsunoji and Y. Ooyama, *New J. Chem.*, 2021, **45**, 4164–4173.
65. S. K. Albert, H. V. P. Thelu, M. Golla, N. Krishnan, S. Chaudhary and R. Varghese, *Angew.Chem.*, 2014, **126**, 8492–8497.
66. F. de Lera-Garrido, R. Sánchez-Ruiz, J. Rodríguez-López, J. Tolosa and J. C. García-Martínez, *Dyes Pigm*., 2020, **179**, 108410.
67. S. Mi, J. Wu, J. Liu, Z. Xu, X. Wu, G. Luo, J. Zheng and C. Xu, *ACS Appl. Mater. Interfaces*, 2015, **7**, 2751127517.
68. Y. Zhang, J. Huang, L. Kong, Y. Tian and J. Yang, *CrystEngComm*, 2018, **20**, 12371244.
69. X. Y. Shen, Y. J. Wang, E. Zhao, W. Z. Yuan, Y. Liu, P. Lu, A. Qin, Y. Ma, J. Z. Sun and B. Z. Tang, *J. Phys. Chem. C*, 2013, **117**, 7334–7347.
70. H. - Q. Peng, X. Zheng, T. Han, R. T. K. Kwok, J. W. Y. Lam, X. Huang and B. Z. Tang, *J. Am. Chem. Soc.*, 2017, **139**, 10150–10156.
71. J. Huang, X. Yang, J. Wang, C. Zhong., L. Wang, J. Qin and Z. Li, *J. Mater. Chem.*, 2012, **22**, 2478–2484.
72. Y. Li, Y. Dong, L. Cheng, C. Qin, H. Nian, H. Zhang, Y. Yu and L. Cao, *J. Am. Chem. Soc.*, 2019, **141**, 8412–8415.
73. M. Shyamal, P. Mazumdar, S. Maity, G. P. Sahoo, G. S. - Morán and A. Misra, *J. Phys. Chem. A*, 2016, **120**, 210–220.
74. R. Deans, J. Kim, M. R. Machacek and T. M. Swager, *J. Am. Chem. Soc.*, 2000, **122**, 8565 – 856.
75. D. G. Whitten, *Acc. Chem. Res.*, 1993, **26**, 502509.
76. J. Saltiel, A. Waller, Y. P. Sun and D. F. S. Jr., *J. Am. Chem. Soc.*, 1990, **112**, 4580–4581.

77. J. Zhang, J. K. Whitesell and M. A. Fox*, Chem. Mater.*, 2001,13, 2323-2331.
78. L. Zhu and Y. Zhao*, J. Mater. Chem. C*, 2013, **1**, 10591065.
79. P. Jana, M. Paramasivam, S. Khandelwal, A. Dutta and S. Kanvah, *New J. Chem.*, 2020, **44**, 218–230.
80. J. Seo, J. W. Chung, J. E. Kwon and S. Y. Park, *Chem. Sci.*, 2014, **5**, 4845–4850.
81. V. Palakollu, A. K. Vasu, V. Thiruvenkatam and S. Kanvah, *New J. Chem.*, 2016, **40**, 4588–4594.
82. S. Guo, J. Pan, J. Huang, L. Kong and J. Yang, *RSC Adv.*, 2019, **9**, 26043–26050.
83. B. – K. An, J. Gierschner and S. Y. Park, *Acc. Chem. Res.*, 2012, **45**, 544–554.
84. B. - K. An, D. - S. Lee, J. - S. Lee, Y. - S. Park, H. - S. Song and S. Y. Park, *J. Am. Chem. Soc*., 2004, **126**, 10232–10233.
85. A. K. Vasu, M. Radhakrishna and S. Kanvah, *J. Phys. Chem. C*, 2017, 121, **40**, 22478–2248.
86. Y. Zhang, C. Liang, H. Shang, Y. Maa and S. Jiang, *J. Mater. Chem. C*, 2013,**1**, 4472-4480
87. V. Palakollu and S. Kanvah, *New J. Chem.*, 2014, **38**, 5736–5746.
88. (a) H. - J. Kim, J. Gierschner and S. Y. Park, 2020, *J. Mat. Chem. C*, **8**, 7417–7421; (b) S. - J. Yoon, J. W. Chung, J. Gierschner, K. S. Kim, M. - G. Choi, D. Kim and S. Y. Park, *J. Am.Chem.Soc.*, 2010*,* **132***,* 13675–13683.
89. J. Zhao, W. Chen, J. Liu, H. Guo, F. Lu and L. Chen, *ChemNanoMat.*, 2018, **4**, 785789.
90. (a) B. - K. An, J. Gierschner and S. Y. Park, *Acc. Chem. Res.*, 2012, **45**, 544–554; (b) N. Yamamoto, *J. Phys. Chem. C*, 2018, **122**, 12434–12440.

91. N. L. C. Leung, N. Xie, W. Yuan, Y. Liu, Q. Wu, Q. Peng, Q. Miao, J. W. Y. Lam and B. Z. Tang, *Chem. Eur. J.*, 2014, **20**, 1534915353.
92. (a). B. L. Feringa, *Acc. Chem. Res.*, 2001, **34**, 504–513; (b) S. Lin, K. G. Cuevas, X. Zhang, J. Guo and Q. Li, *Adv. Funct. Mater*., 2021, **31**, 2007957; (c) J. Li, H. K. Bisoyi, J. J. Tian, J. B. Guo and Q. Li, *Adv. Mater.*, 2019, **31**, 1807751; (d) J. Li, H. K. Bisoyi, S. Lin, J. Guo and Q. Li, *Angew. Chem., Int. Ed*., 2019, **58**, 1605216056.
93. (a) M. Mathews and N. Tamaoki, *J. Am. Chem. Soc.*, 2008, **130**, 11409–11416; (b) D. Gust, T. A. Moore and A. L. Moore, *Chem. Commun*., 2006, 1169–1178; (c) B. L. Feringa, R. A. vanDelden, N. Koumura and E. M. Geertsema, *Chem. Rev.*, 2000**, 100**, 1789–1816; (d) X. Zhang, B. Koz, H. K. Bisoyi, H. Wang, K. G. Gutierrez-Cuevas, M. E. McConney, T. J. Bunning and Q. Li, *ACS Appl. Mater. Interfaces*, 2020, **12**, 55215–55222.
94. R. Kumar, A. Sharma, H. Singh, P. Suating, H. S. Kim, K. Sunwoo, I. Shim, B. C. Gibb and J. S. Kim, *Chem. Rev*., 2019, **119**, 9657–9721.
95. C. Zhang, Y. Wang, S. Cheng, X. Zhang, B. Fu and W. Hu, *Adv. Electron. Mater.*, 2017, **3**, 1700209.
96. L. Fabbrizzi and A. Poggi, *Chem. Soc. Rev.*, 1995, **24**, 197–202.
97. A. Bajpai, S. K. Shukla, S. Bhanu and S. Kankane, *Prog. Polym. Sci.*, 2008, **33**, 1088–1118.
98. Z. Shen, F. Chen, X. Zhu, K. T. Yong and G. Gu *J. Mater. Chem. B*, 2020, **8**, 89728991.
99. I. Nunez, E. Merino, M. Lecea, S. Pieraccini, G. P Spada, C. Rosini, G. Mazzeo, M. Ribagorda and M. C. Carreño, *Chem. Eur. J*, 2013, **19**, 3397-3406.
100. M. Shellaiah, T. Simon, V. Srinivasadesikan, C. - M. Lin, K. W. Sun, F. - H. Ko, M. - C. Lin and H. - C. Lin, *J. Mater. Chem. C*, 2016, **4**, 2056–2071.

101. X. Wan, Z. Ding, Y. Ma, Y. Zhang, H. Shanga and S. Jiang, *Soft Matter*, 2019, **15**, 16581665.

102. Z. Wang, L. Gao, Y. Zheng, Y. Zhu, Y. Zhang, X. Zheng, C. Wang, Y. Li, Y. Zhao and C. Yang, *Angew. Chem. Int. Ed.*, 2022, **61**, e202203254.

103. J. Li, Y. Zhang, J. Mei, J. W. Y. Lam, J. Hao and B. Z. Tang, *Chem. Eur. J.*, 2015, **21**, 907–914.

104. H. Goyal, P. Kumar and R. Gupta, *Chem. Asian J.*, 2023, **18**, e202300355.

105. K. Wang, H. Zhang, S. Chen, G. Yang, J. Zhang, W. Tian, Z. Su and Y. Wang, *Adv. Mater.*, 2014, **26**, 61686173.

106. C. Wang and Z. Li, *Mater. Chem. Front.*, 2017, **1**, 21742194.

107. Y. Liu, A. Li, S. Xu, W. Xu, Y. Liu, W. Tian and B. Xu, *Angew. Chem. Int. Ed.*, 2020, **59**, 1509815103.

108. G. Huang, Y. Jiang, S. Yang, B. S. Li and B. Z. Tang, *Adv. Funct. Mater.*, 2019, **29**, 1900516.

109. X. Wu, J. Guo, Y. Cao, J. Zhao, W. Jia, Y. Chen and D. Jia, *Chem. Sci.*, 2018, **9**, 52705277.

110. Y. Ren and T. Baumgartner, *Inorg. Chem.*, 2012, **51**, 26692678.

111. T. Butler, F. Wang, M. Sabat, C. L. Fraser, *Mater. Chem. Front.*, 2017, **1**, 18041817.

112. Y. Sagara and T. Kato, *Nat. Chem.*, 2009, **1**, 605610.

113. (a) G. X. Huang, Y. Q. Jiang, S. F. Yang, B. S. Li and B. Z. Tang, *Adv. Funct. Mater.*, 2019, **29**, 190051; (b) X. Luo, W. Zhao, J. Shi, C. Li, Z. Liu, Z. Bo, Y. Q. Dong and B.Z. Tang, *J. Phys. Chem. C*, 2012, **116**, 41, 21967–21972.

114. J. Wang, J. Mei, R. Hu, J. Zhi Sun, A. Qin and B. Z.Tang, *J. Am. Chem. Soc.*, 2012, **134**, 9956–9966.

115. J. Xiong, K. Wang, Z. Yao, B. Zou, J. Xu and X.H. Bu, *ACS Appl. Mater. Interfaces*, 2018, **10**, 5819–5827.

116. A . Z. Wang, H. Nie, Z. Yu, A. Qin, Z. Zhao and B. Z. Tang , *J. Mater. Chem. C*, 2015, **3**, 91039111.

117. N. Zhao, M. Li, Y. Yan, J. W. Y. Lam, Y. L. Zhang, Y. S. Zhao, K. S. Wong and B. Z. Tang, *J. Mater. Chem. C*, 2013, **1**, 46404646.

118. Y. Qi, W. Liu, Y. Wang, L. Ma, Y. Yu, Y. Zhanga and L. Ren, *New J. Chem.*, 2018, **42**, 1137311380.

119. A. T. Miteva, L. Palmer, L. Kloppenburg, D. Neher and U.H. F. Bunz, *Macromolecules*, 2000, **33**, 652–654.

120. R. Gupta, R. Thomas and G. U. Kulkarni, *J. Mater. Chem.*, 2012, **22**, 1913919145.

121. S. Roy, D. Samanta, P. Kumar and T. K. Maji, *Chem. Commun.*, 2022, **58**, 41494167.

122. Y. Sagara, C. Weder and N. Tamaoki, *RSC Adv.*, 2016, **6**, 8040880414.

123. G. Fan and D. Yan, 2014, *Sci. Rep.*, **4**, 4933.

124. Z. Wang, H. Nie, Z. Yu, A. Qin, Z. Zhao and B. Z. Tang, *J. Mater. Chem. C*, 2015, **3**, 91039111.

125. Z. Zhang, X. Liu, Y. Feng, Z. - Q. Yu, L. Wang, X. - K. Ren and Y. Liu, *J. Mater. Chem. C*, 2021**, 9**, 975981.

126. R. Kaneko, Y. Sagara, S. Katao, N. Tamaoki, C. Weder, H. Nakano, *Chem. Eur. J.*, 2019, **25**, 61626169.

127. Y. Zhang, C. Liang, H. Shang, Y. Maa and S. Jiang, *J. Mater. Chem. C*, 2013, **1**, 44724480.

128. B. – K. An, S. - K. Kwon, S. - D. Jung and S. Y. Park, *J. Am. Chem. Soc*., 2002, **124**,14410–14415.

129. X. Zhang, Z. Chi, X. Zhou, S. Liu, Y. Zhang and J. Xu, *J. Phys. Chem. C*, 2012, **116**, 23629–23638.

130. L. Wen, J. Sun, C. Li, C. Zhu, X. Zhang, Z. Wang, Q. Song, C. Lv and Y. Zhang, *New J. Chem*., 2021**, 45,** 1153011535.

131. (a) T. Ikeyama, C. Kabuto and M. Sato*, J. Phys. Chem.*, 1996, **100**, 19289–19291; (b) H. Goerner*, J. Phys. Chem.*, 1989, **93**, 1826–1832; (c) T. Ikeyama and T. Azumi, *J. Phys. Chem.*, 1985, **89**, 5332–5333.

Chapter 2

Materials and methods

2.1 Synthesis and Characterization

All the starting materials and solvents were procured from commercial sources and used without purification. The procedures for the synthesis of all the compounds were discussed under the experimental sections of respective chapters.

2.1.1 Crystallization Techniques

The quality of the single crystal is a necessary criterion for single-crystal X-ray diffraction studies. Although various methods have been adopted for the preparation of good quality single crystals, the slow evaporation of the dilute solution has been adopted as the widely used method for preparing the single crystals of organic compounds. The uniform dimensions of the crystals are also quite important to obtain good quality single-crystal X-ray diffraction data. Here in this work, the technique used for crystallization is the slow evaporation method. The single crystals of some of the compounds were grown by slow solvent evaporation at room temperature while the single crystals of some compounds were grown at low temperatures (4 ℃). Single solvent and solvent mixtures were also used for the crystal growth process. Crystals mentioned in Chapter 3 were mainly grown from pure dioxane by dissolving the samples in minimum quantity of pure dioxane followed by slow evaporation at room temperature. Dichloromethane is also used as a solvent for the crystallization of one of the isomers mentioned in this chapter. The crystals analysed in Chapter 4 were grown from various pure solvents and solvent mixtures. Dichloromethane, toluene, ethyl acetate and ethyl acetate/ hexane mixture etc. were used to grow crystals analysed in Chapter 4. The single crystals of the cholesterol-based system explored in Chapter 5 was grown from toluene.

2.1.2 X-ray diffraction analysis

The X-ray diffraction is based on Bragg's diffraction law, which helps to understand the relationship between diffraction and the position of objects in matter. In this method, the conditions are such that the X-rays incident on planes of crystals with an incident angle θ diffracted constructively. Hence according to Bragg's law, the angle θ and the interplanar distance d of crystal planes are related by the expression $n\lambda = 2d \sin \theta$. The diffraction pattern obtained for each sample under study is characteristic of the structure of the sample under investigation.

2.1.2.1 Powder X-ray diffraction analysis

The powder X-ray diffraction technique is a non-destructive method for the structural characterization of matter. The peaks in the PXRD pattern help to determine the crystallinity and phase of the sample under observation. In the PXRD technique the material under investigation was subjected to X-rays of wavelength, λ and electrons were scattered from the sample with certain velocities and the incident X-rays diffracted repeatedly according to Braggs law of diffraction, $n\lambda = 2d \sin\theta$, and diffraction patterns were obtained which is characteristics of the sample under investigation. In the thesis, the major focus is on the stimuli-responsive nature of the compounds. The stimuli-responsive emission in a particular aggregate is due to the crystal-to-crystal transition or crystal-to-amorphous transition or vice versa. The phase changes in the solid forms of the compounds on applying various stimuli can be characterized by comparing the powder X-ray diffraction patterns, and structural variations can be explored by indexing diffraction patterns. The PANalytical X'Pert3 (Cu Kα radiation (λ = 1.5406 Å) radiation source operating at 45 kV and 40 mA) and PANanlytical Aeris (using Cu Kα

radiation (λ = 1.5406 Å) radiation source operating at 40 kV and 15 mA). powder X-ray diffractometers were used to obtain the diffraction patterns discussed in various Chapters of the thesis. The diffraction patterns were recorded over a 2θ scan ranging from 5° - 60° at a step size of 0.01° and 0.05 respectively for PANalytical X'Pert3 and PANanlytical Aeris diffractometers. The temperature-dependent X-ray diffractograms were recorded on a Bruker D8 Discover diffractometer with 2θ scans ranging from 5° - 60°. The sample was placed on a copper sample holder fitted with a heating element and the diffraction experiments were conducted after stabilizing the required temperature over 5 minutes. The Cu Kα radiation source operating at 40 kV and 40 mA is used as an X-ray source for recording the diffractograms.

2.1.2.2 Single crystal X-ray diffraction studies

Single crystal X-ray diffraction is a molecular structure determining method which provides detailed structural and bonding information. In addition to the molecular structure, the single-crystal X-ray diffraction provides intermolecular interactions and molecular packing in the crystals.

2.1.2.2.1 Data collection for structural analysis

An Olympus SZ-61stereozoom microscope attached with a polarizing filter is used for selecting good quality single crystals of various compounds discussed in this thesis. The crystals with dimensions in the range of approximately 0.1 to 0.4 mm were chosen for single-crystal X-ray data collection. The crystal was mounted on a glass fibre placed on a copper pip and placed on goniometer head. The goniometer head is placed on the diffractometer and the crystal is adjusted to the X-ray beam using an optical microscope with crosshairs and an attached monitor.

The X-ray diffraction intensity data for various crystals were collected on Bruker D8 Quest Eco diffractometer operating at 50 kV and 30 mA attached with Photon -III detector or Bruker D8 Venture diffractometer operating at 50 kV and 40 mA attached with Photon-II detector with CMOS sensor. The data of compounds except compound **CSO** presented in Chapter 3 were collected at room temperature (298 K), whereas the data of **CSO** was collected at 130 K under a stream of liquid nitrogen. All the data collection was carried out using Mo Kα radiation (0.71073 Å) while the crystal structure of compound **CS-1** presented in Chapter 5 was collected using CuKα radiation (1.5406 Å). The crystal-to-detector distance was set to 4.5 cm for the intensity data collection. The data preparation of data collection strategy and monitoring of the data collection was carried out using APEX-III program suit.[1] Data integration, Lorentz and polarization corrections and merging of data were carried out using SAINT.[1] The program SADABS was used to perform the absorption correction on the merged data and the data was averaged using SORTAV software of the WINGX program suit.[2] The structure was solved by direct methods using SHELXS-2014[3] and refined by SHELXL-2014[4] programs incorporated to WINGX program.[5] The hydrogen atoms on all the carbon atoms, except those with disorder were located from the difference Fourier map and were refined isotropically. The ORTEP plots of all the compounds at a 50 % probability level are drawn using ORTEP3 software. The molecular and packing diagrams were generated using the software Mercury version 4.2.0.[6] Intermolecular interactions were computed using the program PLATON.[7]

2.1.4 Photoluminescence spectroscopy

Photoluminescence spectroscopy (P L) is a method used to determine the electronic structure of matter. It is a contactless non-destructive method. The

intensity of the emitted photons and the spectral positions gives various information about the electronic structure of the materials under investigation. Fluorescence spectra discussed in Chapter 3 were obtained using Horiba-Jobin-Yvon Fluorolog-3-11 spectrofluorimeter. Both the solution and solid state quantum yields were measured on an EDINBURGH FLS 1000 spectrometer attached with an integrating sphere. The time-resolved fluorescence lifetime experiments were performed on a time correlated single photon counting system (TCSPC) Fluorocube (Horiba-Jobin-Yvon). Photoluminescence spectra and lifetime experiments mentioned in chapter 4 were performed using a Horiba Fluorolog-3 spectrofluorometer with TCSPC set up (model FL 3C-221). Phosphorescence spectra of compounds were recorded using a pulsed UV xenon lamp with each pulse having a full-width at half-maximum (FWHM) of 3 μs. Samples were excited with pulsed light and the emitted phosphorescence was measured with a variable delay between 50 μs and 10 s and an open window between pulse and detection. The Photoluminescence spectral analysis and lifetime experiments of Chapter 5 were performed using Fluorolog-3 spectrofluorimeter attached with TCSPC (model FL 3C-221). The quantum yields of each sample were measured on the EDINBURGH FLS 1000 instrument attached with an integrating sphere.

2.2. References

1. Bruker, APEX2, SAINT and SADABS, 2006
2. R. H. Blessing, Outlier Treatment in Data Merging, *J. Appl. Crystallogr.*, 1997, **30**, 421–426.
3. G. M. Sheldrick, A short history of SHELX, *Acta Crystallogr. Sect. A Crystallogr.*, 2008, **64**, 112–122.
4. G. M. Sheldrick, Crystal structure refinement with SHELXL, Acta *Crystallogr. Sect. C Struct. Chem.*, 2015, **71**, 3–8.
5. L. J. Farrugia, *J. Appl. Crystallogr.*, 2012, **45**, 849–854.
6. C. F. Macrae, P. R. Edgington, P. McCabe, E. Pidcock, G. P. Shields, R. Taylor, M. Towler and J. Van De Streek, *J. Appl. Crystallogr.*, 2006, **39**, 453–457.
7. A. L. Spek, *J. Appl. Crystallogr*., 2003, **36**, 713.

Chapter 4

Aggregation Induced Photophysical Behaviour of *o*-Alkyloxy Substituted Dicyanodistyrylbenzene Derivatives

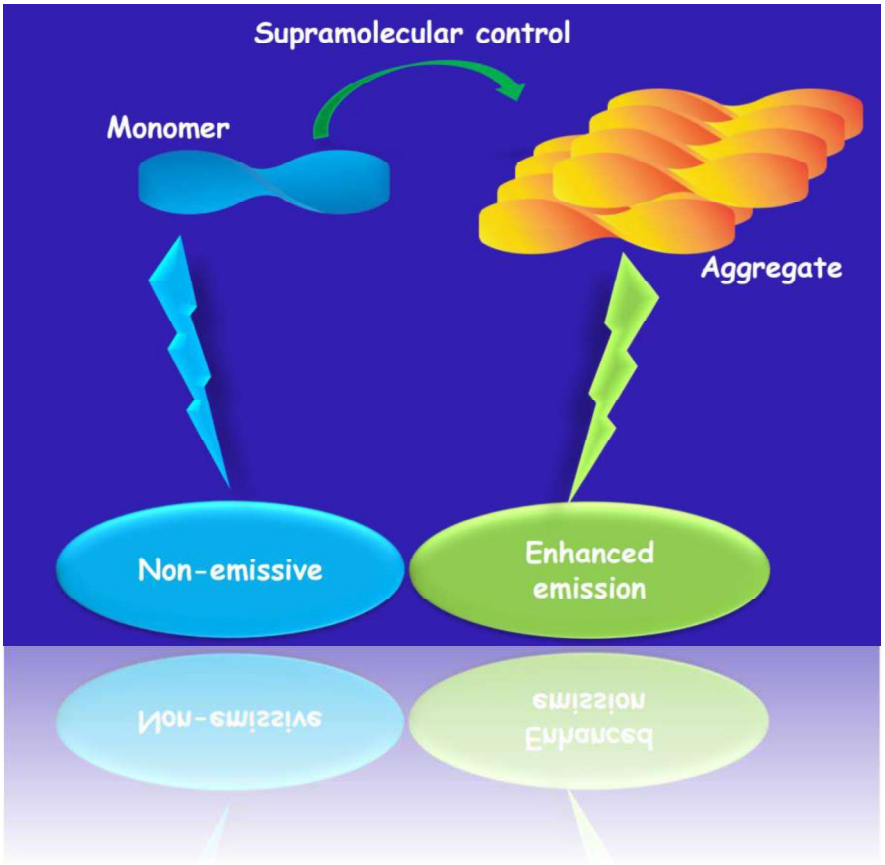

4.1 Abstract

This chapter discusses the role of various structural factors influencing the luminescence efficiency of a series of ortho-alkyloxy substituted dicyanodistyrylbenzene derivatives. This work also explores the importance of restricted intramolecular rotations in achieving stable triplet states in dicyanodistyrylbenzene derivatives in solution at 77 K. All the ortho-alkyloxy derivatives of dicyanodistyrylbenzenes reported in this work demonstrated aggregation induced emission behaviour in solid state in comparison to the respective dilute solutions of the compounds in THF. This study investigates the importance of structural and packing parameters in the solid state such as twist in π-backbone, overlap and interplanar distance of the π-system in determining the fluorescence efficiency of the compounds in the solid state. All the isomers showed comparable luminescence spectra at room temperature in dilute 2-MeTHF solutions with a lifetime in the regime of nanoseconds, while the spectra at 77 K showed different spectral nature with redshifted maxima. The emission of the compounds recorded at room temperature with a delay of 0.5 ms showed highly redshifted emission with a lifetime in the order of milliseconds. The red shifted emission spectra with a lifetime in milliseconds confirm phosphorescence in the ortho alkyloxy dicyanodistyrylbenzene derivatives at 77 K. The crystalline samples of all the molecules showed different spectra from that of respective solutions in THF along with enhanced, but varying, quantum yield in the solid state. The structural factors behind the incomparable spectral

features and enhanced quantum efficiency of all the compounds were explored using single-crystal X-ray diffraction studies. By correlating the photophysical properties with the structural parameters in the solid state confirmed that the interplay between the twist in the molecular structure along with the π-π overlap and the interplanar distance plays a crucial role in determining the enhanced emission in the solid state.

4.2. Introduction

Aggregation induced emission (**AIE**) is suggested as one of the major contributing factors of the unquenched solid state luminescence in organic π-systems.[1-9] The photoluminescence of organic conjugated molecules mainly depends on the nature of the aggregate formed in the solid state. Previous reports on π-conjugated molecules indicated that the formation of J-aggregate or X-aggregate can result in increased luminescence efficiency.[10-14] Various optoelectronic applications of organic materials call for improved quantum efficiency, where a suitable tuning of the aggregate structure largely contributes to enhanced quantum efficiency.[15]

4.3 Scope of Present Investigation

The molecular structure and the packing mode in the aggregate structure are quite important in the making of AIE materials. One can regulate the aggregate packing by suitable molecular design. Here the aim behind the present exploration is to rationalize the design strategies in a simple molecular system namely, α-cyanostilbene, to obtain enhanced quantum yield in the solid state. Owing to the cyano group in the α-position, several α-cyanostilbene derivatives have shown a twisted geometry in the solid state.[16] Expecting that the substitution in the *ortho* position of dicyanodistyrylbenzene system would give rise to more twisted molecular geometry in the solid state, *ortho* alkyloxy variants of

dicyanodistyrylbenzene **OCS-1** to **OCS-6** were designed and synthesized (Scheme 4.1, The molecule **CSO** previously discussed in chapter 3 also incorporated in this study for comparison of emission behaviour and renamed as **OCS-5** for convenience.). In addition to the enhanced fluorescence in the solid state it is expected that the inherently twisted α- cyanostyryl systems with *ortho* alkyloxy substitution may give rise to a molecular geometry with higher twist in π-backbone leading to stable triplet states and thereby phosphorescence at 77 K. A similar observation of phosphorescence was made previously in stilbene systems at 77 K owing to the restriction of the intramolecular rotation.[17] To explore the possibility of a stable triplet state by restricting the molecular motions the luminescence spectra and lifetime were conducted at 77 K applying various time delay. To understand the underlying structural factors of the origin of enhanced photophysical properties a detailed analysis of photophysical properties in conjunction with the structural details obtained from single crystal X-ray diffraction, was conducted. The present investigation aims to demonstrate the supramolecular control on increased fluorescence quantum yields in the solid state. This investigation also aims to understand the interplay between the structural parameters such as molecular twist, π-overlap, and interplanar distance on varied solid state fluorescence quantum yield of *ortho*-alkyloxy dicyanodistyrylbenzene derivatives.

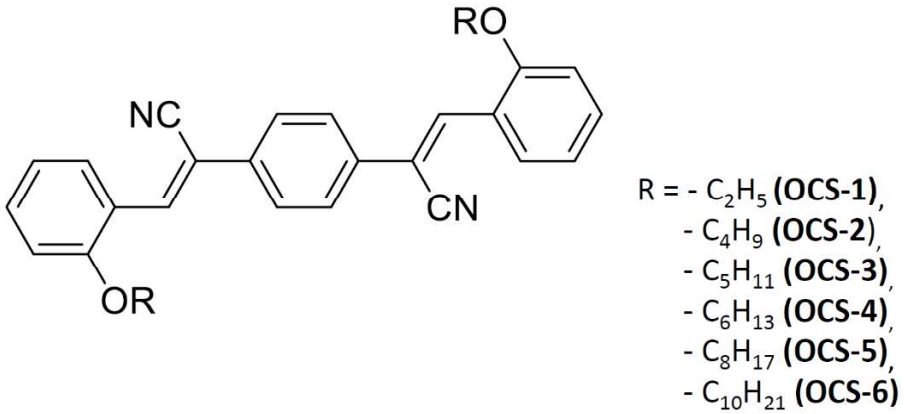

Scheme 4.1: Molecular structure of *ortho* alkyloxydicyanodistyrylbenzenes.

4.4 Experimental Section

Solvents and chemicals for the synthesis and photophysical studies were purchased from Sigma Aldrich, Alfa Aeser, and TCI and used without further purification. The ^{1}H NMR and ^{13}C NMR spectra were recorded on a Bruker Avance 400 MHz spectrometer operating at room temperature. The mass spectra of the compounds were recorded on a Waters Xevo G2 XS QToF mass spectrometer. Photoluminescence spectra and lifetime experiments were performed using a Horiba Fluorolog-3 spectrofluorometer with TCSPC set up (model FL 3C-221). Phosphorescence spectra of compounds OCS-1 to OCS-6 were recorded using a pulsed UV xenon lamp with each pulse having a full-width at half-maximum (FWHM) of 3 μs. Samples were excited with pulsed light and the emitted phosphorescence was measured with a variable delay

between 50 μs and 10 s and an open window between pulse and detector. The single crystal X-ray diffraction data of**OCS-3**, **OCS-4** and **OCS-6** were collected on Bruker D8 Venture diffractometer attached with PHOTON II detector with CMOS-sensor while that for the **OCS-1** and **OCS-2** were collected on a Bruker D8 Quest Eco diffractometer with PHOTON III detector. All the data collections were conducted at room temperature using Mo Kα radiation operated at 50 kV and 40 mA.

4.4.1 Synthesis and Characterization

4.4.1.1 General method for the synthesis

4.4.1.1.1 *Synthesis of ortho-alkyloxy substituted hydroxy benzaldehyde*

Ortho-alkoxy substituted benzaldehyde derivatives were prepared by adopting the previously reported procedure (Scheme 4.2).[18,19] A mixture of 2-hydroxybenzaldehyde (20 mmol), K_2CO_3 (30 mmol), and corresponding 1-bromo alkane (20 mmol) was stirred at 80 ℃ in DMF under an inert atmosphere for 12 hours. The reaction mixtures were evaporated and the organic phase was extracted with DCM and washed with water (2 x 50 ml). The organic phase in all the cases were column

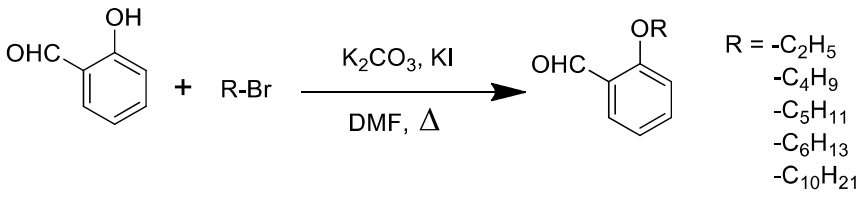

Scheme 4.2: Route to the synthesis of *ortho*-alkyloxy benzaldehydes.

chromatographed over silica gel using ethyl acetate/hexane (1:9) to obtain the target compounds as oily liquids. The products were characterized using ^{1}H NMR and ^{13}C NMR spectroscopy.

2-ethoxybenzaldehyde: Yield: 80.0 %, **^{1}H NMR** (400 MHz, $CDCl_3$) δ (ppm) 10.47 (s, 1H), 7.78 (d, *J* = 7.7 Hz, 1H), 7.62 – 7.34 (m, 1H), 7.05 – 6.84 (m, 2H), 4.10 (q, *J* = 7.0 Hz, 2H), 1.43 (t, *J* = 7.0 Hz, 3H). **^{13}C NMR** (400 MHz, $CDCl_3$) δ (ppm) 189.97, 161.22, 136.24, 128.25, 125.38, 120.54, 112.39, 64.19, 14.89.

2-butoxybenzaldehyde: Yield: 79.7 %, **^{1}H NMR** (400 MHz, $CDCl_3$) δ (ppm) 10.49 (s, 1H), 7.79 (dd, *J* = 7.7, 1.84 Hz, 1H), 7.48 (m, 1H), 6.97 - 6.92 (m, 2H), 4.03 (t, *J* = 6.4 Hz, 2H), 1.79 (m, 2H), 1.54 - 1.44 (m, 2H) 0.96 (t, *J* = 7.36 Hz, 3H). **^{13}C NMR** (400 MHz, $CDCl_3$) δ (ppm) 189.93, 161.65, 136.01, 128.19, 124.93, 120.49, 112.57, 68.26, 31.18, 19.34, 13.88.

2-pentyloxy benzaldehyde: Yield: 78.9 %, **^{1}H NMR** (400 MHz, $CDCl_3$) δ(ppm) 10.52 (s, 1H), 7.82 (dd, *J* = 7.7, 1.8 Hz, 1H), 7.52 (m, 1H), 7.06 6.93 (m, 2H), 4.07 (t, *J* = 6.4 Hz, 2H), 1.84 (m, 2H), 1.52 – 1.35 (m, 4H), 0.94 (t, *J* = 7.1 Hz, 3H). **^{13}C NMR** (400 MHz, $CDCl_3$) δ (ppm) 190.02, 161.66, 136.01, 128.23, 124.94, 120.74, 112.56, 68.56, 28.36, 31.18, 22.49, 14.10.

2-hexyloxy benzaldehyde: Yield: 76.8 %, **^{1}H NMR** (400 MHz, $CDCl_3$) δ (ppm) 10.50 (s, 1H), 7.81 (m, 1H) 7.51 (m, 1H), 6.97 (m, 1H), 6.90 (m, 1H) 4.05 (t, 2H, *J* = 6.4 Hz), 1.851.78 (m, 2H), 1.501.40 (t, 2H, *J* = 8 Hz) 1.36-1.26 (m, 4H), 0.89 (t, 3H, *J* = 7.2 Hz) **^{13}C NMR** (400MHz, $CDCl_3$)

δ (ppm) 189.99, 161.67, 136.0, 128.23, 124.95, 120.51, 112.57, 68.60, 31.58, 29.12, 25.81, 22.65, 14.09.

2-decyloxy benzaldehyde: Yield: 79.7 %, **^{1}H NMR** (400 MHz, $CDCl_3$) δ(ppm) 10.52 (s, 1H), 7.83 (dd, *J* = 7.7, 1.8 Hz, 1H), 7.52 (m, 1H), 7.03 – 6.94 (m, 2H), 4.07 (t, *J* = 6.4 Hz, 2H), 1.89 – 1.79 (m, 2H), 1.54 – 1.43 (m, 2H), 1.35 – 1.24 (m, 12H), 1.05 – 0.68 (m, 3H). **^{13}C NMR** (400 MHz, $CDCl_3$) δ (ppm) 190.30, 161.56, 135.56, 128.47, 125.06, 120.72, 112.71, 68.44, 31.67, 29.64, 29.43, 29.40, 28.87, 26.17, 26.14, 22.77, 14.09.

4.4.1.1.2 *Synthesis of the o-alkylated dicyanodistyrylbenzenes*

All the alkoxy derivatives of the dicyanodistyrylbenzenes were synthesized following Knoevenagel condensation with phenylenediacetonitrile and the corresponding alkyloxy benzaldehyde (Scheme 4.3).[18, 19] Alkyloxy benzaldehyde (3.66 mmol) was taken in an oven dried round bottom flask and dissolved in 18 ml ethanol. To this solution 1, 4-phenylene diacetonitrile (2 mmol) and ^{t}BuOK (2.8 mmol) were added. The reaction mixture was stirred for 2 hrs at 80 ℃ under an inert atmosphere. The reaction mixture was filtered and

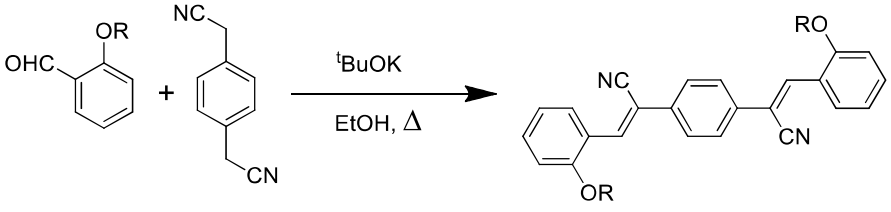

Scheme 4.3: Synthetic route to (2Z,2'Z)-2,2'-(1,4-phenylene)bis(3-(2-alkoxyphenyl)acrylonitrile) derivatives.

washed with excess ethanol and reprecipitated from dichloromethane solution using excess methanol (3 x 20 ml). The compounds were recrystallised from various solvents. The compound **OCS-1** was crystallized from dichloromethane while **OCS-2** and **OCS-4** were crystallized from ethyl acetate/hexane mixture. The **OCS-3** was crystallized from ethyl acetate while **OCS-6** was crystallized from toluene. All of the dicyanodistyrylbenzene derivatives were characterized using ^{1}H NMR (Figure 4.1 - 4.10), ^{13}C NMR, HRMS and single-crystal X-ray diffraction (Table 4.1).

OCS-1: Yield: 80.3 % **^{1}H NMR** (400 MHz, $CDCl_3$) δ (ppm) 8.19 (dd, *J* = 7.8, 1.5 Hz, 2H), 8.06 (s, 2H), 7.77 (s, 4H), 7.41 (m, 2H), 7.07 (t, *J* = 7.6 Hz, 2H), 6.94 (d, *J* = 8.3 Hz, 2H), 4.13 (q, *J* = 6.9 Hz, 4H), 1.48 (t, *J* = 7.0 Hz, 6H). **^{13}C NMR** (400 MHz, $CDCl_3$) δ (ppm) 157.48, 138.05, 135.38, 132.27, 128.57, 126.56, 122.90, 120.72, 118.04, 111.69, 110.39, 64.12, 14.81. **HRMS (ESI)** calculated for $C_{28}H_{24}N_2O_2$: 420.5024, Found: 421.1912 $[M+H]^+$.

OCS-2: Yield: 89 % **^{1}H NMR** (400 MHz, $CDCl_3$) δ (ppm) 8.20 (dd, *J* = 7.8, 1.5 Hz, 2H), 8.07 (s, 2H), 7.76 (s, 4H), 7.41 (m, 2H), 7.06 (t, *J* = 7.9 Hz, 2H), 6.95 (d, *J* = 9.0 Hz, 2H), 4.07 (t, *J* = 6.5 Hz, 4H), 1.84 (m, 4H), 1.55 – 1.47 (m, 4H), 1.01 (t, *J* = 7.4 Hz, 6H). **^{13}C NMR** (400 MHz, $CDCl_3$) δ (ppm) 157.62, 137.90, 135.35, 132.28, 128.48, 126.51, 122.90, 120.69, 118.05, 111.73, 110.24, 68.27, 31.19, 19.36, 13.88. **HRMS (ESI)** calculated for $C_{32}H_{32}N_2O_2$: 476.6087, Found: 477.2533 $[M+H]^+$.

OCS-3: Yield: 80.6 % **^{1}H NMR** (400 MHz, $CDCl_3$) δ(ppm) 8.20 (dd, *J* = 7.7, 1.6 Hz, 2H), 8.08 (s, 2H), 7.76 (s, 4H), 7.41 (m, 2H), 7.06 (t, *J* =

7.4 Hz, 2H), 6.95 (d, *J* = 8.3 Hz, 2H), 4.06 (t, *J* = 6.6 Hz, 4H), 1.85 (m, 4H), 1.52 – 1.37 (m, 8H), 0.95 (t, *J* = 7.1 Hz, 6H). **^{13}C NMR** (400 MHz, $CDCl_3$) δ(ppm) 157.64, 137.92, 135.37, 132.28, 128.48, 126.50, 122.92, 120.71, 118.04, 111.77, 110.23, 68.61, 28.82, 28.32, 22.42, 14.08. **HRMS (ESI)** calculated for $C_{34}H_{36}N_2O_2$: 504.6618, Found: 505.2849 $[M+H]^+$.

OCS-4: Yield: 82 % **^{1}H NMR** (400 MHz,$CDCl_3$) δ(ppm) 8.21 (dd, *J* = 7.9, 1.6 Hz, 2H), 8.07 (s, 2H), 7.76 (s, 4H), 7.41 (m, 2H), 7.07 (t, *J* = 7.5 Hz, 2H), 6.95 (d, *J* = 8.2 Hz, 2H), 4.06 (t, *J* = 6.5 Hz, 4H), 1.91 – 1.78 (m, 4H), 1.49 (q, *J* = 7.0 Hz, 4H), 1.40 – 1.32 (m, 8H), 0.93 – 0.87 (m, 6H). **^{13}C NMR** (400 MHz, $CDCl_3$) δ(ppm) 157.63, 137.91, 135.36, 132.28, 128.47, 126.49, 122.91, 120.70, 118.03, 111.76, 110.24, 68.61, 31.50, 29.09, 25.79, 22.60, 14.00. **HRMS (ESI)** calculated for $C_{36}H_{40}N_2O_2$: 532.7150, Found: 533.3159 $[M+H]^+$

OCS-6: Yield: 84.1 % **^{1}H NMR** (400 MHz, $CDCl_3$) δ (ppm) 8.20 (dd, *J* = 7.8, 1.6 Hz, 2H), 8.07 (s, 2H), 7.76 (s, 4H), 7.41 (m, 2H), 7.06 (t, *J* = 7.5 Hz, 2H), 6.95 (d, *J* = 8.1 Hz, 2H), 4.05 (t, *J* = 6.6 Hz, 4H), 1.91 – 1.78 (m, 4H), 1.52 – 1.44 (m, 4H), 1.40 – 1.21 (m, 24H), 0.91 – 0.81 (m, 6H). **^{13}C NMR** (400 MHz, $CDCl_3$) δ(ppm) 157.62, 137.88, 135.34, 132.26, 128.48, 126.49, 122.21, 120.69, 118.02, 111.76, 110.24, 68.61, 31.91, 29.68, 29.65, 29.61, 29.35, 29.11, 26.12, 22.68, 14.11. **HRMS (ESI)** calculated for $C_{28}H_{24}N_2O_2$: 644.9276, Found: 645.44 [M+H]+

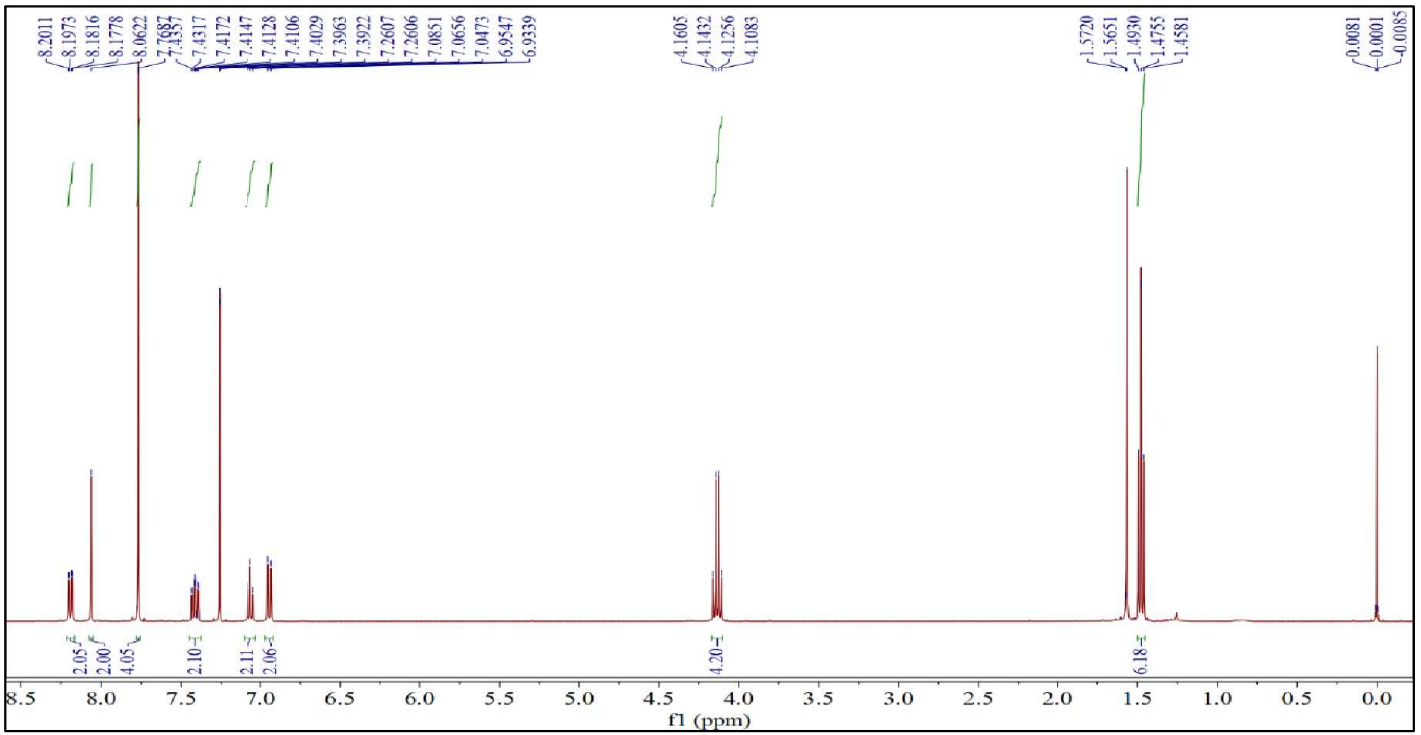

Figure 4.1: ^{1}H NMR spectra of **OCS-1**

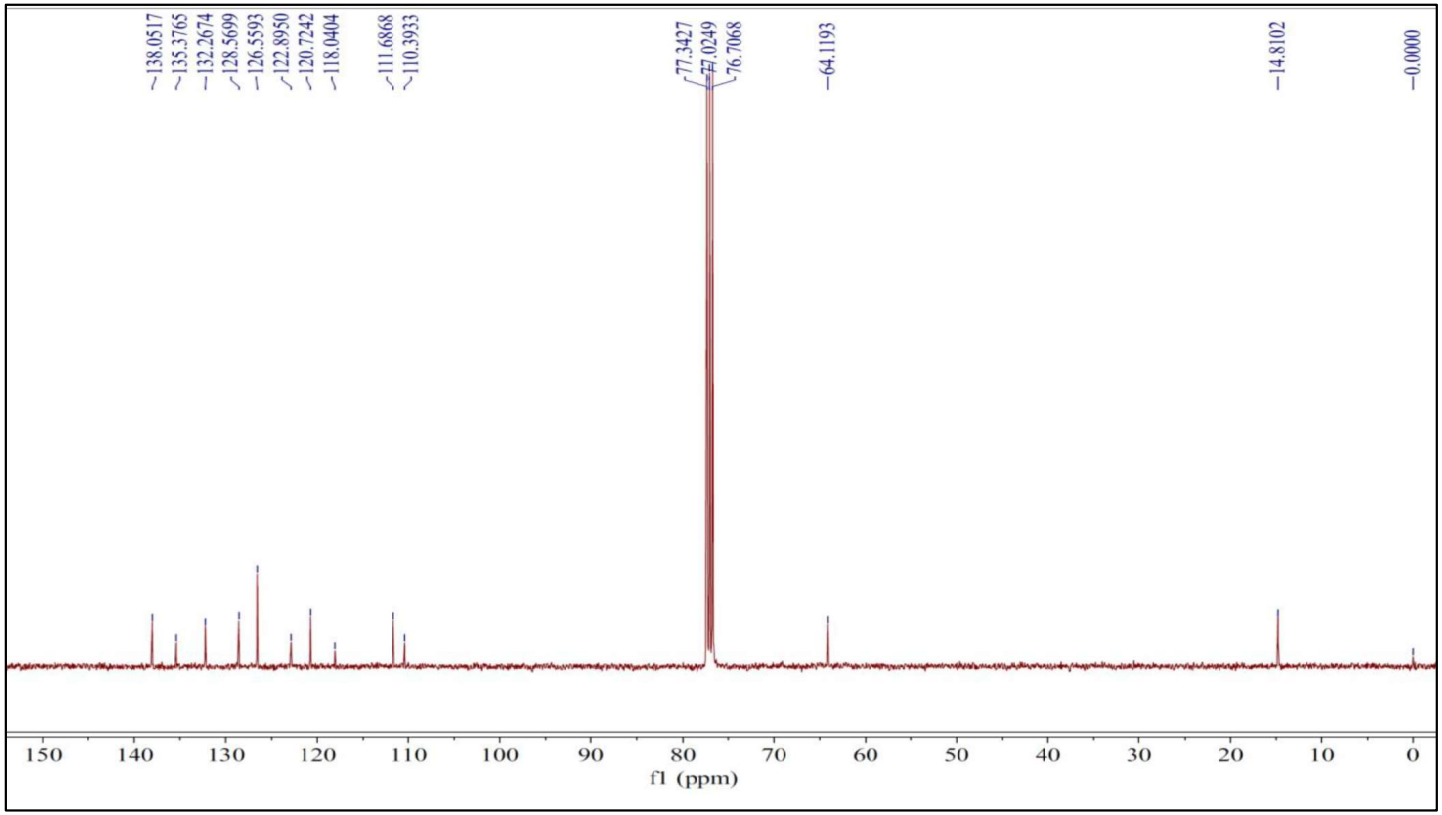

Figure 4.2: ^{13}C NMR spectra of **OCS-1**

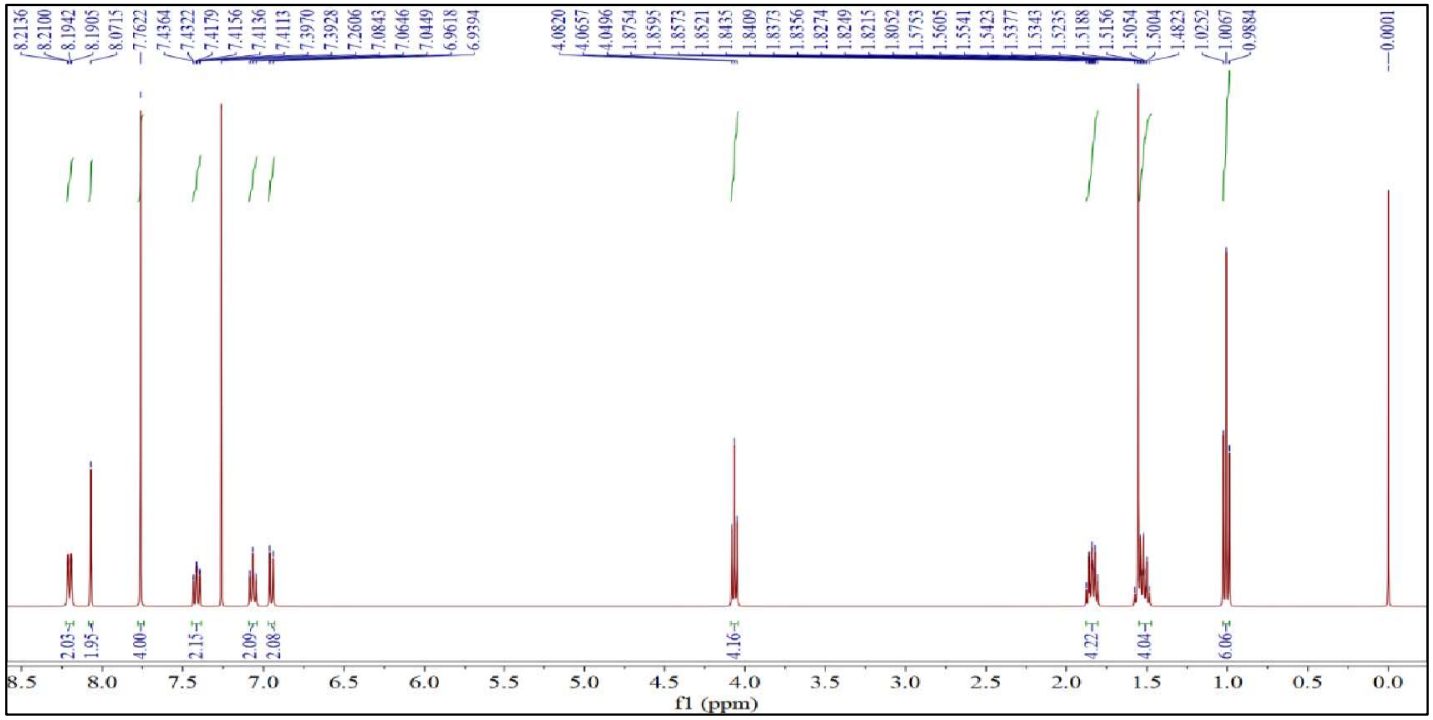

Figure 4.3: ^{1}H NMR spectra of **OCS-2**

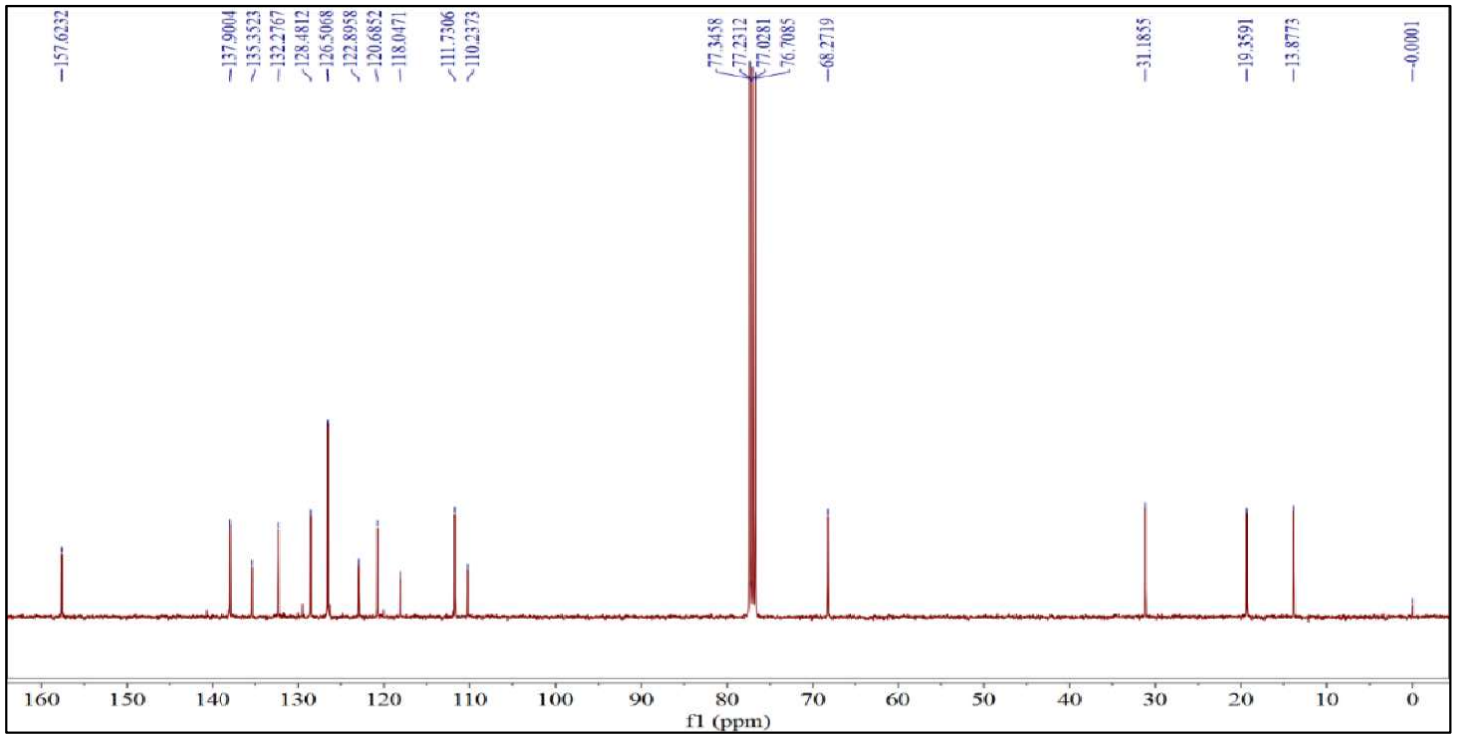

Figure 4.4: The [13] C NMR spectra of compound **OCS-2**

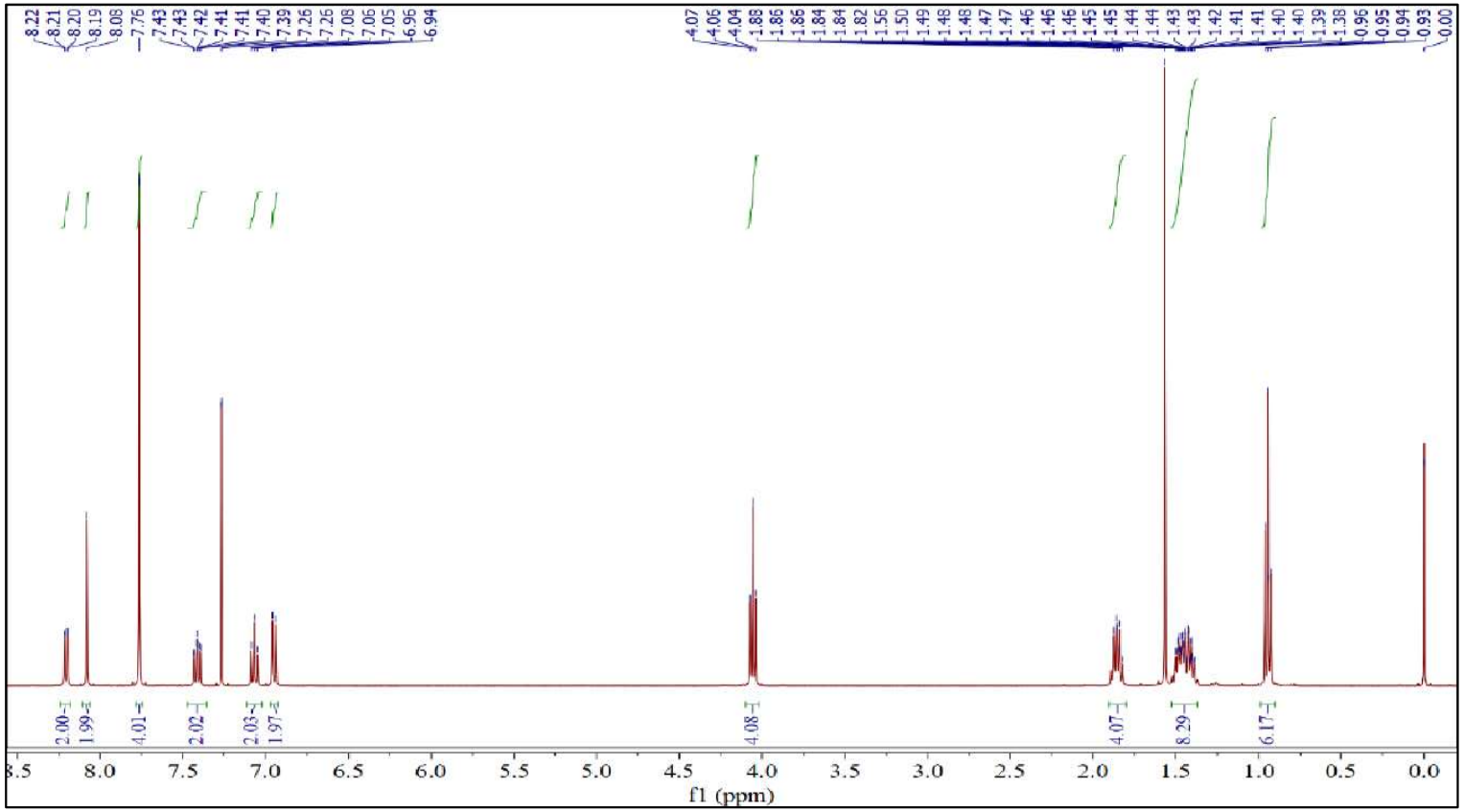

Figure 4.5: ^{1}H NMR spectra of the compound **OCS-3**

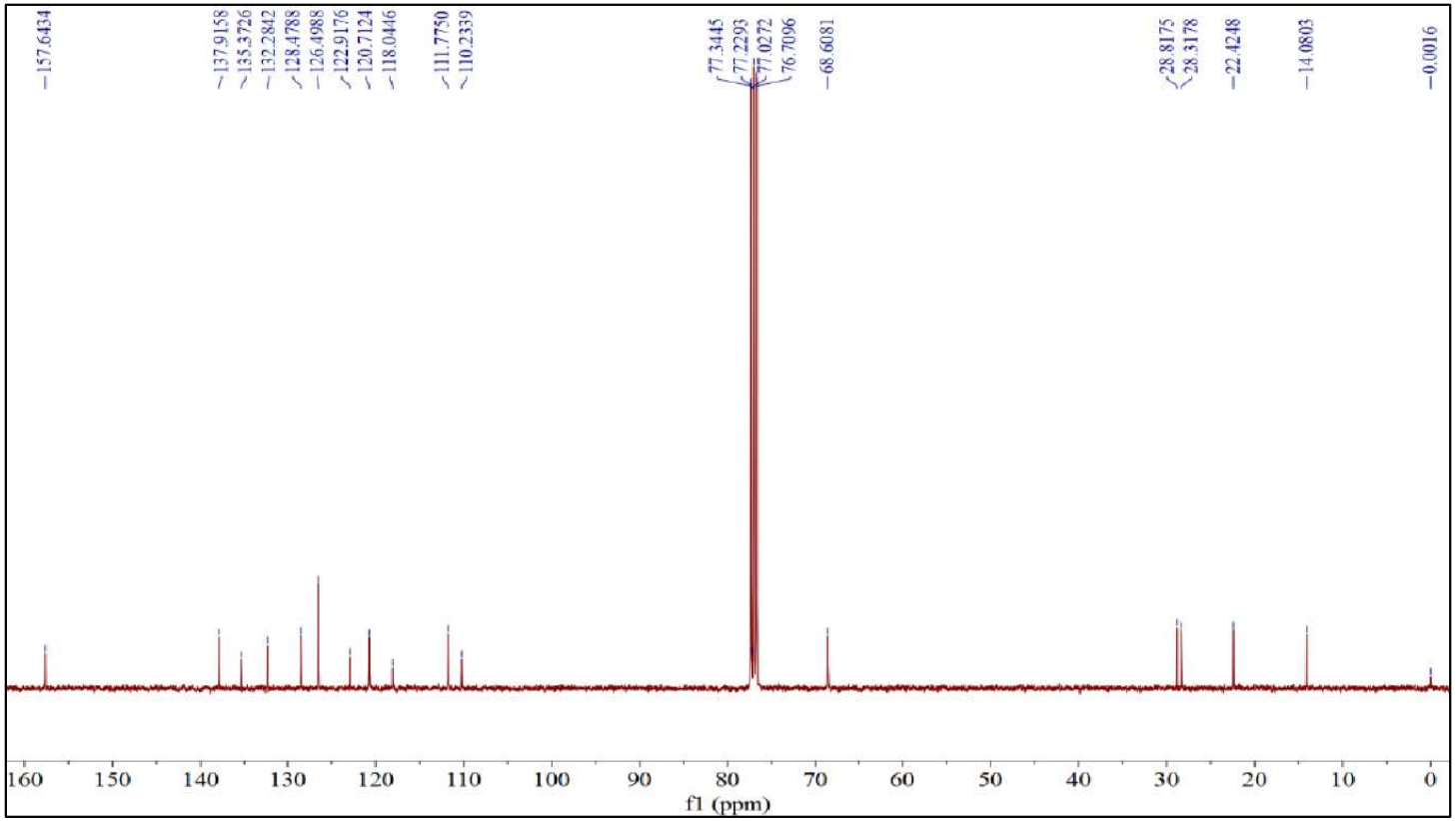

Figure 4.6: ^{1}H NMR spectra of the compound **OCS-3**

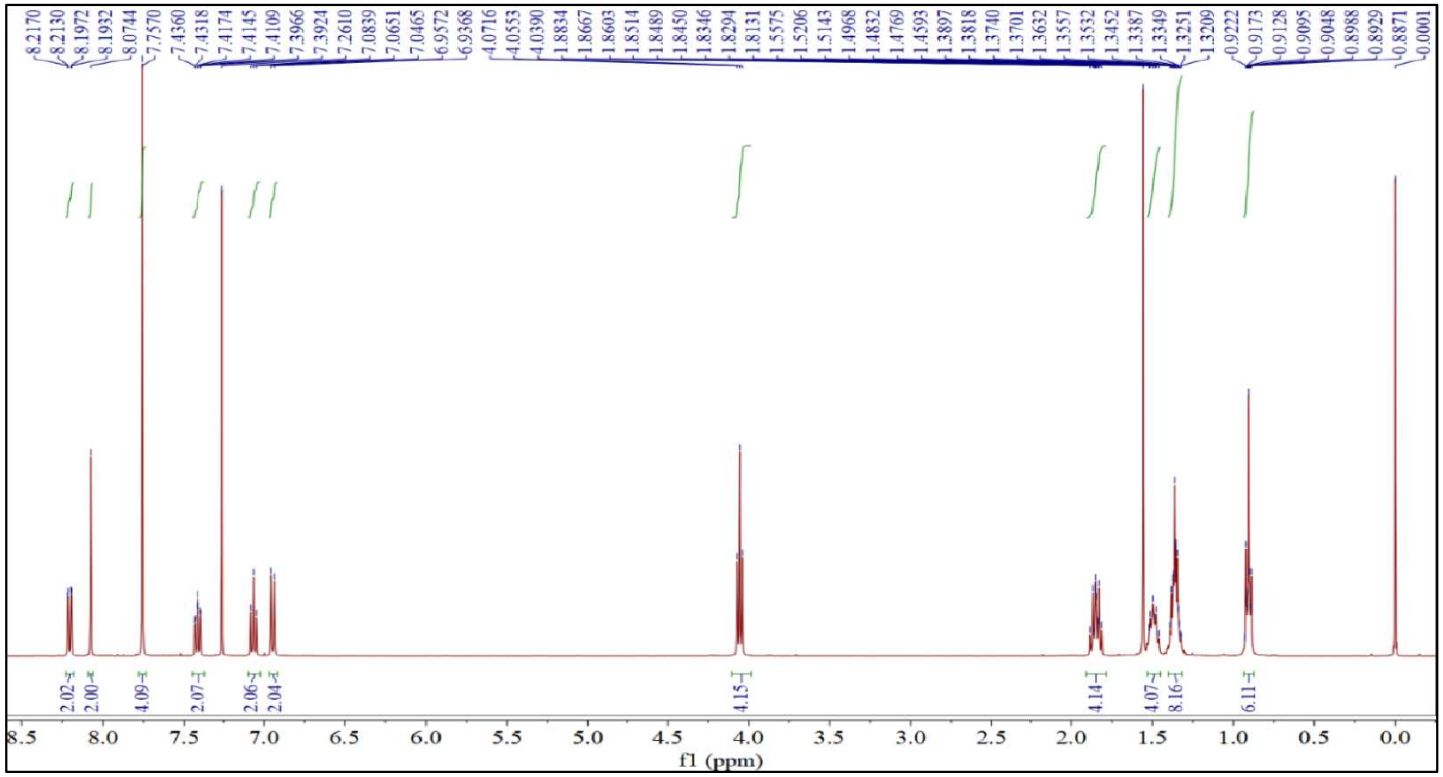

Figure 4.7: [1]HNMR spectra of the compound **OCS-4**

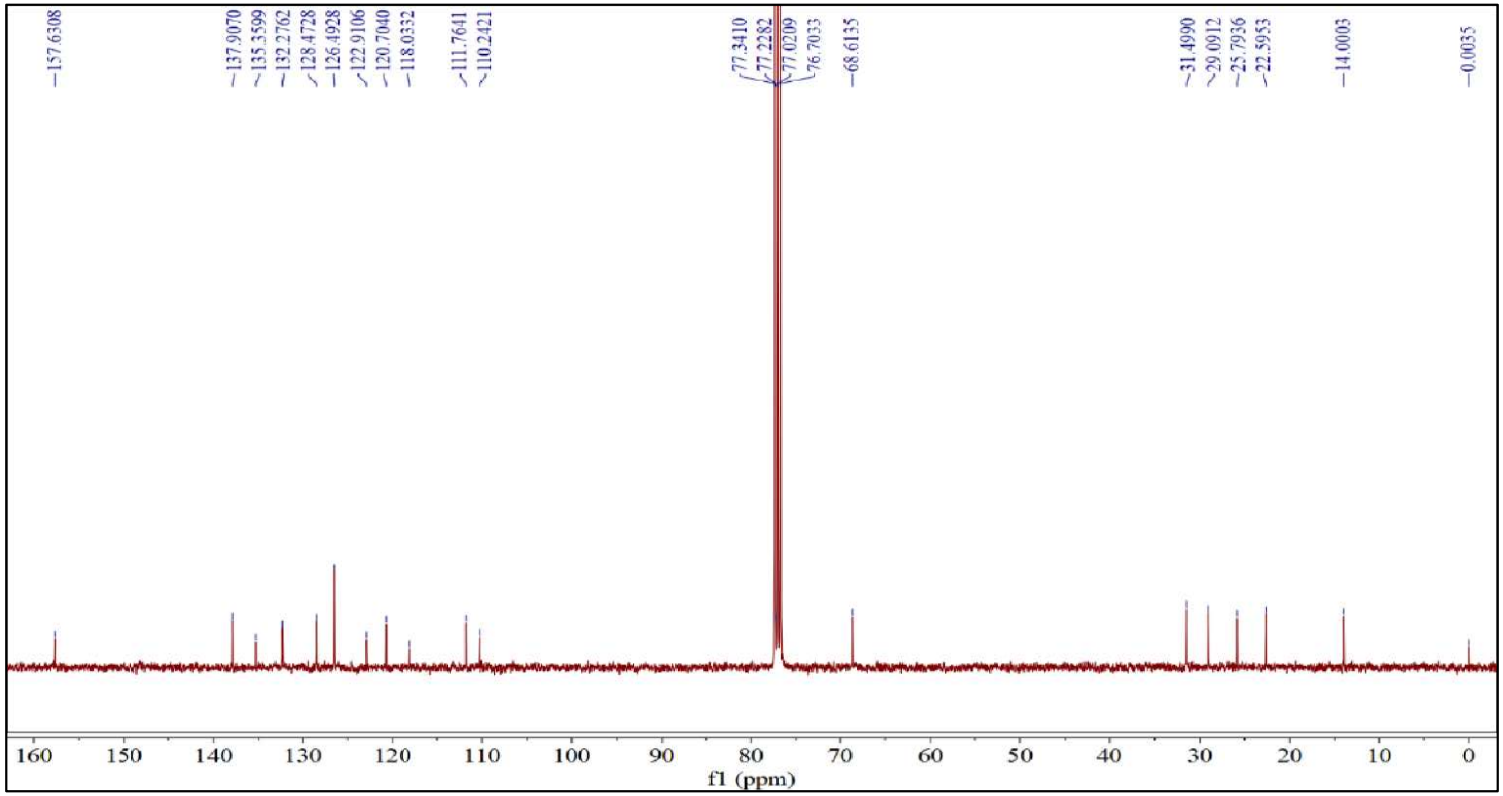

Figure 4.8: ^{13}C NMR spectra of the compound **OCS-4**

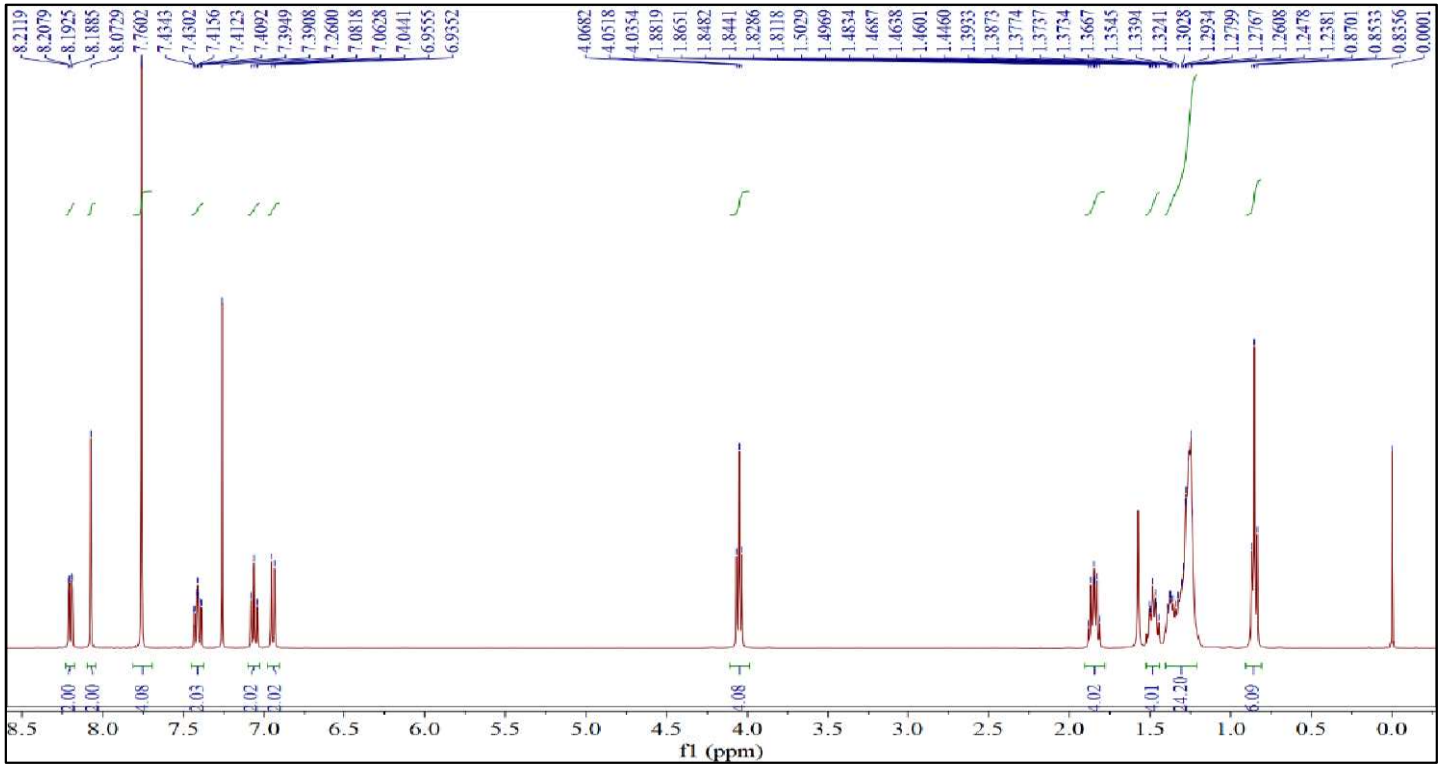

Figure 4.9: ^{1}H NMR spectra of the compound **OCS-6**

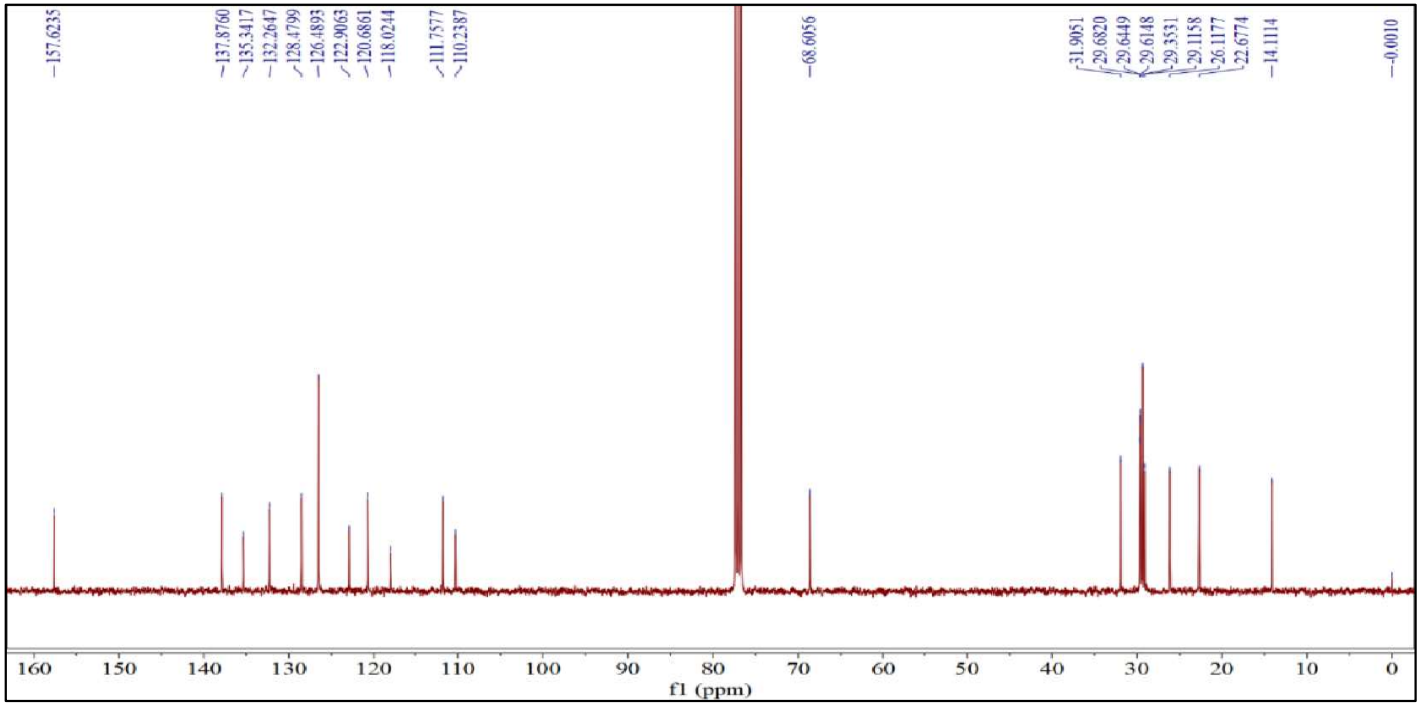

Figure 4.10: ^{1}H NMR spectra of the compound **OCS-6**

Table 4.1: Crystallographic information table for *ortho*-alkyloxy substituted dicyanodistyrylbenzens

Compound	**OCS-1**	**OCS-2**	**OCS-3**	**OCS-4**	**OCS-5**
Formula weight	420.49	476.59	504.65	532.70	644
Cell setting	Monoclinic	Monoclinic	Triclinic	Triclinic	Triclinic
Space group	C2/c	P21/c	P-1	P-1	P-1
A (Å)	27.1752 (6)	4.7163 (17)	7.7829 (4)	8.3834 (11)	8.3260 (3)
B (Å)	4.1440 (1)	19.178 (8)	9.4031 (4)	9.7444 (12)	14.9118 (5)
C (Å)	19.8481 (4)	15.0650 (6)	12.0556 (5)	11.4786 (15)	17.7963 (6)
α (°)	90	90	67.903 (2)	108.814 (5)	65.643 (1)
β (°)	93.376 (1)	95.354 (15)	85.591 (2)	96.433 (5)	88.409 (1)
γ (°)	90	90	66.489 (2)	112.798 (5)	76.349 (1)
Cell volume ($Å^3$)	2231.30 (9)	1356.6 (9)	746.82 96)	787.50 (18)	1950.23 (12)
Z	4	2	1	1	2
F	888	508	270	286	700
ρ (Mg/m^3)	1.252	1.167	1.122	1.123	1.098
Crystal size (mm)	0.55x0.26x0.14	0.40x0.20x0.10	0.78x0.77x0.32	0.30x0.25x0.10	0.88x0.62x0.15
Index ranges	-36≤h≤36 -5≤k≤5 -26≤ l≤26	-6≤h≤4 -24≤k≤24 -19≤ l≤19	-10≤h≤10 -12≤k≤12 -15≤ l≤16	-10≤h≤10 -11≤k≤11 -13≤ l≤13	-10≤h≤9 -18≤k≤18 -21≤ l≤21
Reflections collected	23628	23458	22313	29933	36377
Number of independent Reflections	2781	2944	3586	2917	7252
R_1	0.0440	0.0623	0.0684	0.0735	0.0828
wR_2 (all)	0.1361	0.1918	0.2362	0.2559	0.2341
S	1.084	1.028	1.141	1.040	1.032
No. parameters	193	164	209	264	533
Max. $eÅ^{-3}$	0.240	0.372	0.480	0.388	0.395
CCDC Number	2252530	2252531	2252529	2252532	2252533

4.5 Results and Discussion

4.5.1 Solution state photophysical properties

To explore the photophysical behaviour, the UV-visible absorption spectra of molecules **OCS-1** to **OCS-6** were recorded from their respective dilute solutions in 2-Methyltetrahydrofuran (2-MeTHF). All the compounds showed comparable absorption features with the absorption maxima centered around 370 nm and a shoulder peak at 320 nm (Figure 4.11). The dilute solutions of **OCS-1** to **OCS-6** in 2-MeTHF with an optical density of 0.1 were excited at 370 nm and photoluminescence spectra were recorded at

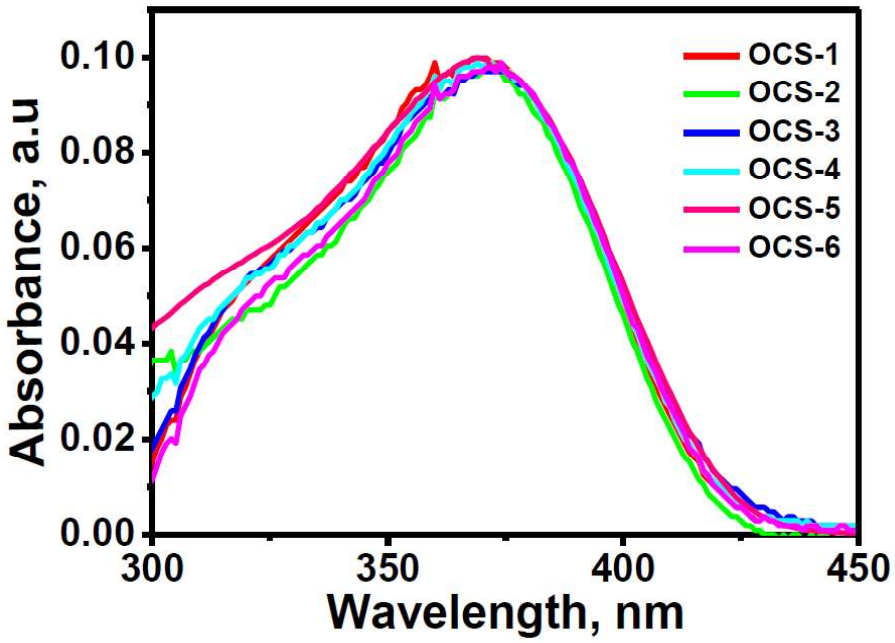

Figure 4.11: The UV-Visible spectra of **OCS-1** to **OCS**-6 in 2-MeTHF (2.4x10-^{6} mol L^{-1})

room temperature and 77 K (Figure 4.12). The spectra of **OCS-1** recorded at room temperature showed two distinct bands centered at 413 nm and 431nm (Figure 4.12a). The bands at 413 nm and 431 nm correspond to fluorescence emission from the isolated molecules The photoluminescence spectrum recorded for **OCS-1** in 2-MeTHF at 77 K showed a distinct band structure with a maximum at 452 nm. To explore the possibility of phosphorescence emission in **OCS-1** with twisted molecular geometry, the photoluminescence spectrum was recorded from 2-MeTHF at 77 K with a delay of 0.5 ms (Figure 4.12 red curve). The emission spectrum (λ_{em}= 510 nm) showed a redshift of 58 nm in comparison to the photoluminescence spectra recorded at 77 K without delay The emission spectra of **OCS-2** to **OCS-6** recorded at room temperature, 77 K, and 77 K with a delay of 0.5 ms showed similar behaviour as that observed with the molecule **OCS-1** (Figure 4.12). The photoluminescence maxima and lifetime data for all the compounds at different conditions are listed in table 4.2. The photoluminescence decay recorded for **OCS-1** from solution in 2-MeTHF at room temperature is fitted using biexponential decay with lifetime τ_1 = 0.95 ns and τ_2 = 1.58 ns. The quantum yield obtained for the compound **OCS-2** in solution is very low with a value of 8.47 x 10^{-3} %. For the other derivatives the solution phase quantum yield values were not obtained with better reliabity due to poor emission in solution. .The photoluminescence decay recorded for compounds **OCS-2** to **OCS-6** also showed similar decay as in the case of **OCS-1**, however with different lifetime values (Figure 4.13 and Table 4.2). To confirm the phosphorescence in **OCS-1** at

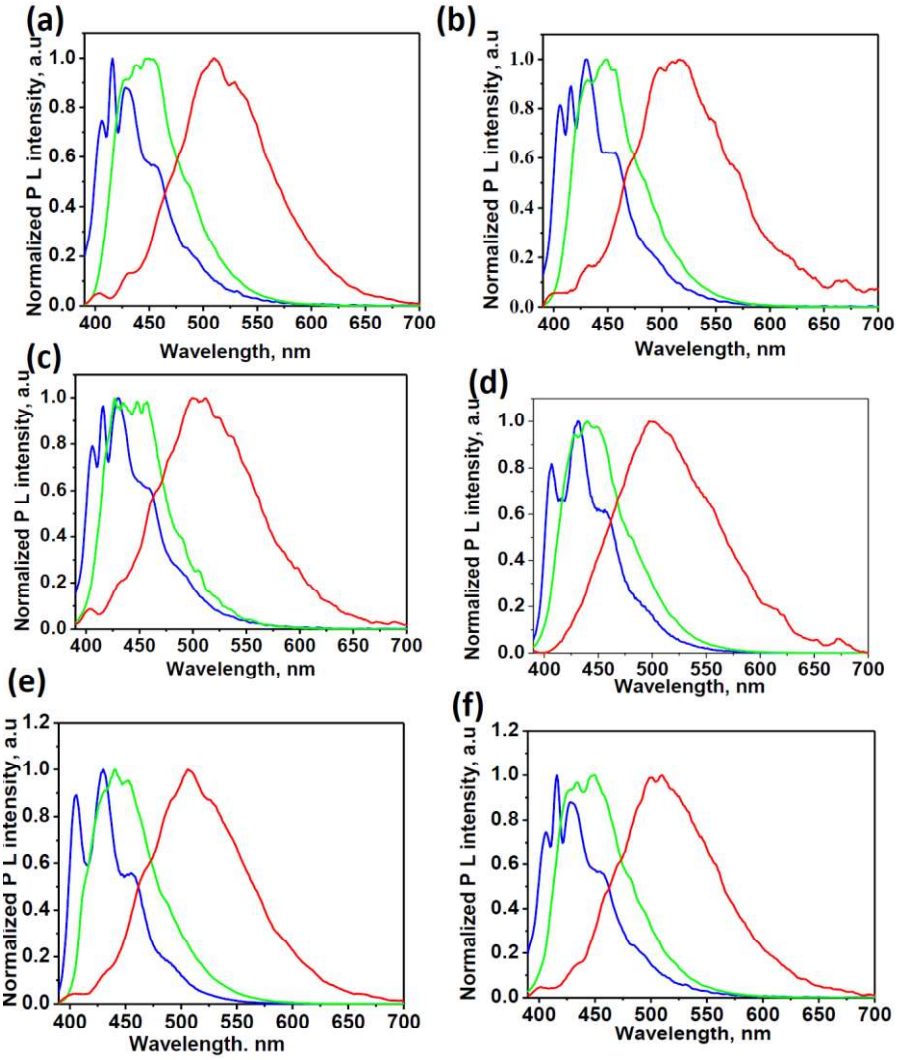

Figure 4. 12: The emission spectra of (a) **OCS-1**, (b) **OCS-2**, (c) **OCS-3**, (d) **OCS-4**, (e) **OCS-5** and (f) **OCS-6**, in 2-MeTHF at room temperature (blue curve), 77 K (green curve) and 77 K with a delay of 0.5 ms red curve).

77 K in 2-MeTHF the photoluminescence decay was recorded with a delay of 0.5 ms (Figure 4.14a). The decay was fitted with biexponential decay with a lifetime value τ_1 = 0.96 ms and τ_2 = 16.75 ms. The redshifted emission with a concomitant lifetime enhancement at 77 K with a time delay of 0.5 ms is attributed to phosphorescence. All other derivatives from **OCS-2** to **OCS-6** showed similar behaviour as that of **OCS-1** in the lifetime and photoluminescence spectral features. The compound **OCS-2** showed a bi-exponential decay with a lifetime of 0.128 ms and 1.90 ms at 77 K (time delay 0.5 ms). The transient emission decay of **OCS-3** also showed bi-exponential decay (time delay 0.5 ms) with a lifetime of τ_1 = 1.76 ms and τ_2 = 28.09 ms. The molecules **OCS-4** (τ_1 = 1.5 ms, τ_2 = 17.39 ms) and **OCS-5** (τ_1 = 1.15 ms, τ_2 = 25.41 ms) and **OCS-6** (τ_1 = 1.02 ms, τ_2 = 7.69 ms) also showed similar behaviour with red shifted emission and phosphorescence emission with lifetime in the range of milliseconds indicating the existence stable triplet state and phosphoresce at 77 K.

To rule out the possibility of charge transfer (CT) character in the molecule the photoluminescence spectra of **OCS-1** were recorded from solvents of varying polarity such as toluene, chloroform and acetonitrile. The fluorescence spectra showed no shift in wavelength with increasing the polarity of the solvents indicating the absence of CT state in the molecule (Figure 4.15)

.

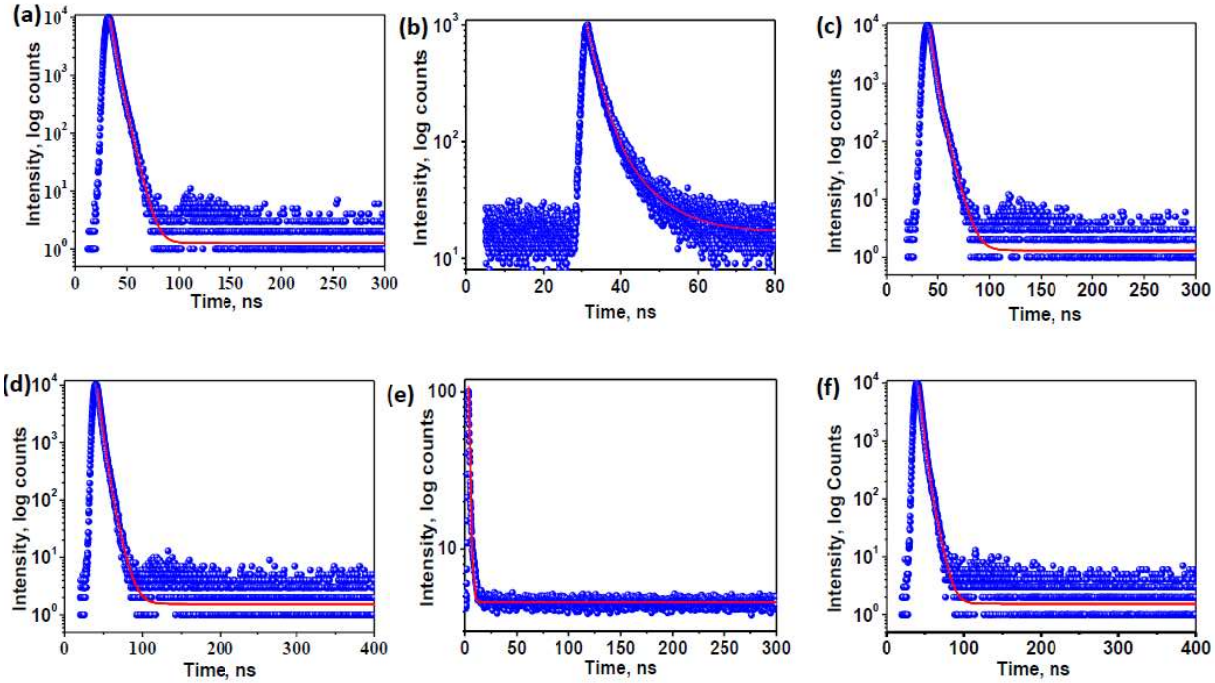

Figure 4.13: Photoluminescence decay curve of (a) **OCS-1,** (b) **OCS-2,** (c) **OCS-3,** (d) **OCS-4** (e) **OCS-5** and (f) **OCS-6** in 2 MeTHF at room temperature.

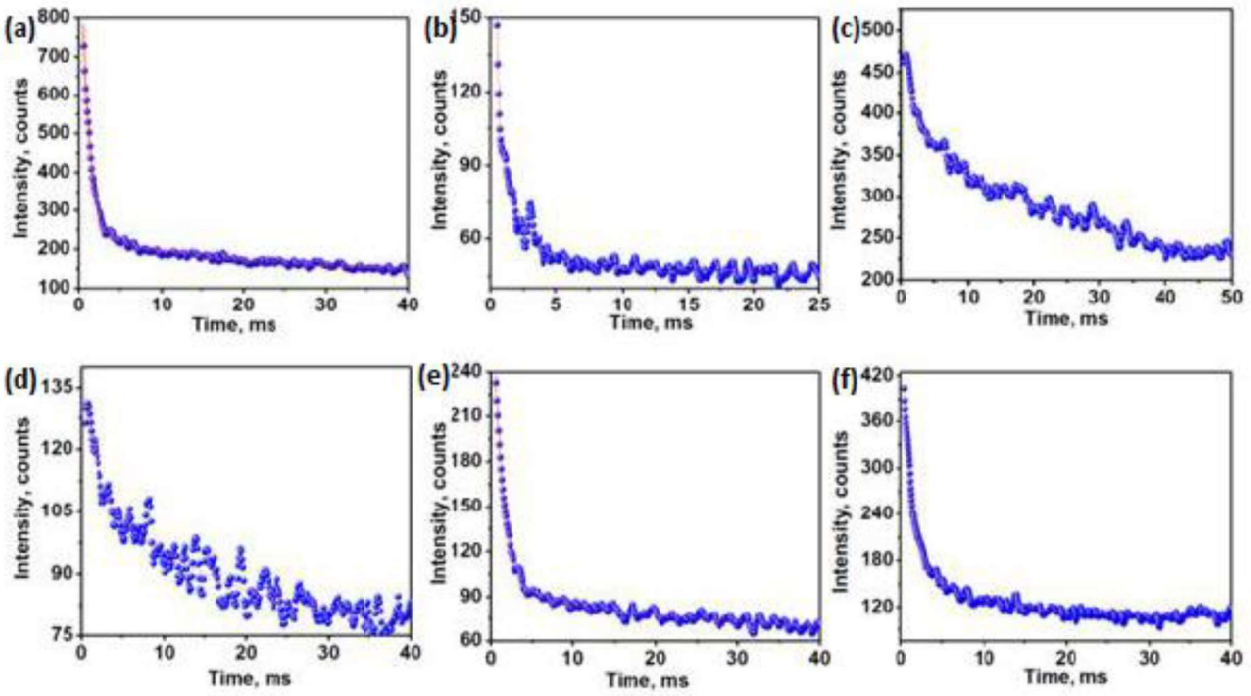

Figure 4.14: Phosphorescence decay curve of (a) **OCS-1,** (b) **OCS-2,** (c) **OCS-3,** (d) **OCS-4** (e) **OCS-5** and (f) **OCS-6** in 2 Me-THF at room temperature.

Table 4.2: The photoluminescence maximum (room temperature (RT), 77 K and 77 K with 0.5 ms delay) and lifetime data (room temperature (RT), 77 K with 0.5 ms delay) recorded for compounds **OCS-1** to **OCS-6** in 2-Me THF.

Sample	**λ_{max}, nm (RT)**	**λ_{max}, nm (77K)**	**λ_{max}, nm (77K, delay 0.5 ms)**	**Lifetime, ns (ns, RT)**		**Lifetime, ms (77 K, delay of 0.5 ms)**	
				τ_1	τ_2	τ_1	τ_2
OCS-1	415	449	509	0.95	1.58	16.75	0.969
OCS-2	429	448	516	2.0	6.94	1.90	0.128
OCS-3	430	447	510	1.73	0.85	1.76	28.09
OCS-4	430	443	499	2.08	1.03	7.39	1.50
OCS-5	431	441	507	0.79	3.55	1.15	25.41
OCS-6	428	440	507	0.88	1.82	7.69	1.02

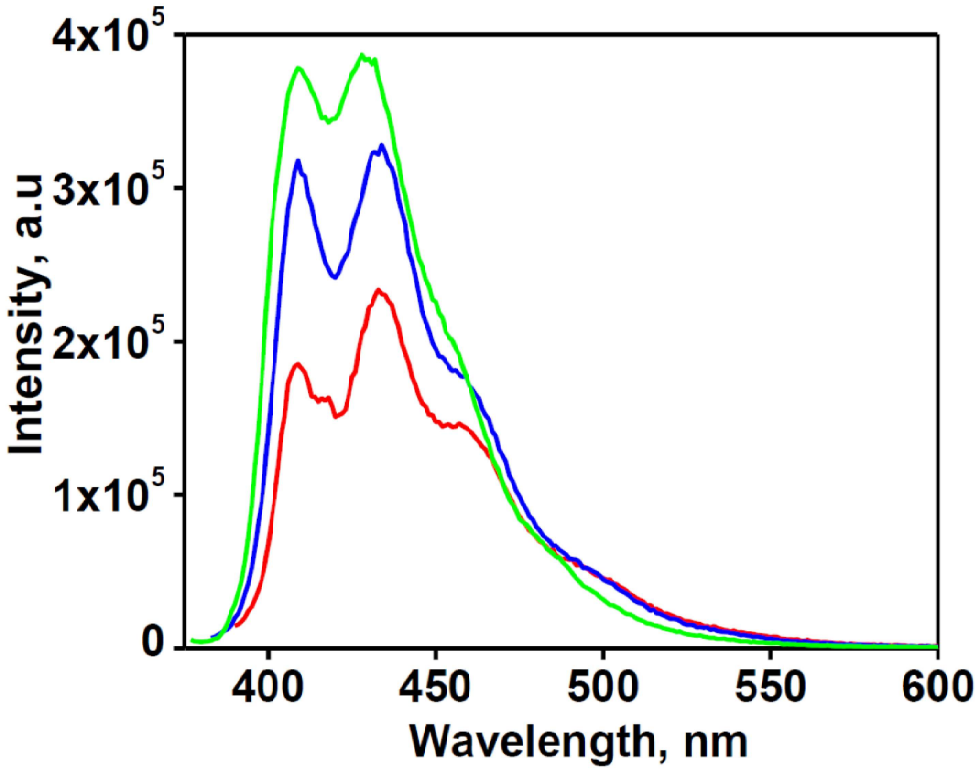

Figure 4.15: The emission spectra of **OCS-1** in toluene (red curve), in chloroform (blue curve) and in acetonitrile (green curve).

4.5.2 Solid state photoluminescence properties

To explore the photophysical behaviour of the molecule in the solid state the UV visible spectra of all the compounds were recorded at room temperature. The UV-visible spectra showed similar spectral features varying absorption maxima (Figure 4.16). Figure 4.17 shows the solid state luminescence spectra of all the compounds recorded by exciting at 370 nm. The compounds **OCS-1**, **OCS-2**, **OCS-3** and **OCS-6** showed single banded emission spectra with various emission maxima, while the compound **OCS-4** and **OCS-5** showed emission spectra with a shoulder band respectively at 502 nm and 493 nm. Among the six *ortho* alkyloxy derivatives of dicyanodistyrylbenzenes, **OCS-2** showed a redshifted spectrum with a maximum centred at 534 nm while the luminescence maximum for **OCS-4** was at relatively shorter wavelength maximum centred around 478 nm. The difference in luminescence emission maxima of the compounds with varying alkyl chains are due to the variation of the molecular conjugation and dipolar coupling in the solid state. The quantum yield of all the compounds were recorded to compare the luminescence efficiency in the solid state. Among the six alkyloxy derivatives of dicyanodistyrylbenzene, the compound **OCS-1** showed the highest quantum yield value of 0.86. This quantum efficiency of molecule **OCS-1** is quite promising for possible optoelectronic applications. The other derivatives from **OCS-2** to **OCS-6** also showed appreciable quantum yield values with variation of 0.08 to 0.78 (Table 4.3). The lowest quantum efficiency of all the derivatives was shown by **OCS-4** and **OCS-5** with values 0.11 and 0.08 respectively. Figure 4.18 shows the photoluminescence decay recorded for compounds **OCS-1** to

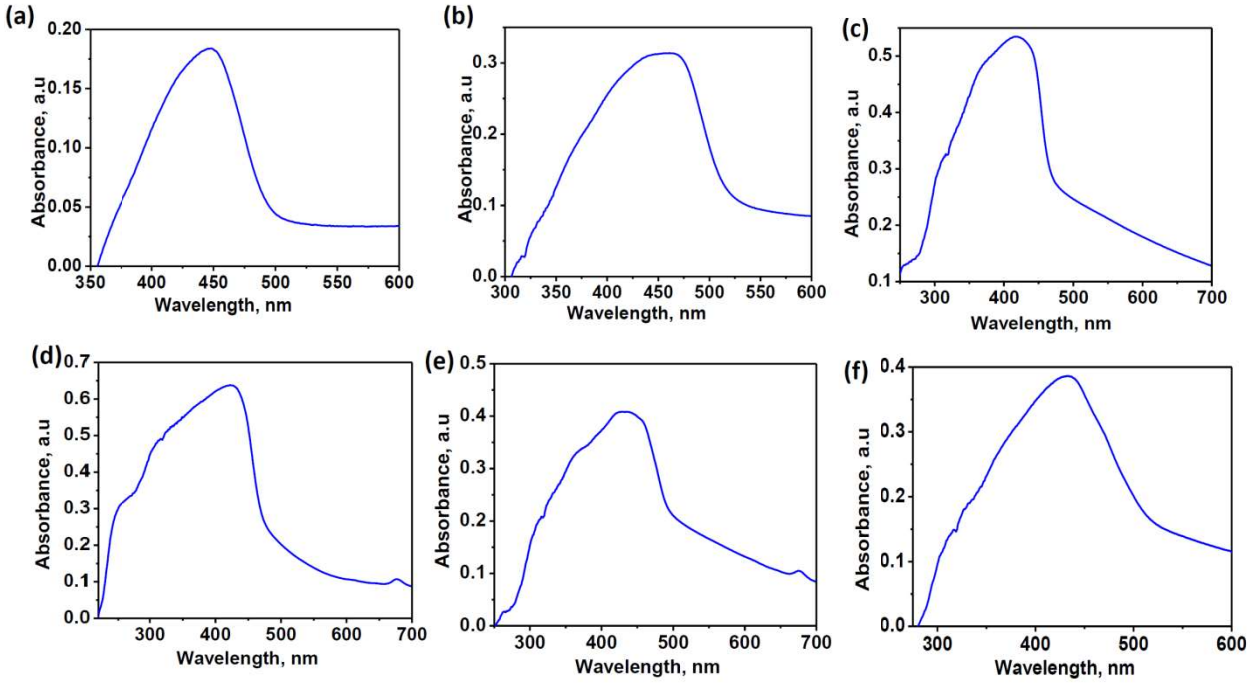

Figure 4.16: Solid state UV-Visible absorption spectra of (a) **OCS-1**, (b) **OCS-2**, (c) **OCS-3**, (d) **OCS-4**, (e) **OCS-5** and (f) **OCS-6**.

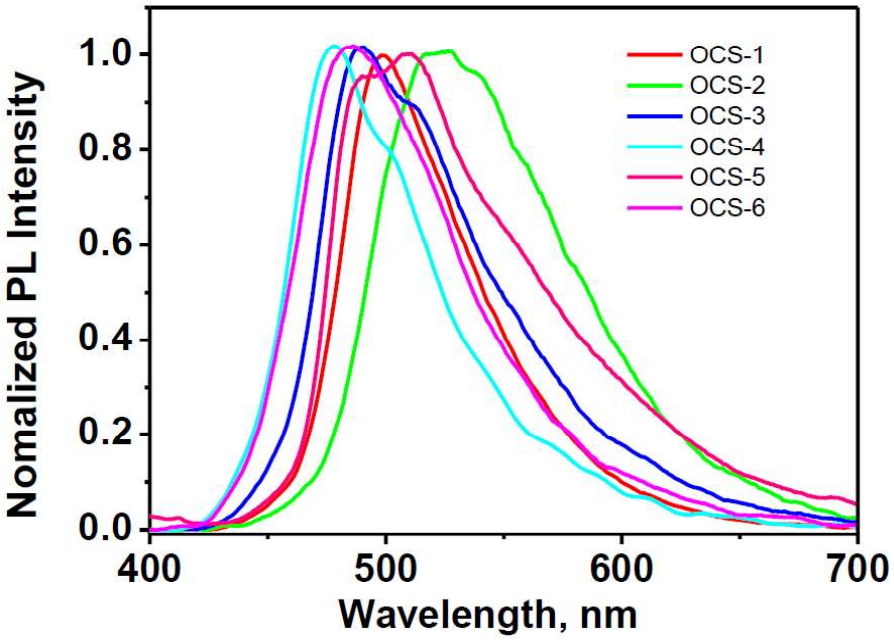

Figure 4.17: Solid state photoluminescence spectra of compounds **OCS-1** to **OCS-6**.

Table 4.3: Photophysical parameters of **OCS-1** to **OCS-6**.

Sample	λ_{em} (nm)	τ_F (ns)	Φ_F	k_r (ns^{-1})	k_{nr} (ns^{-1})
OCS-1	502	2.41	0.86	0.36	0.05
OCS-2	534	1.34	0.78	0.58	0.17
OCS-3	484	1.27	0.49	0.38	0.40
OCS-4	478	1.32	0.11	0.08	0.68
OCS-5	508	2.09	0.08	0.04	0.44
OCS-6	510	1.44	0.44	0.30	0.39

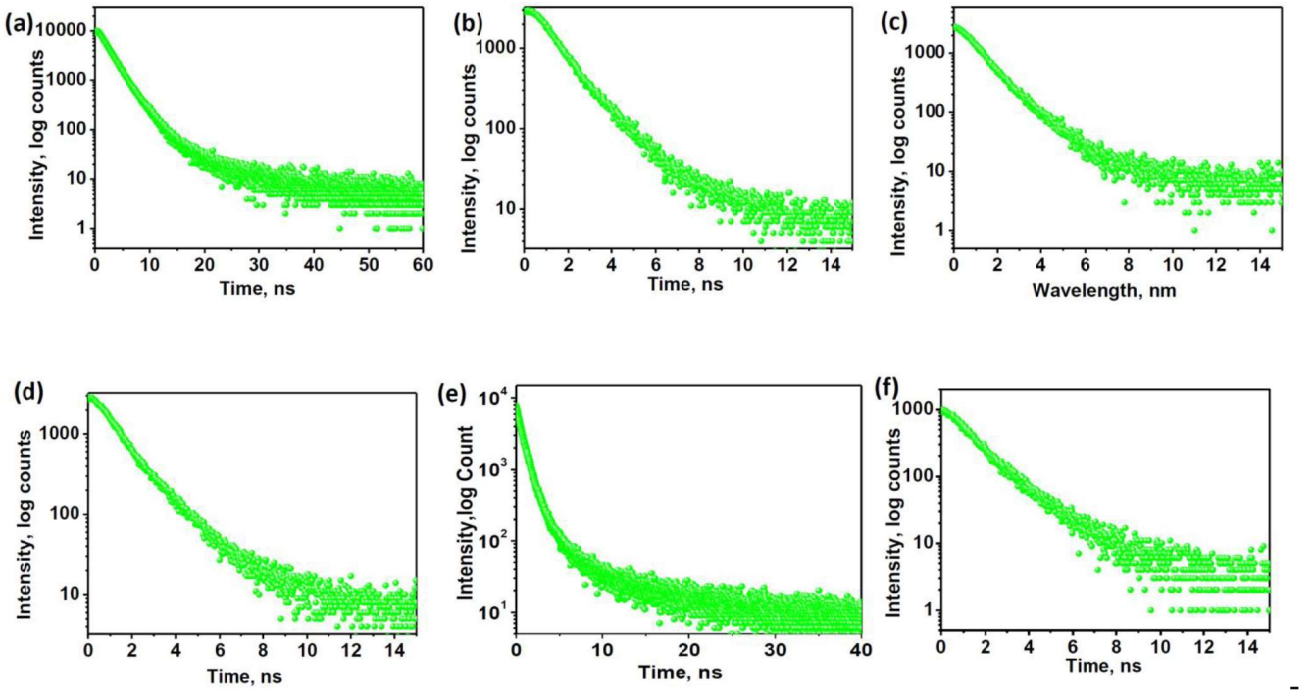

Figure 4.18: Fluorescence decay curve of (a) **OCS-1**, (b) **OCS-2**, (c) **OCS-3**, (d) **OCS-4**, (d) **OCS-5** and (f) **OCS-6** in the solid state

OCS-6 by exciting at 405 nm. All the transient decay of emission were fitted with triexponential decay with lifetime values in the range nanoseconds. The observed lifetime values clearly indicate that the emission in the solid state is fluorescence. To account for the variation in fluorescence quantum yield in the solid state a detailed comparison of fluorescence lifetime, quantum yield, and radiative and nonradiative decay rate constants were carried out (Table 4.3). The molecules **OCS-1** and **OCS-2** which are showing higher quantum yield in solid state (0.86 and 0.78) have higher radiative decay constant value of 0.36 and 0.58 respectively. Among the two molecules **OCS-1** having higher quantum yield showed lower non-radiative decay constant (0.05), which imply that the non-radiative decay pathways are effectively blocked in **OCS-1**. Among the six *ortho* alkoxy derivatives the molecules **OCS-4** and **OCS-5** showed lowest quantum yield values since they have lower radiative decay constant values (0.08 and 0.04 ns^{-1}). The higher values of nonradiative decay constants of these molecules indicate that various decay pathways are operating in the solid state of these molecules originating from molecular packing. According to previous literature the molecular structure and packing parameters largely determines the quantum efficiency of organic luminophores in the solid state.[20] Hence it is be expected that the variation in quantum efficiency in compounds **OCS-1** to **OCS-6** can be due to the difference in molecular packing in the crystalline state. To probe the variable emission behaviour in these molecules, it is quite important to explore the structure and packing of the **OCS-1** to **OCS-6** in the solid state.

4.5.3 Single crystal X-ray diffraction studies and structure-property correlation

To understand the role of molecular structure and packing in determining the emission properties of *ortho* alkyloxy substituted dicyanodistyrylbenzenes in the solid state, we carried out a detailed analysis of structural data obtained from single crystal X-ray diffraction. All the compounds showed different molecular packing with various intermolecular interactions such as C-H···O, C-H···π, and π···π interactions, accommodating different levels of twist in π-back bone constituting an aggregate pair as shown in Figure 4.19a. To establish the role of structure and packing on increased quantum yield obtained for all the *ortho*-substituted dicyanodistyrylbenzene derivatives, the difference in twist in π-backbones, π-π overlap and interplanar distance in **OCS-1** to **OCS-6** were analyzed. It is a fact that the twisted architectures show aggregation induced emission compared to the planar counterpart where the planar architectures are prone to aggregation caused quenching owing to the increased π-π stacking.[21] The comparison of molecular twist could not provide a systematic input to the observed quantum yield in the solid phases of **OCS-1** to **OCS-6**, indicating that in addition to the molecular twist some other structural parameters may also be crucial in dictating the emission properties of **OCS-1** to **OCS-6** in the crystalline state. Some of the recent studies showed that molecular rigidity in the aggregated state also contributes to high quantum yield.[22] To explore the role of molecular rigidity on varying quatum yield of compounds **OCS-1** to **OCS-6**, we measured the π-overlap (o) and the interplanar distance

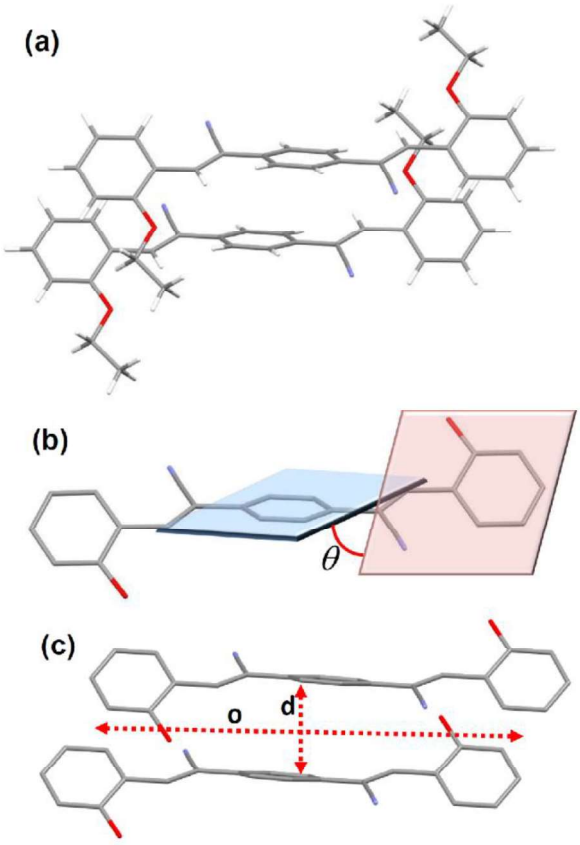

Figure 4. 19: (a) Aggregate pairs seen in single crystalline samples of **OCS-1**. A schematic representation of (b) twist angle, θ, (c) π-overlap, o and interplanar distance, d in *ortho* alkyloxy dicyanodistyrylbenzenes (Alkyl chains and hydrogen atoms are removed for clarity).

(d) between the aggregate pairs in crystals of various dicyanodistyrylbenzene derivatives (Figure 4.19). The compounds **OCS-1** to **OCS-6** showed different extents of π-overlap and interplanar spacing in the crystals (Figure 4.20 and Table 4.4). The molecule **OCS-1** with a maximum twist in the π-system ($\theta = 50.3°$)

with percentage overlap of 90.5% and an optimum interplanar distance, showed the highest quantum yield (Φ_F = 90.5 %) among all the molecules (Table 4.4). Despite the comparable twist (θ = 47.8°) with that of **OCS-1**, the molecule **OCS-4** showed the lowest quantum yield among all the molecules owing to the reduced percentage of overlap (o = 39.7%) along with an increased interplanar distance (3.56 Å). This observation indicates that larger interplanar distance results in a loosely packed aggregate structure resulting in a relatively inefficient orbital overlap. In **OCS-2**, with a nearly planar geometry (8.2°), the compound showed an appreciably high quantum yield (Φ_F = 77. 93 %) which is attributed to an appreciable percentage of overlap (o = 82.5 %). In addition to the molecular twist, improved π-overlap and moderate interplanar distance seem to play an important role in the aggregate formation in **OCS-2**. The molecules **OCS-3** and **OCS-6** with a better molecular twist and rigid molecular packing showed a medium quantum efficiency which is attributed to a moderate π-overlap. The **OCS-5** with minimum twist angle and interplanar distance showed a lowest quantum yield indicating the luminescence quenching in the crystalline state of these molecules.

Table 4. 4: Photophysical and structural parameters of *ortho* alkyloxy substituted dicyanodistyrylbenzene derivatives.

Sample	λ_{max} (nm)	Φ_F (%)	Twist angle (°)	Overlap (%)	Interplanar distance (Å)
OCS-1	502	86.39	50.3	90.5	3.47
OCS-2	534	77.93	8.2	82.5	3.48
OCS-3	484	49.00	52.1	36.2	3.47
OCS-4	478	10.83	47.8	39.7	3.56
OCS-5	508	8.00	8.0	40.0	3.37
OCS-6	510	43.61	41.1	32.0	3.38

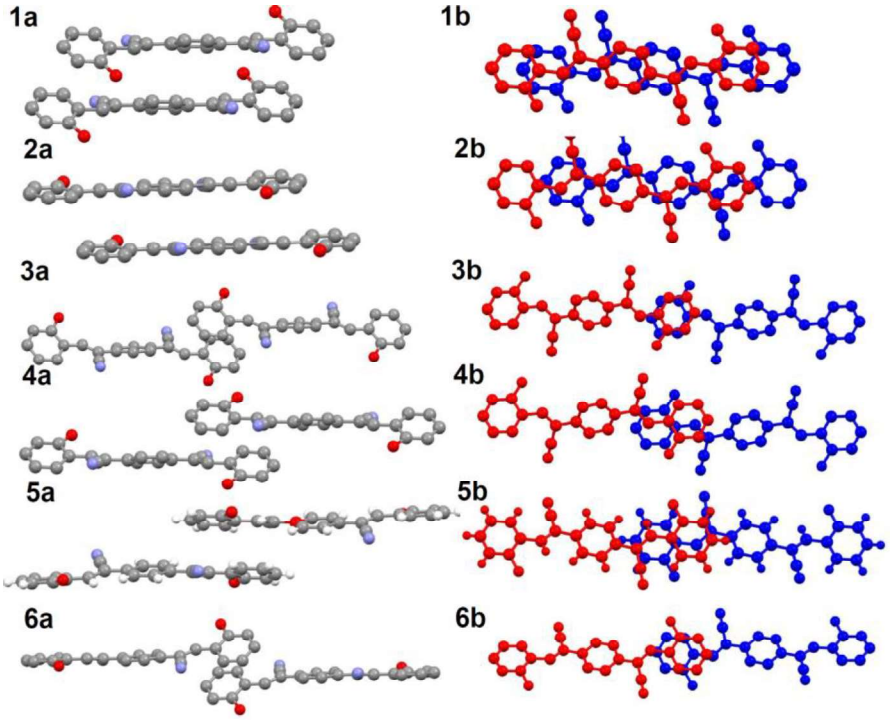

Figure 4.20: Aggregate pairs in **OCS-1** (1a and 1b), **OCS-2** (2a and 2b), **OCS-3** (3a and 3b) **OCS-4** (4a and 4b), **OCS-5** (5a and 5b) and **OCS-6** (6a and 6b). (Alkyl chains and hydrogen atoms are removed for clarity

4.6. Conclusion

In summary, a series of *ortho*-alkyloxy dicyanodistyrylbenzenes were synthesized, solution state and solid-state luminescence properties were investigated. A detailed analysis of photoluminescence properties of compounds **OCS-1** to **OCS-6** in 2-MeTHF was carried out at room temperature, 77K and 77K with delay. The lifetime obtained for all the compounds in 2-MeTHF at room temperature indicated fluorescence emission while luminescence decay recorded at 77 K with a delay of 0.5 ms demonstrated the phosphorescence in these molecules in solution at 77 K. This work substantiates the importance of restriction of intramolecular motion in achieving the stable triplet state and phosphorescence emission. The study further explored the various structural factors that affect the quantum efficiency of the molecules in the solid state. The work demonstrated the interplay between the structural parameters such as twist in π-backbone, overlap between the π-system of the neighbouring molecules and the interplanar distance between the molecules in determining the quantum efficiency of molecules **OCS-1** to **OCS-6** in the solid state**.** The alkyloxy substitution in the *ortho* position of dicyanodistyrylbenzene introduces molecular twist and rigid packing in the solid state which plays a pivotal role in achieving high quantum yields in *ortho* alkyloxy substituted dicyanodistyrylbenzene systems.

4.7. References

1. B. Xu, W. Li, J. He, S. Wu, Q. Zhu, Z. Yang, Y.- C. Wu, Y. Zhang, C. Jin, P.- Y. Lu, Z. Chi, S. Liu, J. Xu and M. R. Bryce, *Chem Sci*, 2016, **7**, 5307–5312.
2. Z. He, C. He and B. Z. Tang. *ACS Omega*, 2018, **3**, 3267–3277.
3. Y. Hong, J. W. Y. Lam and B. Z. Tang, *Chem. Soc. Rev.*, 2011, **40**, 53615388.
4. S. Dong, Z. Li and J. Qin*, J. Phys. Chem. B*, 2009, **113**, 434–441.
5. Y. Wang, D. Xu, H. Gao, Y. Wang, X. Liu, A. Han, C. Zhang and L. Zang*, J. Phys. Chem. C*, 2018, 122, **4**, 2297–2306.
6. E. Ubba, Y. Tao, Z. Yang, J. Zhao, L. Wang and Z. *Chi, Chem. Asian J.*, 2018, **13**, 31063121.
7. W. Qin, Z. Yang, Y. Jiang, J. W. Y. Lam, G. Liang, H. S. Kwok and B. Z. Tang*, Chem. Mater.*, 2015, **27**, 3892–3901.
8. H.- X. Yu, J. Zhi, T. Shen, W. Ding, X. hang and J. - L. Wang, *J. Mater. Chem. C*, 2019, **7**, 88888897.
9. S. Xu, Y. Duan and B. Liu, *Adv. Mater.*, 2020, **32**, 1903530.
10. S. B. Anantharaman, J. Kohlbrecher, G. Rainò, S. Yakunin, T. Stöferle, J. Patel, M. Kovalenko, R. F. Mahrt, F. A. Nüesch and J. Heier, *Adv. Sci.*, 2021, **8**, 1903080.
11. T. E. Kaiser, H. Wang, V. Stepanenko and F. Würthner, *Angew. Chem.*, 2007, **119**, 5637–5640.
12. Z. Q. Xie, B. Yang, F. Li, G. Cheng, L. L. Liu, G. D. Yang, H. Xu, L. Ye, M. Hanif, S. Y. Liu, D. G. Ma and Y. G. Ma, *J. Am. Chem. Soc.*, 2005, **127**, 14152–14153.
13. J. *Zhang*, B. Xu, J. Chen, S. Ma, Y. Dong, L. Wang, B. Li, L. Ye and W. Tian, *Adv. Mater*., 2014, **26**, 739–745.
14. S. Ma, Y. Liu, J. Zhang, B. Xu, and W. Tian, *J. Phys. Chem. Lett.*, 2020, **11**, 1050410510.
15. W. Li, Y.- Mo Zhang, T. Zhang, W. Zhang, M. Li and S. X.- An Zhang, *J. Mater. Chem. C*, 2016, **4**, 1527-1532.
16. (a) S.- J. Yoon, J. H. Kim, K. S. Kim, J. W. Chung, B. Heinrich, F. Mathevet, P. Kim, B. Donnio, A.- J. Attias, D. Kim and S. Y. Park, *Adv. Funct. Mater.*, 2012,

22, 6169; (b) D. Zhang, Y. Liu, H. Gao, Q. Changa and X. Cheng, *J. Mater. Chem. C*, 2020, **8**, 1747417481; (c) K. A. N. Upamali, L. A. Estrada, P. K. De, X. Cai, J. A. Krause, and D. C. Neckers, *Langmuir*, 2011, **27**, 1573–1580.

17. (a) T. Ikeyama, C. Kabuto and m. Sato*, J. Phys. Chem.*, 1996, **100**, 19289–19291; (b) H. Goerner*, J. Phys. Chem.*, 1989, **93**, 1826–1832; (c) T. Ikeyama and T. Azumi, *J. Phys. Chem.*, 1985, **89**, 5332–5333.
18. H. J. Kim, J. Gierschner, S. Y. Park, *J. Mater. Chem. C*, 2020, **8**, 74177421.
19. S. J. Yoon, J. W. Chung, J. Gierschner, K. S. Kim, M. G. Choi, D. Kim, S. Y. Park, *J. Am. Chem. Soc.*, 2010, **132**, 1367513683.
20. (a) J. Fan, L. Lin and C.- K. Wang*, Phys. Chem. Chem. Phys.*, 2017, **19**, 30147-30156. (b) C. Wang and Z. Li, *Mater. Chem. Front.*, 2017, 1, 21742194; (c) S. Xue, X. Qiu, Q. Sun and W. Yang, *J. Mater. Chem. C*, 2016, **4**, 15681578.
21. (a) Y. Cai, X. Ji, Y. Zhang, C. Liu, Z. Zhang, Y. Lv, X. Dong, H. He, J. Qi, Y. Lu, D. Ouyang, W. Zhao and W. Wu, *Aggregate*, 2023, **4**, e277; (b) L. L. Bras, K. Chaitou, S. Aloïse, C. Adamo and A. Perrier, *Phys. Chem. Chem. Phys.*, 2019, **21**, 4656.
22. (a) Z. Wei, Z. - Y. Gu, R. K. Arvapally, Y.- P. Chen, R. N. McDougald, J. F. Ivy, A. A. Yakovenko, D. Feng, M. A. Omary and H.- C. Zhou, *J. Am. Chem. Soc.*, 2014, 2014, **136**, 8269–8276; (b) K. Kokado, R. Taniguchi and K. Sada, *J. Mater. Chem. C*, 2015, **3**, 85048509; (c) T. Hirose, K. Higashiguchi and Matsuda, K. S, *Chem. Asian J.*, 2011, **6**, 1, 0571063.

Chapter 5

Multistimuli Responsive Emission in Cholesterol Appended Cyanostyryl Thiophene Positional Isomers with Liquid Crystalline Properties

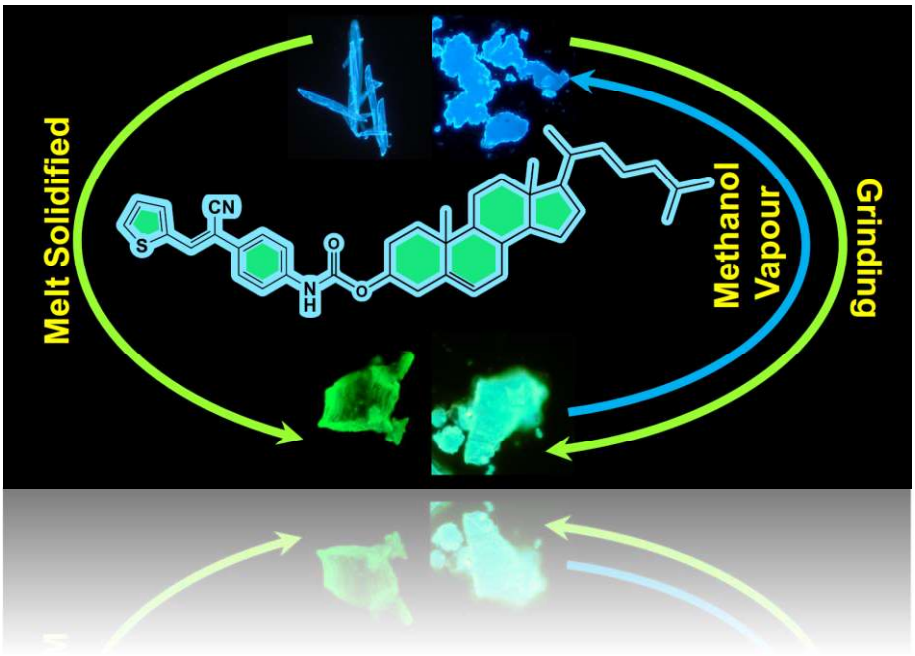

5. 1 Abstract

*The present work describes the synthesis of two cholesterol appended cyanostyryl thiophene positional isomers **CS-1** and **CS-2** and their stimuli responsive solid-state emission and liquid crystalline properties. Both compounds showed enhanced emission in the solid state due to the aggregation-induced emission. Interestingly, **CS-1** and **CS-2** showed emission switching under the influence of thermal and/or mechanical stimuli. The difference in emission properties of pristine **CS-1** and its melt-processed sample **CS-1M** is attributed to the formation of two different crystalline phases. The powder X-ray diffractogram simulated from the single crystal X-ray diffraction data of **CS-1** and **CS-1M** showed similar features indicating that the molecules in the melt-cooled phase adopt a packing similar to the one observed in the single crystal. In addition to heat-induced changes in fluorescence properties, compound **CS-2** showed mechanofluorochromism and methanol vapour-induced reversible emission switching. The observed emission switching in **CS-2** under thermal and shear stress was due to crystalline to amorphous transition. The emission recovery from the grounded sample of **CS-2** under methanol vapours was attributed to the reversible transition from amorphous to a crystalline phase similar to pristine **CS-2**. A detailed analysis of various photophysical parameters of compounds under different stimuli is reported. The liquid crystalline properties of the compounds were studied using polarizing optical microscopy (POM) and differential scanning calorimetry (DSC). Both **CS-1** and **CS-2** showed the formation of an enantiotropic cholesteric (N*) liquid crystalline phase. Interestingly, the N* phase was stabilized down to room temperature in a glassy state.*

5.2 Introduction

Cyanostyrylbenzenes are an important class of compounds with aggregation-induced emission and multistimuli response.[1,2] Stimuli-responsive cyanostyryl systems were studied by various research groups and established the role of diverse packing modes in the solid state emission.[3,4] In one of the explorations, Park and coworkers demonstrated the mechanochromic emission switching in alkyloxy substituted symmetrical dicyanodistyrylbenzene and established the crucial role of molecular arrangement in the observed stimuli response.[5] In addition, the report on different polymorphic crystals of dicyanodistyrylbenzene derivatives revealed the dependence of intermolecular interaction in the solid-state emission.[6] A report by Fan et al. demonstrated the use of positional isomerism obtained by suitably placing the cyano group on the stilbene unit in achieving tunable solid state emissions.[7] A recent report demonstrated the positional isomerism modified intramolecular charge transfer to create molecular assemblies with switchable emission.[8,9] Hence positional isomers are good candidates for stimuli responsive emission behaviour.

5.3 Scope of the present investigation

The positional isomerism has evolved as an indispensable tool in generating materials with varied emissions in the solid state from a single structural unit. Herein, we synthesize two cholesterol based compounds **CS-1** and **CS-2** (Scheme 5.1) containing cyanostyryl thiophene as fluorophore to explore the role of positional isomerism on solid-state emission behaviour. The present molecular design comprised appending a mesogenic cholesterol moiety to the cyanostyryl thiophene luminescent core that is conducive for stabilizing liquid crystalline phases.[10,11] Liquid crystals with luminescent properties are demonstrated to be an ideal class of functional materials for the next generation of electronic and optoelectronic devices.[12] Inducing liquid crystallinity to luminescent cores or doping fluorescent dyes into the mesophase has been the strategy to obtain luminescent liquid crystals.[13-16] In addition to the liquid crystalline properties, the present report aims to demonstrate the multistimuli responsive emission behaviour in **CS-1** and **CS-2** and explores the structural origin of observed switchable emission properties.

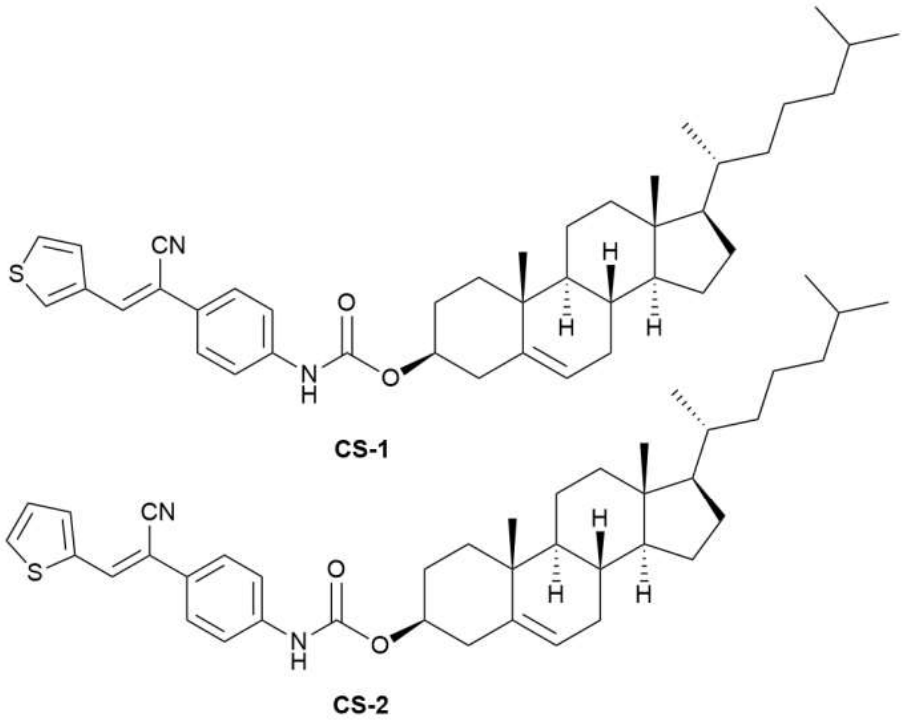

Scheme 5.1: Structure of cholesterol functionalized cyanostyrylthiophene derivatives, **CS-1** and **CS-2**.

5.4 Experimental Section

Solvents and chemicals for the synthesis and photophysical studies were purchased from Sigma Aldrich, Alfa Aeser, TCI and used without further purification. The ^{1}H NMR and ^{13}C NMR spectra were obtained from a Bruker Avance 400 MHz spectrometer operating at room temperature. Photoluminescence spectra and lifetime experiments were performed using Fluorolog-3 with TCSPC spectrofluorometer (model FL 3C-221). The mass spectra of the compounds were recorded on a Waters Xevo G2 XS QToF mass spectrometer. The single crystal X-ray diffraction data of **CS-1** was collected on Bruker D8 Venture diffractometer attached with PHOTON II detector with CMOS-sensor. The data collection was conducted at room temperature using CuK α ($\lambda = 0.15418$ nm) radiation operated at 50 kV and 40 mA. The powder X-ray diffraction data was collected using PANalytical X'Pert3 Powder X-ray diffractometer

5.4.1. *Synthesis of 2,3,4,7,8,9,10,11,12,13,14,15,16,17-tetradecahydro-10,13-dimethyl-17-(6-methylheptan-2-yl)-1H-cyclopenta[a]phenanthren-3-yl 4 (cyanomethyl) phenylcarbamate, 1*

The compound **1** was synthesized following the reported procedure.[12] 2-(4-aminophenyl) acetonitrile (5 mmol) is dissolved in minimum quantity of dichloromethane and cooled to 0 ^{0}C in an ice bath. The cholesterol chloroformate (4.8 mmol) was added to the reaction mixture followed 0.5 ml pyridine and stirring was continued for 6 hours. The reaction mixture was washed with water and extracted with dichloromethane. Combined organic layers were washed with brine, and dried over Na_2SO_4. Solvent was evaporated and the residue was purified by column chromatography on silica gel using hexane ethyl acetate (4/1) as eluent to afford compound **1** as a colourless crystalline solid on re-crystallization form ethyl acetate. The product was characterized using ^{1}H NMR and ^{13}C NMR spectroscopy (Figure 5.1 and 5.2).

Yield: 87 %, ^{1}H NMR (400 MHz, CDCl3) δ (ppm): 0.67 (s, 3H), 0.87 (m, 6H), 0.91 (t, *J* = 6 Hz, 3H), 0.98 (m, 6H), 1.13 (m, 7H), 1.29 (m, 4H), 1.47 (m, 5H), 1.62 (m, 1H), 1.91 (m, 5H), 2.38 (m, 2H), 3.69 (s, 2H), 4.59 (m, 1H), 5.40 (m, 1H), 6.57 (s, 1H), 7.24 (d, *J* = 8 Hz, 3H), 7.38 (d, *J* = 12 Hz, 2H).

^{13}C NMR (400 MHz, $CDCl_3$) δ (ppm): 11.87, 18.71, 19.34, 21.04, 22.57, 22.83, 23.02, 23.83, 24.29, 28.02, 28.07, 28.24, 31.86. 35.80, 36.18, 36.57, 39.51, 39.72, 42.31, 49.99, 56.12, 56.68, 75.18, 117.94, 119.00, 122.87, 124.38, 128.64, 137.99, 139.49, 152.90.

5. 4.2 General method for the synthesis of the compounds CS-1and CS-2.

The compounds **CS-1** and **CS-2** were synthesized by adopting reported procedures incorporating suitable modifications (Scheme 5.2).[13] The compound **1** (545 mg, 1 mmol) and thiophene-2-carbaldehyde or thiophene-3-carbaldehyde (1 mmol) were dissolved in

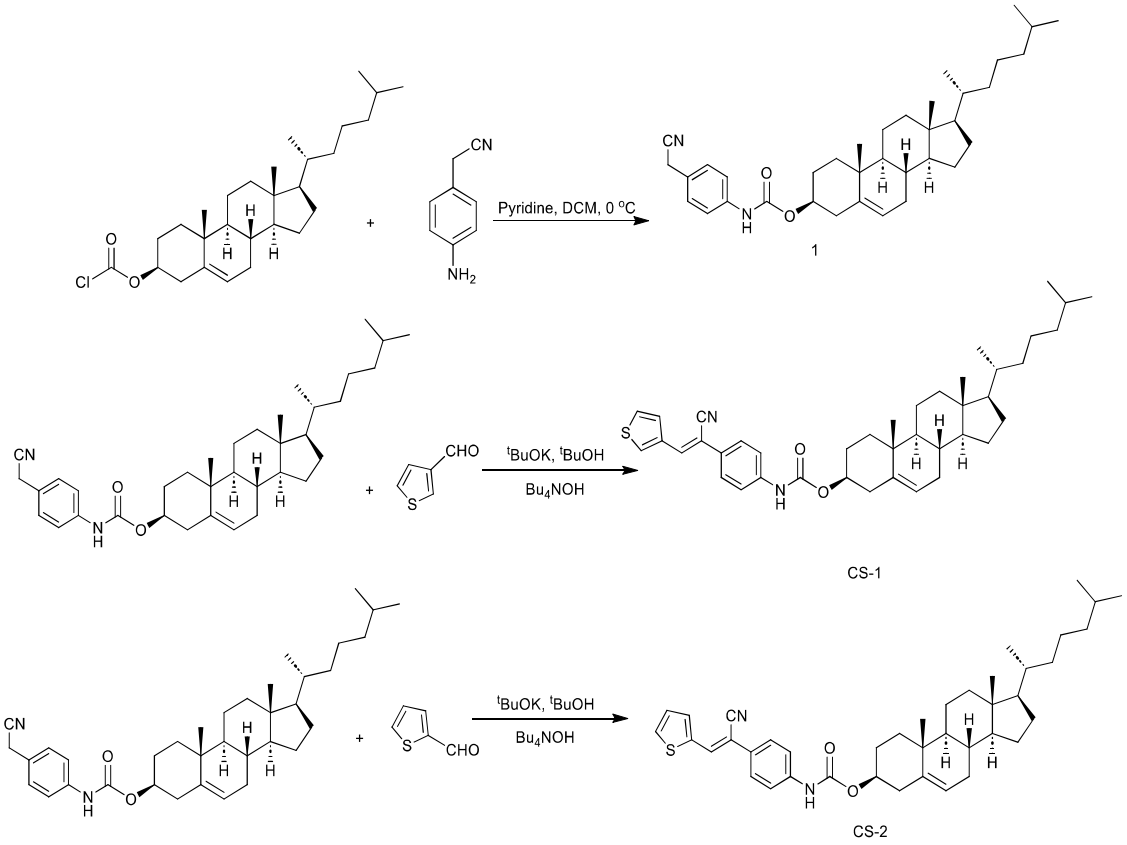

Scheme 5.2: Synthetic route to **CS-1** and **CS-2**

a mixture of ^{t}BuOH (11 ml) and THF (5 ml) at 50 °C. ^{t}BuOK (0.11 ml of a 1 M solution in THF, 0.11 mmol) and n-Bu_4NOH (1 ml of a 1 M solution in MeOH, 1 mmol) were added. An orange precipitate started to form immediately and was stirred for 15 minutes at 70 °C. The reaction mixture was cooled to room temperature and poured into acidified methanol (50 ml containing 1 drop of conc.CH_3COOH). The resulting precipitate was filtered and washed with methanol. The compounds were further re-precipitated 5 times from dichloromethane solutions by adding excess methanol and the products were charecterized by ^{1}HNMR, ^{13}CNMR (Figure 5.3 to 5.6) and mass spectral analysis.

Compound CS-1: Yield: 87 %, M.P. 188 ^{0}C, ^{1}H NMR (400 MHz, CDCl3) δ (ppm): 0.69 (s, 3H), 0.86 (d, 3H, *J* =1.84 Hz), 0.88 (d, 3H, *J* = 1.84 Hz), 0.92 (d, 3H, *J* = 6.52 Hz), 0.99 (m, 3H), 1.04 (s, 4H), 1.13 (m, 7H), 1.24 (m, 2H), 1.35 (m, 3 H), 1.49 (m, 5H), 1.66 (m, 1H), 1.86 (m, 2H), 1.99 (m, 3H), 2.42 (m, 2H), 4.62 (m, 1H), 5.42 (m, 1H), 6.66 (s,

1H), 7.41 (m, 1H), 7.47 (d, 2H, *J* = 1.96Hz), 7.59 (m, 2H), 7.76 (dd, 1H, *J* = 5.16Hz and 1.32 Hz), 7.92 (m, 1H).

^{13}C NMR (400 MHz, CDCl3) δ (ppm) 11.87, 18.72, 19.34, 21.05, 22.57, 22.83, 23.84, 24.29, 28.02, 28.23, 31.87, 31.91, 35.80, 36.18, 36.58, 36.95, 38.42, 39.52, 39.72, 42.32, 50.00, 56.13, 56.68, 75.31, 109.36, 118.45, 118.67, 122.92, 126.54. 126.63, 127.33, 128.95, 129.02, 134.05, 136.11, 138.87, 139.47, 152.69. HRMS (ESI) m/z calculated 638.3906; Found: 639.4040 $[M+H]^+$.

Compound CS-2: Yield: 83 %, M.P. 179 ^{0}C, ^{1}H NMR (400 MHz, CDCl3) δ (ppm): 0.69 (s, 3H), 0.88 (m, 6H), 0.93 (t, 3H, *J* = 6Hz), 1.01 (m, 6H), 1.12 (m, 7H), 1.30 (m, 5H), 1.48 (m, 5H), 1.63 (m, 2H), 1.92 (m, 5H), 2.41 (m, 2H), 4.62 (m, 1H), 5.41 (d, 1H, *J* = 4Hz), 6.68 (d, 1H, *J* = 4Hz), 7.15 (m, 1H) 7.45 (m, 1H), 7.47 (m, 1H), 7.53 (t, 1H, *J* = 4Hz), 7.58 (t, 2H, *J* = 8Hz), 7.65 (t, 1H, *J* = 4Hz).

^{13}C NMR (400 MHz, CDCl3) δ (ppm) 11.87, 18.72, 19.34, 21.05, 22.57, 22.83, 23.84, 24.29, 28.02, 28.24, 31.87, 31.91, 35.80, 36.18, 36.58, 36.95, 38.42, 39.52, 39.72, 42.32, 50.00, 56.13, 56.68, 75.31, 107.79, 118.17, 118.70, 122.93, 126.49, 127.83, 128.65, 129.68, 132.00, 132.87, 138.08, 138.91, 139.47, 152.78. HRMS (ESI) m/z calculated 638.3906; Found: 639.3990 $[M+H]^+$.

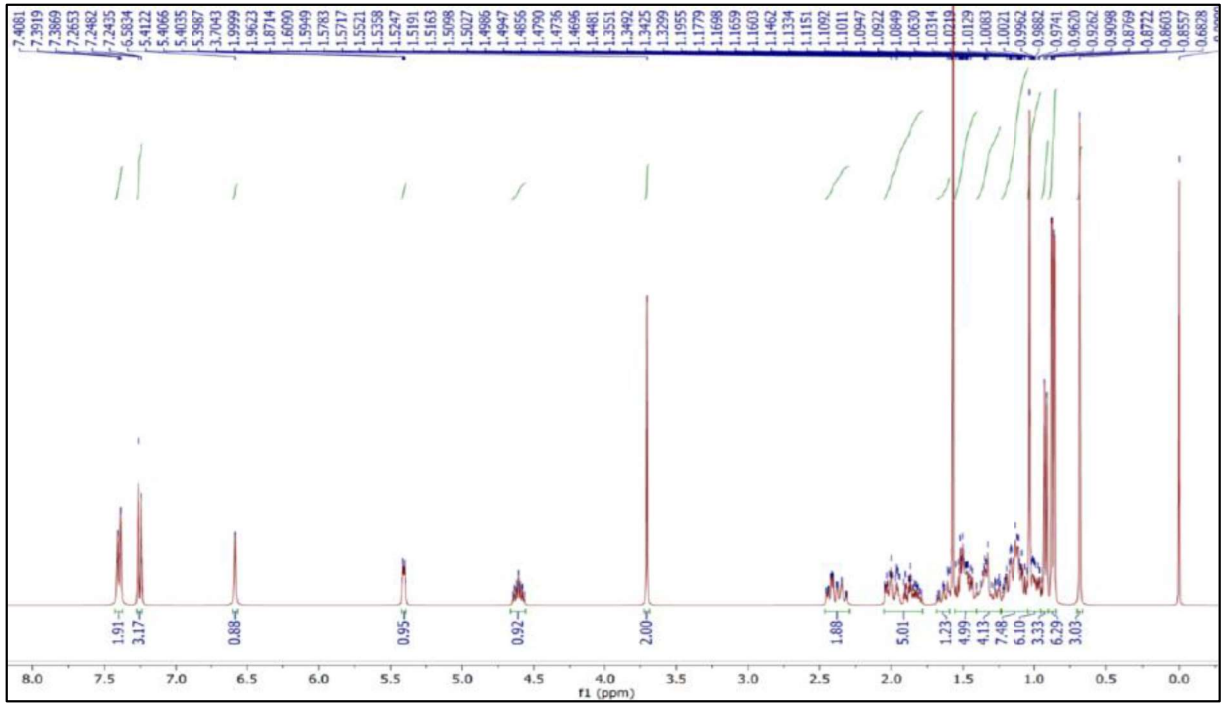

Figure 5.1: ^{1}H NMR spectra of Cholesterol appended 2-(4-aminophenyl)acetonitrile, **1** in $CDCl_3$

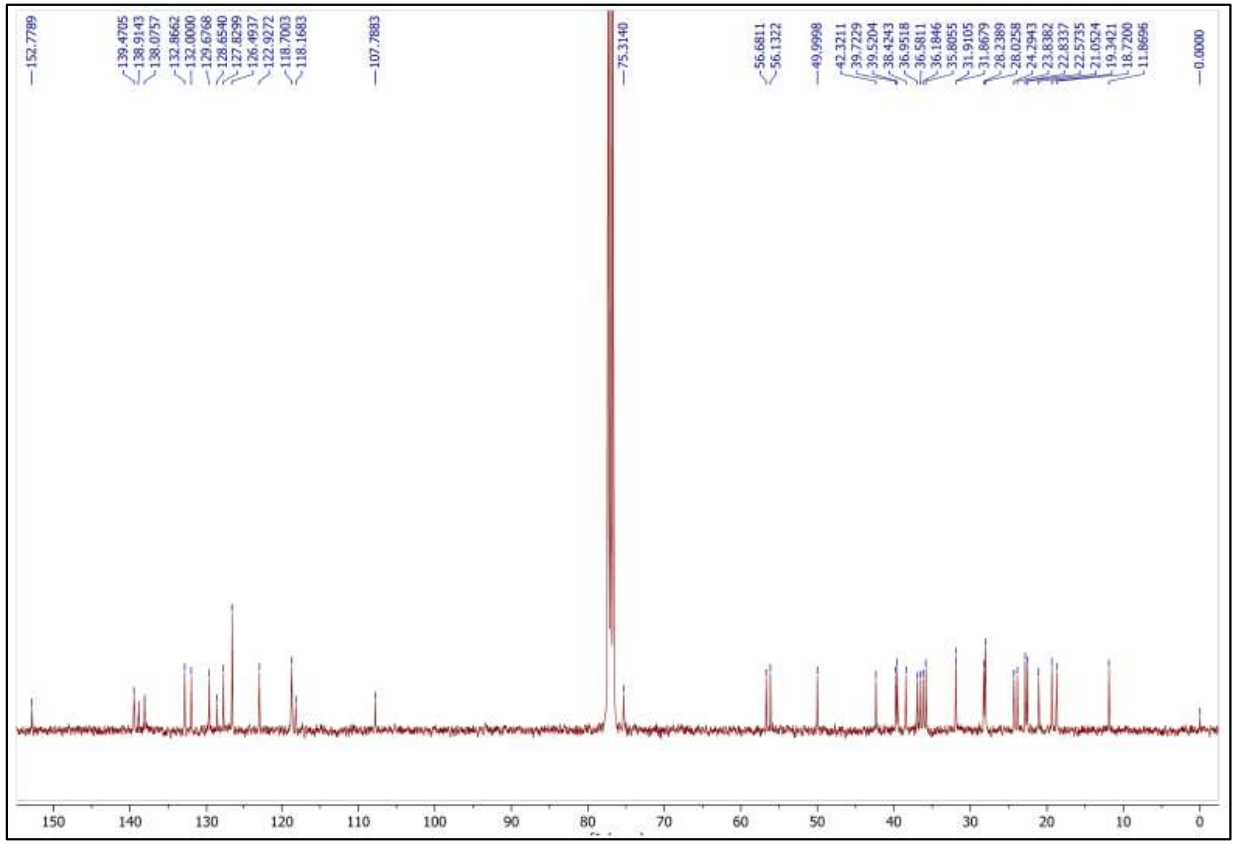

Figure 5.2: ^{13}C NMR spectra of Cholesterol appended 2-(4-aminophenyl)acetonitrile, **1** in $CDCl_3$

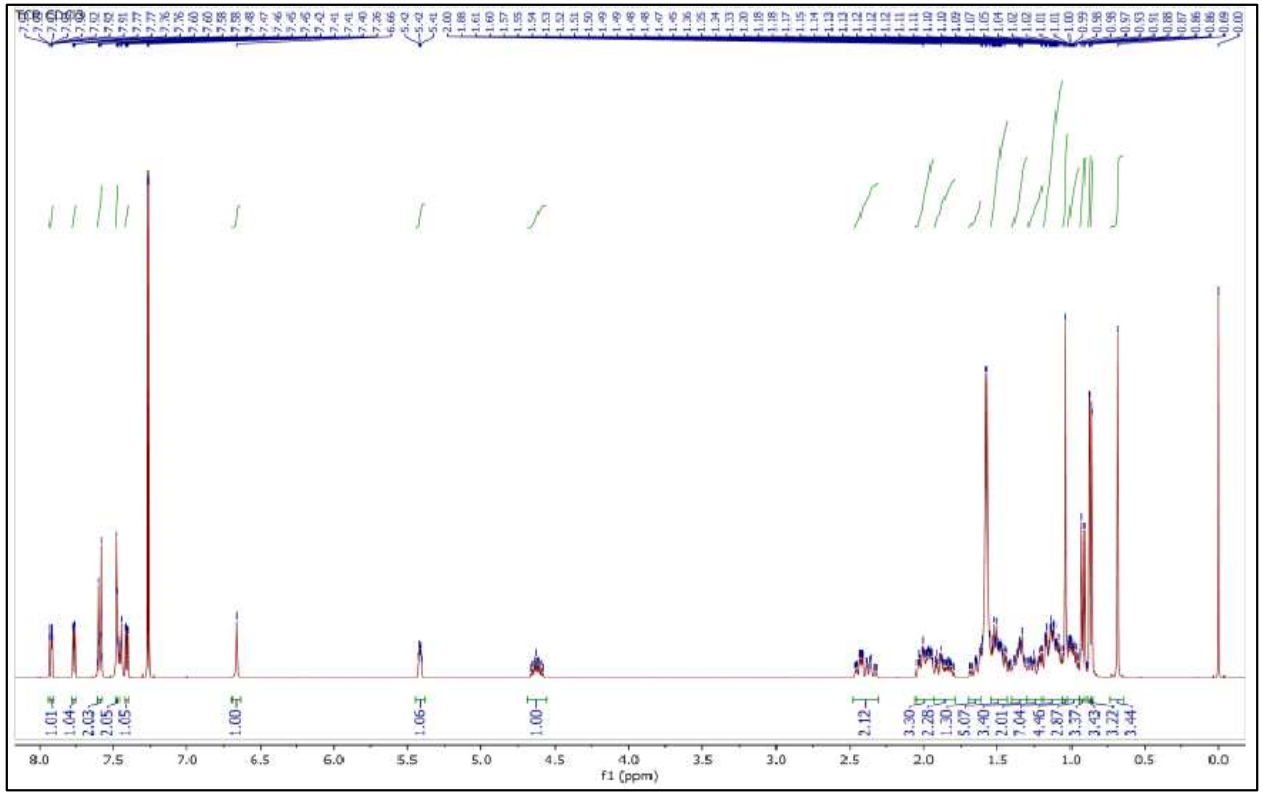

Figure 5.3: ^{1}H NMR spectra of **CS-1** in $CDCl_3$

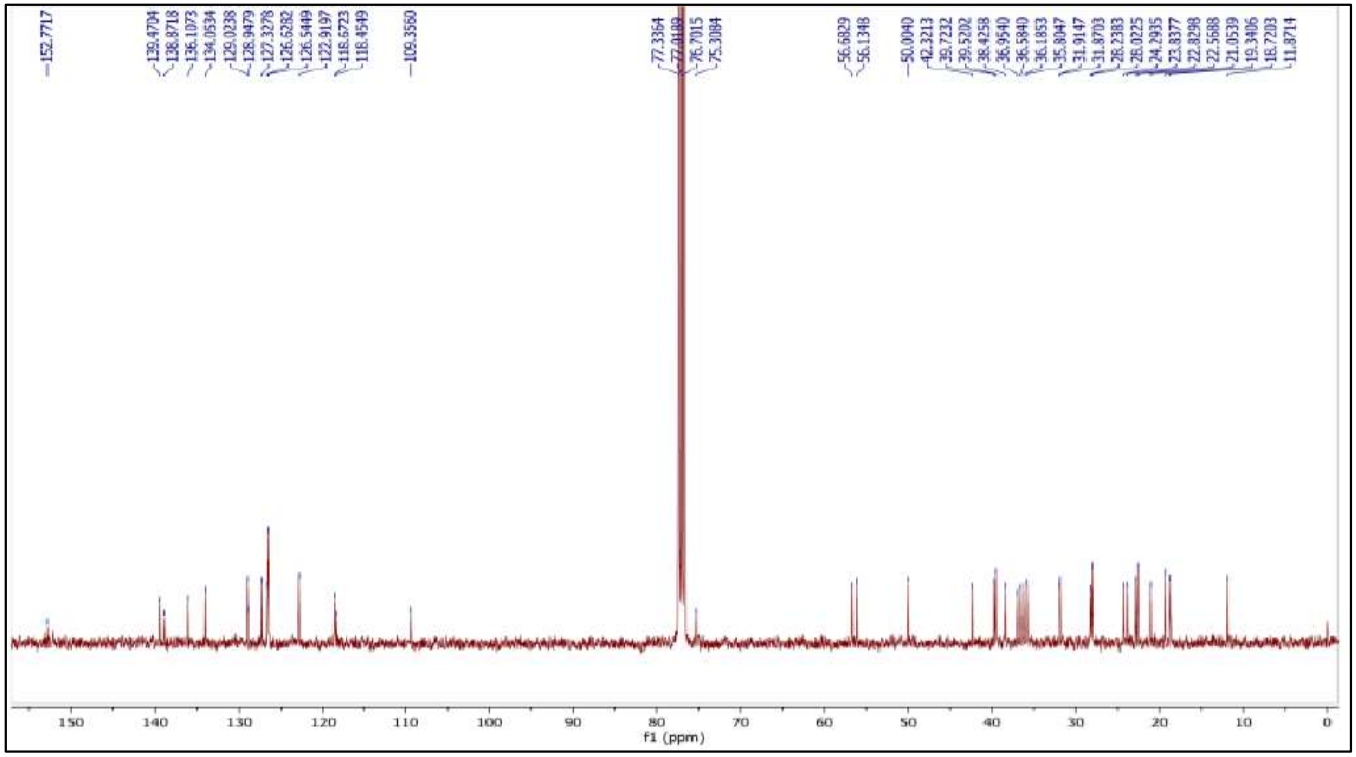

Figure 5.4: ^{13}C NMR spectra of CS-**1** in $CDCl_3$

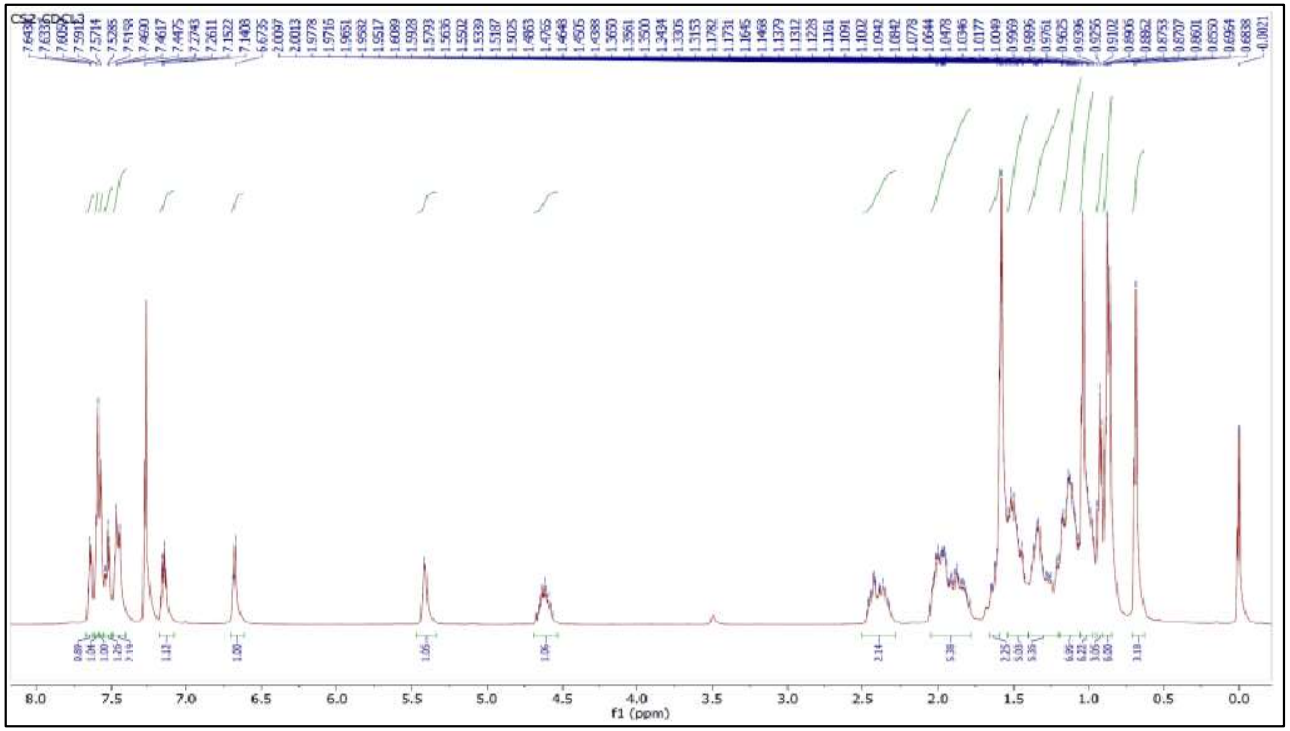

Figure 5.5: ^{1}H NMR spectra of **CS-2** in $CDCl_3$

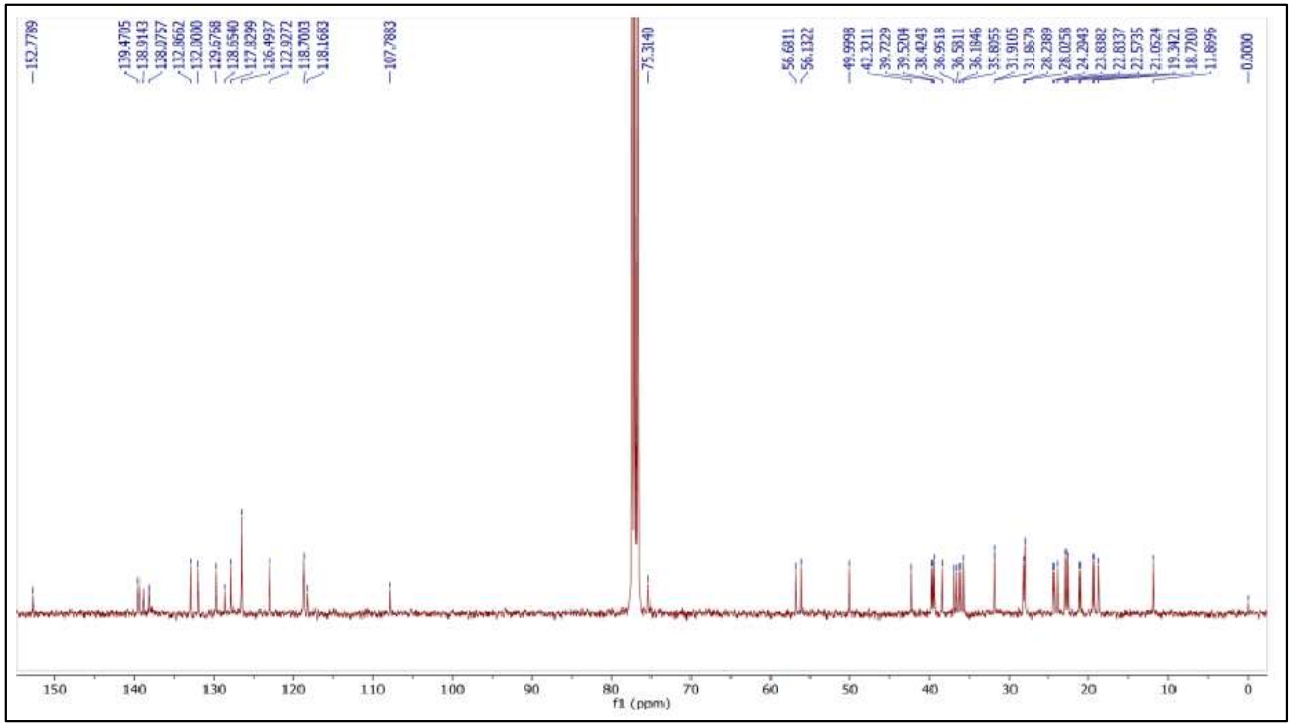

Figure 5.6: ^{13}C NMR spectra of **CS-2** in $CDCl_3$

5. 5 Results and Discussion

5.5.1 Solution and solid state photophysical characterization

The absorption spectra of compound **CS-1** and **CS-2** were recorded from their dilute solutions in THF (1 μM) and the spectra showed single band centered at 343 nm and 363 nm respectively (Figure 5.7). The UV-visible absorption spectra showed a shift in the absorption maximum attributed to the difference in conjugation length originating from positional isomerism. Figure 5.8 shows the fluorescence spectra of compound **CS-1** and **CS-2**

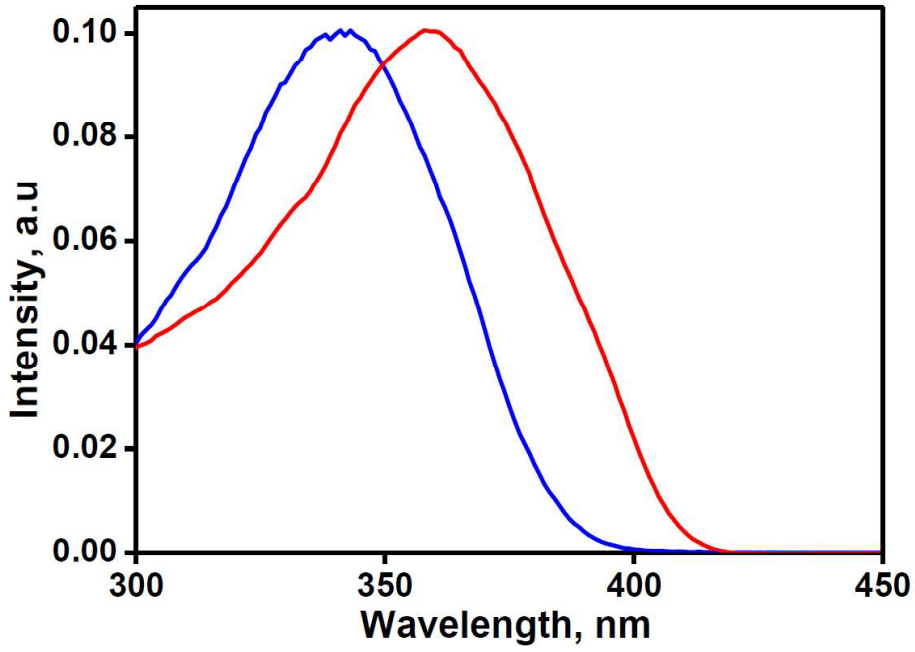

Figure 5.7: UV-visible absorption spectra of **CS-1** (blue curve) and **CS-2** (red curve) in THF (1 μM)

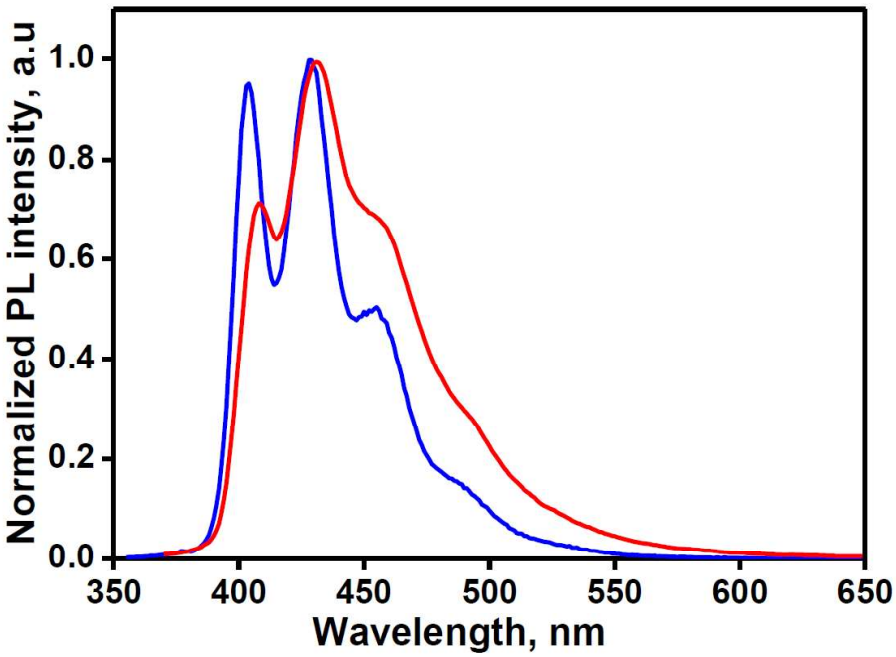

Figure 5.8: Solution state emission spectra of **CS-1** (blue) and **CS-2** (red) (λ_{ex} = 370 nm) in THF (1 μM).

recorded by exciting at 370 nm. The compound **CS-1** showed multiple bands centered at 404 nm, 430 nm, and 455 nm respectively and a comparable emission spectrum with a negligible wavelength shift was observed for **CS-2**. The observed shoulders besides the emission maximum in the emission spectra of **CS-1** and **CS-2** can be attributed to the emission from different vibrational levels. Figure 5.9a shows the emission spectra recorded on pristine solid samples of **CS-1** and **CS-2** by exciting at 370 nm. The compound **CS-1** showed a single band centered at 475 nm while **CS-2** showed two bands centered respectively

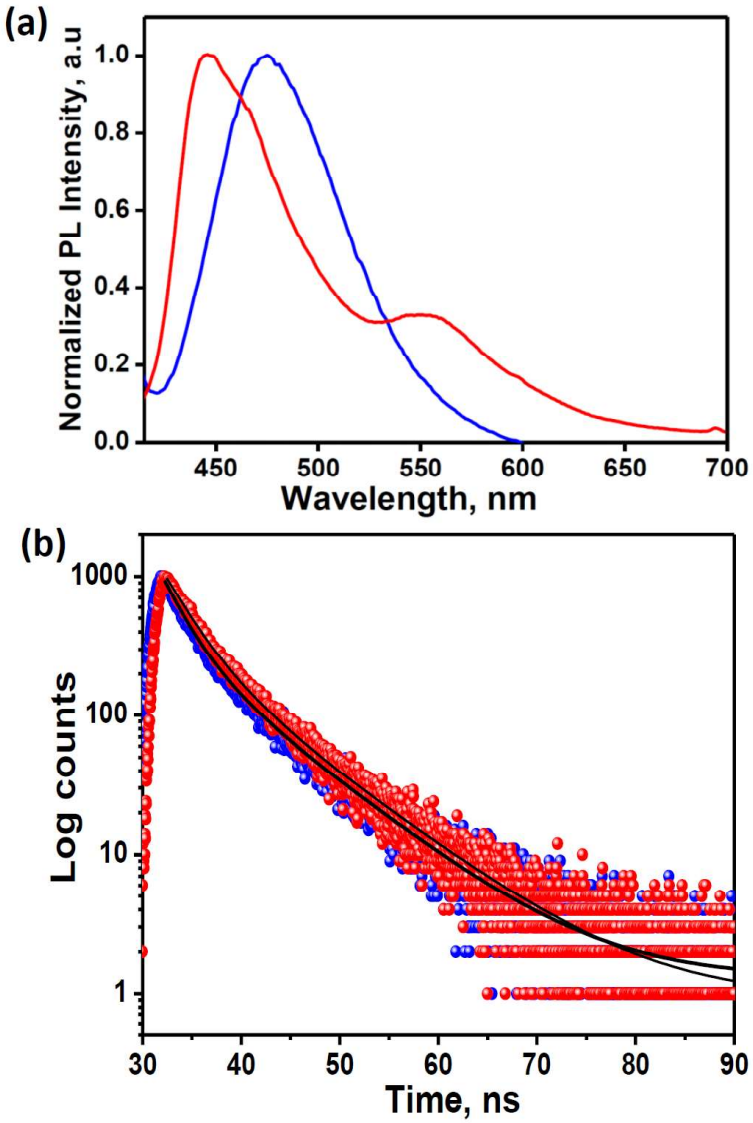

Figure: 5.9 (a) Solid state emission spectra of **CS-1** (blue) and **CS-2** (red) (λ_{ex} = 370 nm) and **(b)** Transient decay of emission recorded for **CS1** (blue, λ_{ex}= 370 nm, λ_{em}= 430 nm,) and pristine **CS2** (red, λ_{ex}= 370 nm, λ_{em}= 428 nm,) from THF solutions

at 447 nm and 555 nm with broad emission towards longer wavelength region. The red shift in the solid state emission spectra of **CS-1** and **CS-2** in comparison to that recorded from their solutions in THF can be attributed to the formation of aggregates in the solid-state. To explore the solution state emission properties of **CS-1** and **CS-2** in detail, the emission quantum yield and lifetime were recorded from dilute solutions of compounds in THF. Both the compounds showed comparable lifetime (Table 5.1 and Figure 5.9b) and quantum yield values. The lower quantum yield and radiative decay rate constants for **CS-1** (Φ_F = 0.013, k_{nr} = 5. 39 x10^{-3} ns^{-1}) and **CS-2** (Φ_F = 0.015, k_{nr}=5. 24 x10^{-3} ns^{-1}) represents the weakly emissive nature of the compounds in solution.

Table 5.1: Fluorescence wavelength maximum, fluorescence quantum yield, and an average lifetime of different emitting states of **CS-1**, and **CS-2**. Radiative and non-radiative rates (k_F, k_{nr}) were calculated using the equation $k_F = \phi_F/\tau_F$ and $\tau_F = (k_F + k_{nr})^{-1}$ (Sol-Solution)

Phases	λ_{em} (nm)	ϕ_F	τ_F (ns)	k_r (ns^{-1})	k_{nr} (ns^{1})
CS-1 Sol	430	0.013	2. 42	5.38 x10^{-3}	0.41
CS-2 Sol	428	0.015	2.86	5.24 x10^{-3}	0.34
CS-1	474	0.45	0.85	0.54	0.65
CS-1M	495	0.13	1.01	0.13	0.86
CS-2	447	0.30	0.10	3.00	7.18
CS-2G	472	0.63	0.18	3.45	2.05
CS-2M	492	0.68	0.34	2.01	0.95

5. 5.2. Aggregation induced emission in CS1 and CS2

To corroborate the aggregation induced red shifted emission in the solid of **CS-1** and **CS-2**, the compounds were tested for similar behavior in their solution phase by mixing different fractions of water in THF solution. Figure 5.10a shows the emission spectra of **CS-1** recorded from the solutions in THF/water mixtures by varying the water fraction from 0 to 90 %. It is noteworthy that the spectral intensity was decreased on increasing the water fraction up to 50 % and a concomitant intensity enhancement was made in the case of **CS-1** with a red shift in emission maximum on increasing the water fraction above 50 % (Figure 5.10). There is an enhancement in the emission intensity of **CS-1** on increasing in poor solvents like water. A similar observation was made in the case of **CS-2** with a red shift in emission maximum (Figure 5.10b). The comparison of emission intensity for THF solution containing a water fraction of 90 % to pure THF solution showed 2.2 and 1.3-times intensity enhancement for compounds **CS-1** and **CS-2** respectively (Figure 5.11). The observed intensity enhancement at high concentrations of poor solvents like water is due to the formation of aggregates in solutions, where this is a clear evidence of aggregation induced enhanced emission (AIEE) in **CS-1** and **CS-2**.

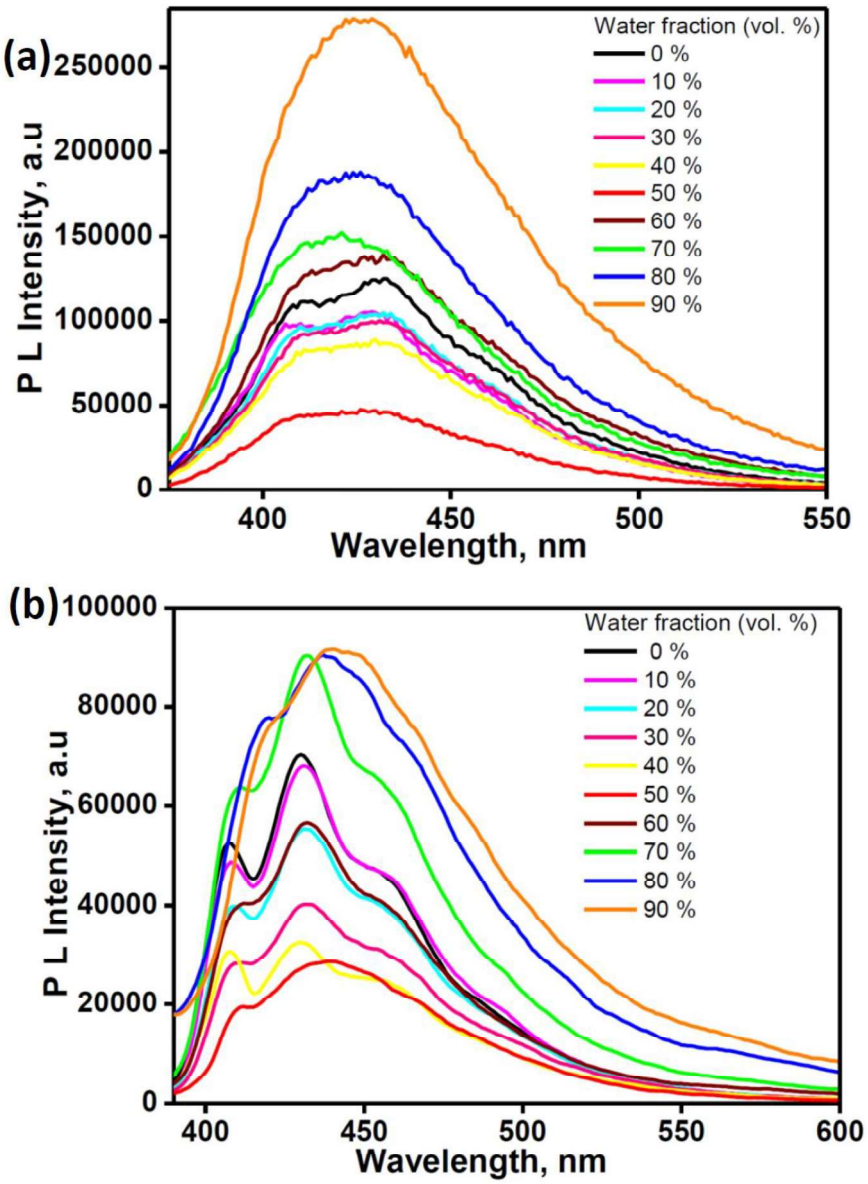

Figure 5.10 Emission spectra of (a) **CS-1** and (b) **CS-2** recorded in THF/water mixtures (50 μM) by varying the water fraction. (λ_{ex} = 370 nm.

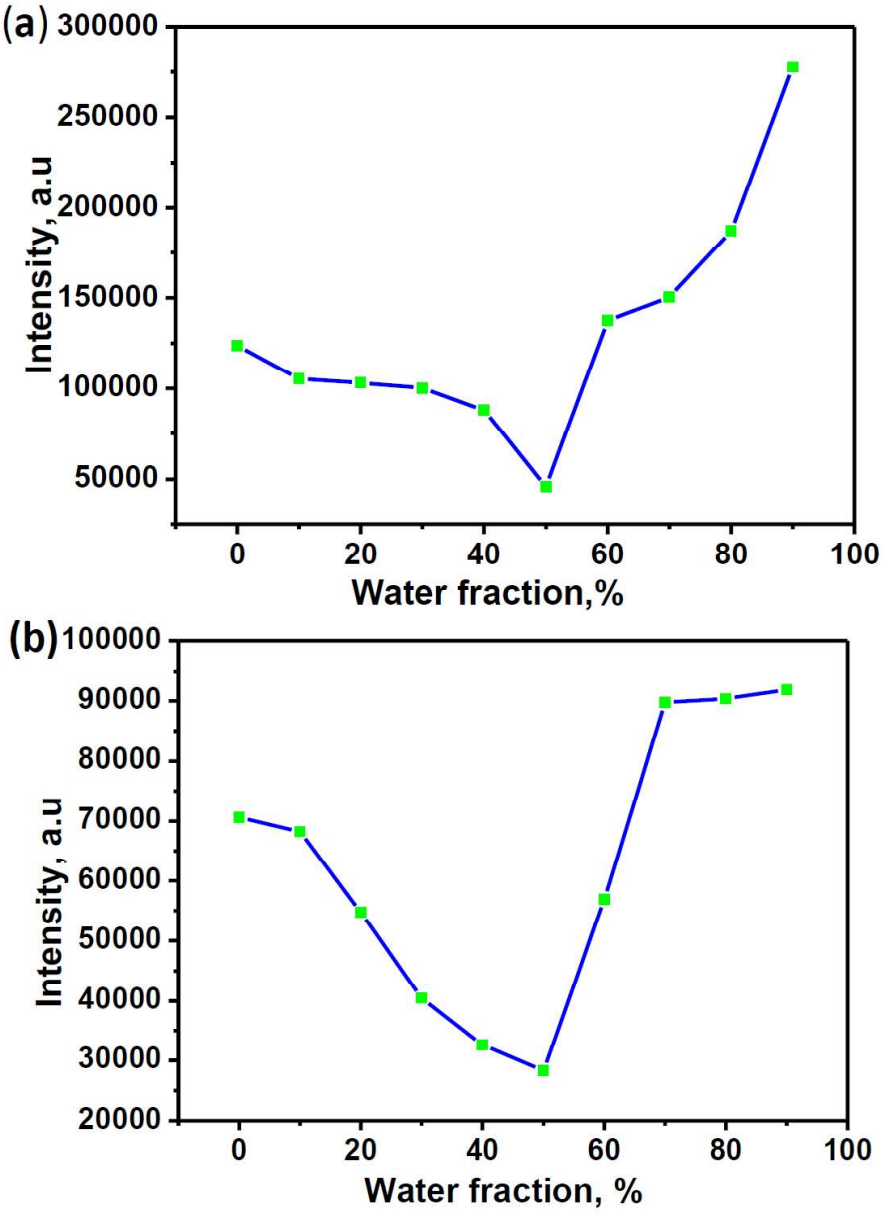

Figure 5.11: Fluorescent intensity in response of (a) **CS-1** and (b) **CS-2** to the changes of water fractions in THF-H_2O mixture.

5.5.3. Stimuli-responsive emission in CS-1 and CS-2

To explore the stimuli responsive emission in molecules **CS-1** and **CS-2** the pristine samples of both compounds were subjected to multiple stimuli. Figure 5.12 shows the emission spectra recorded for the pristine **CS-1** and melt solidified sample of **CS-1** (**CS-1M**). A striking observation can be made from the spectra that the melt solidified samples (red curve) show a red-shifted emission in comparison to the emission from the pristine sample (blue curve) with a corresponding change in emission colour from cyan to bluish green under 365 nm light (Figure 5.12a and Figure 5.13a). The red shift in emission from melt solidified sample can be attributed to the heat induced phase modification with a different molecular arrangement as compared to pristine **CS-1**. Figure 5.13b shows the stimuli responsive emission switching in compound **CS-2**. In contrast to **CS-1**, compound **CS-2** respond to multiple stimuli such as heat, mechanical stress, and solvent vapours. The pristine sample of **CS-2** showed a spectrum with two major bands centered at 436 nm and 551 nm (blue curve) with blue emission colour under 365 nm illumination (Figure. 5.12b), while the sample with applied shear stress (**CS2-G**) showed a red shift in spectrum with emission maximum centered at 474 nm (green curve) and bluish green emission colour. The compound **CS-2** after melt processing (**CS-2M**) showed a maximum redshift in emission spectrum centered around 495 nm with broad emission towards the longer wavelength side along with a green colour emission compared to the pristine

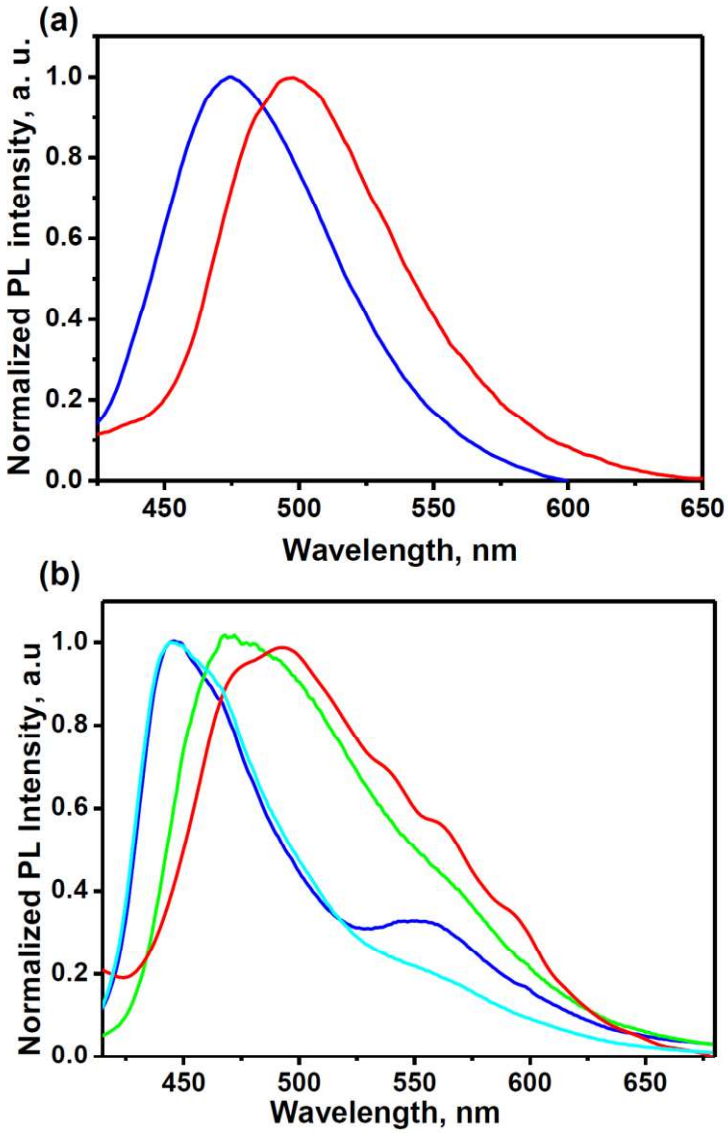

Figure 5.12: Stimuli responsive emission in compounds **CS-1** and **CS-2**: (a) Emission from a pristine sample of **CS-1** (blue) and emission from melt solidified **CS-1** (**CS-1M**, red**)**. (b) Emission from a pristine sample of **CS-2** (blue curve), melt solidified **CS-2** (**CS-2M**, red) and ground sample of **CS-2** (**CS-2G**, green) and emission from sample obtained on exposure to methanol vapours (cyan).

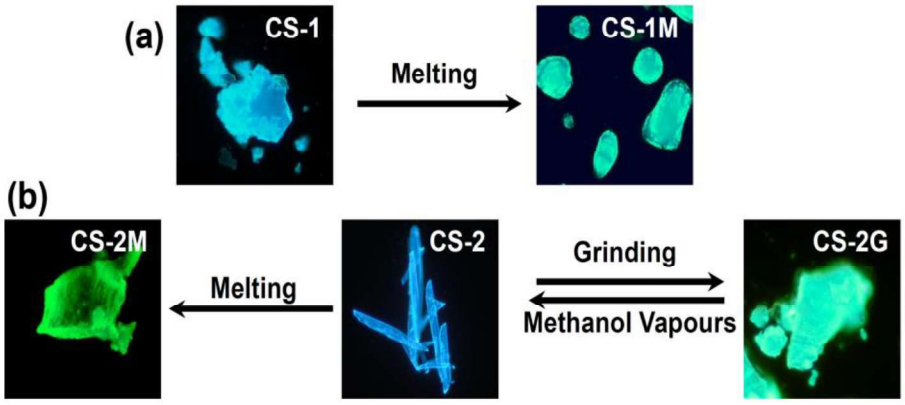

Figure: 5.13: Fluorescent microscopic images of different phases of (a) **CS-1** and (b) **CS-2** samples under different stimuli (λ_{ex} = 365 nm).

sample. The ground sample **CS-2G** showed a methanol vapour induced recovery with emission comparable to that of pristine sample of **CS-2** (Figure. 5.12b and Figure 5.13b (cyan curve).

5.5.4 Comparison of photophysical properties of different phases of CS-1 and CS-2.

The observed switchable emission properties under various stimuli can be explored by analyzing the photophysical parameters such as emission lifetime and quantum yield of different phases. Table 5.1 shows the photophysical parameters of compounds **CS-1** and **CS-2** and their other emissive phases formed by applying stimuli such as heat and shear stress. It is noteworthy that phase **CS-1M** showed a sharp decrease in emission quantum yield in comparison to the pristine **CS-1**, while the fluorescence lifetime of both phases was comparable (Table 5.1 and

Figure 5.14a). Comparatively high nonradiative decay constant (k_{nr}= 0.86 ns^{-1}) in **CS-1M** can be attributed to various quenching pathways

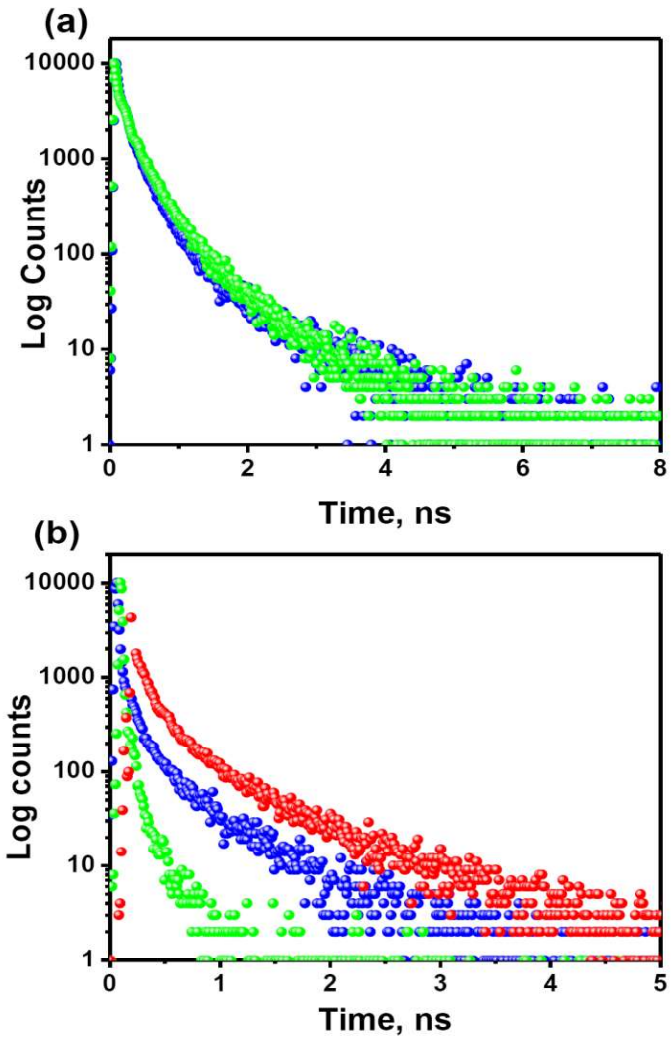

Figure 5.14: (a) Transient decay of emission (λ_{ex} = 370 nm) (a) pristine **CS1** (blue, λ_{em} = 474 nm) and melt solidified sample **CS-1M** (green, λ_{em} = 495 nm) (b) pristine **CS2** (blue, λ_{em} = 447 nm), melt solidified sample **CS-2M** (red, λ_{em} = 492 nm), and ground sample **CS-2G** (green, λ_{em} = 472 nm).

operating in this phase which in turn reflected in decreased emission quantum yield. Figure 5.14b shows the transient decay of fluorescence in different phases of **CS-2**. The various phases of **CS-2** showed appreciable differences in lifetime and quantum yield (Table 5.1). The phases **CS-2M** and **CS-2G** showed a twofold increase in quantum yield in comparison to **CS-2** (Table 5.1). The relatively higher k_r value in comparison to k_{nr} values of **CS-2M** and **CS2-G** is reflected in the enhanced quantum yield of these phases. The pristine **CS-2** with a higher k_{nr} value showed a lower emission quantum yield. The broad emission spectra with enhanced emission quantum yield and lifetime of **CS-2M** and **CS-2G** under applied stimuli can be due to the formation of amorphous states with different types of molecular arrangement with varying levels of dipolar coupling.[21]

5.5.5. Analysis of powder and single crystal X-ray diffraction data

To unravel the mechanism behind the stimuli responsive emission switching in **CS-1** and **CS-2** the powder X-ray diffractograms were recorded on different phases of **CS-1** and **CS-2**. Figure 5.15a shows the powder X-ray diffractograms recorded for **CS-1** (red curve), **CS-1M** (blue curve), and the diffractogram simulated from single crystal X-ray diffraction data (black curve). The diffractogram of **CS-1M** showed a dissimilar diffraction pattern in comparison to the pristine **CS-1** indicating that both **CS-1** and **CS-1M** comprise different crystalline phases thereby resulting in different solid-state emissions. The notable changes in diffractograms indicate that

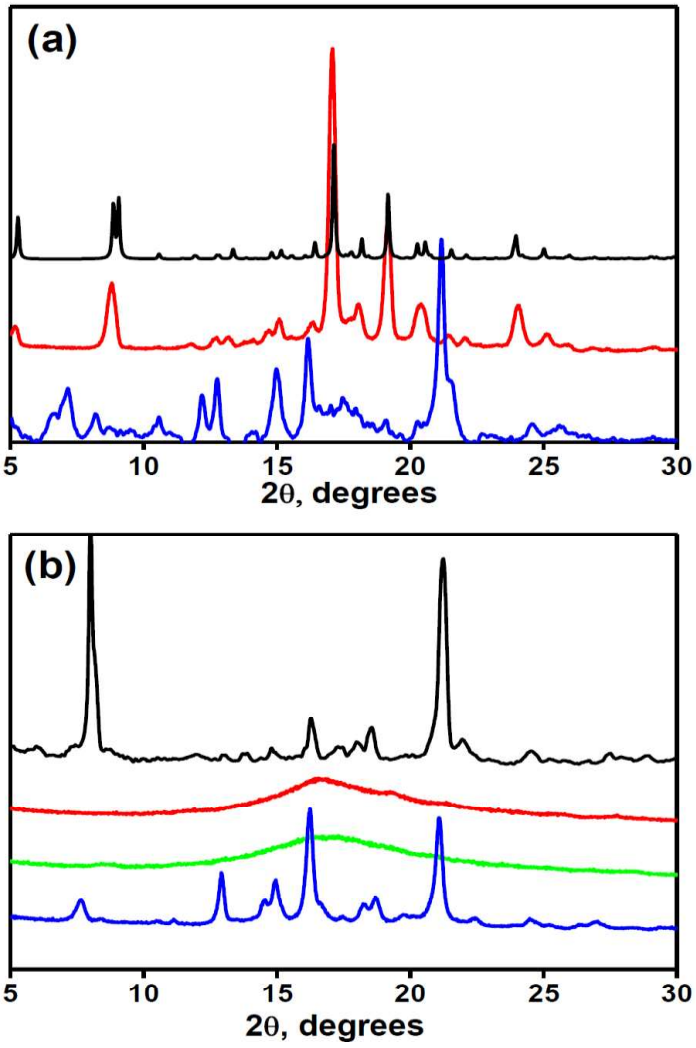

Figure 5.15: Powder X-ray diffractograms of (a) pristine sample of **CS-1**, (blue) **CS-1M** (red) and diffraction pattern simulated from single crystals X-ray diffraction data of **CS-1** (black). (b) Pristine sample of **CS-2** (blue) **CS-2G** (green) **CS-2M** (red) and solvent recovered **CS-2** (black).

the crystalline structure in **CS-1** is changed on thermal treatment resulting in **CS-1M** with red shifted emission. Remarkably, the diffractogram of the melt solidified sample closely resembles the powder X-ray diffractogram simulated from single crystal X-ray diffraction data (black curve), where this is a clear indication of comparable molecular arrangement in **CS-1M** and single crystals of **CS-1**. Figure 5.15b shows the powder X-ray diffractograms recorded on different phases of **CS-2**. The pristine **CS-2** showed a crystalline nature as indicated by the sharp peaks present in the diffractogram (blue curve) while the diffractograms recorded for the ground (**CS-2G**, green curve) and melt solidified (**CS-2M**, red curve) phases were featureless. The **CS-2G** exposed to methanol vapours showed the recovery of pristine CS-2 (Figure 5.15b, black curve) as indicated by the comparable diffraction patterns. From the comparison of powder X-ray diffractograms, it is evident that the emission switching in **CS-2** under shear stress and thermal treatment is attributed to the crystal to amorphous transition, while the emission recovery under methanol vapours is due to the amorphous to crystalline transition.

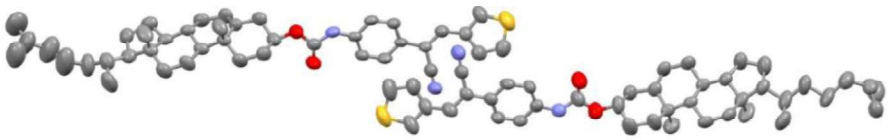

Figure 5.16: ORTEP plot of the asymmetric unit present in the single crystals structure of **CS-1** (ellipsoids are drawn at 50 % probability, and hydrogen atoms are removed for clarity).

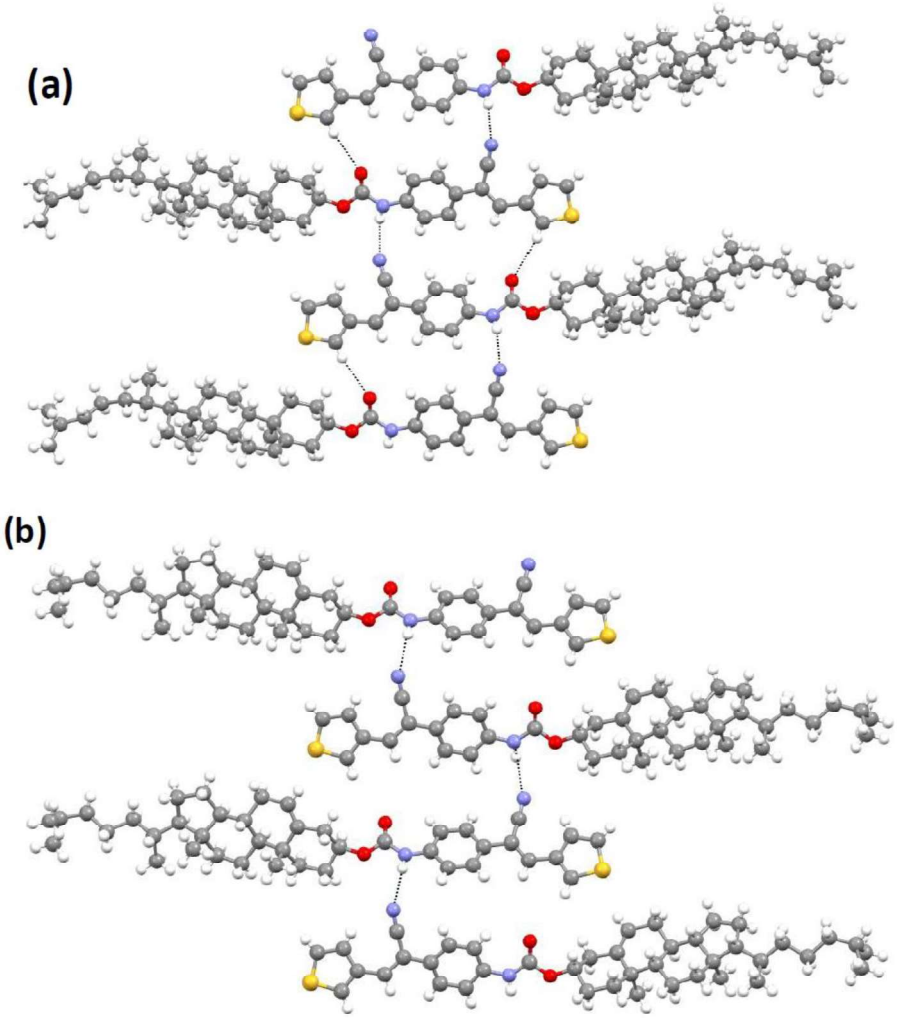

Figure 5.17: Intermolecular interactions present in alternating molecular layers found in the crystal structure of **CS-1**.

To study the structure and molecular packing of conformation in solid state, single crystal X-ray diffraction studies were conducted on crystals of **CS-1** (Table 5.2). The compound **CS-1** resulted in good quality single crystals on slow evaporation from a dilute solution in toluene while the crystallization of **CS-2** did not result in quality single crystals. The molecule **CS-1** crystallized in $P2_1$ space group with two

Table 5.2: Crystallographic and structure refinement details of **CS-1**.

Empirical formula	C41 H54 N2 O2 S
Formula weight	638.92
Temperature	296(2) K
Wavelength	0.71073 Å
Crystal system	Monoclinic
Space group	P 21
Unit cell dimensions	a = 18.357(11) Å α= 90°. b = 12.475(7) Å β= 115.78(2) ° c = 18.564(13) Å γ= 90°.
Volume	3828(4) $Å^3$
Z	4
Density (calculated)	1.109 Mg/m^3
F (000)	1384
Crystal size	0.396 x 0.189 x 0.114 mm^3
Theta range for data collection	2.464 to 25.496°.
Index ranges	-22<=h<=22, -15<=k<=15, -22<=l<=22
Reflections collected	108710
Independent reflections	14206 [R(int) = 0.0836]
Completeness to theta = 25.242°	99.7 %
Max. and min. transmission	0.7455 and 0.6707
Goodness-of-fit on F^2	1.107
Final R indices [I>2sigma(I)]	R1 = 0.0703, wR2 =0.1309
R indices (all data)	R1 = 0.1327, wR2 =0.1616
Largest diff. peak and hole	0.354 and -0.201 e.$Å^{-3}$
CCDC NO	2293176

complete molecules in the asymmetric unit (Figure 5. 16). The molecules showed different level twists in the cyanostyrylthiophene unit with an angle of 26^0 and 23^0. The molecules pack in layers with different types of hydrogen bonding interactions in alternate layers. Figure 5. 17 shows the hydrogen bonding interaction in one of the layers where the molecules show an anti-parallel arrangement connected through NH···N (H···N, 2.307 Å) and CH···O (H···O, 2.704 Å) interactions. The second molecular layer showed a single NH···N (H···N, 2.257 Å) interaction between the molecules (Figure 5.17b). The molecular packing of **CS-1** showed a slipped arrangement of molecules along the molecular long axis.

5.5.6. Liquid crystalline properties

The most commonly used method to study the liquid crystalline properties of compounds is the polarizing optical microscopy (POM) which reveals the characteristic texture of a phase.[22] The optical textures of compounds **CS-1** and **CS-2** were observed in thin layers of the sample between two glass plates. A study using differential scanning calorimetry (DSC) was conducted as a complementary tool to textural observations to know the precise transition temperatures and the enthalpy changes associated with the phase transitions. Both the compounds were found to be liquid crystalline. The chiral nematic (**N***) phase was stabilized in both **CS-1** and **CS-2** over a very wide temperature range. The **N*** phase was identified based on the characteristic oily streak texture for both compounds. Transition temperatures and phase sequences observed for both compounds are summarized in Table 5.3.DSC thermograms of

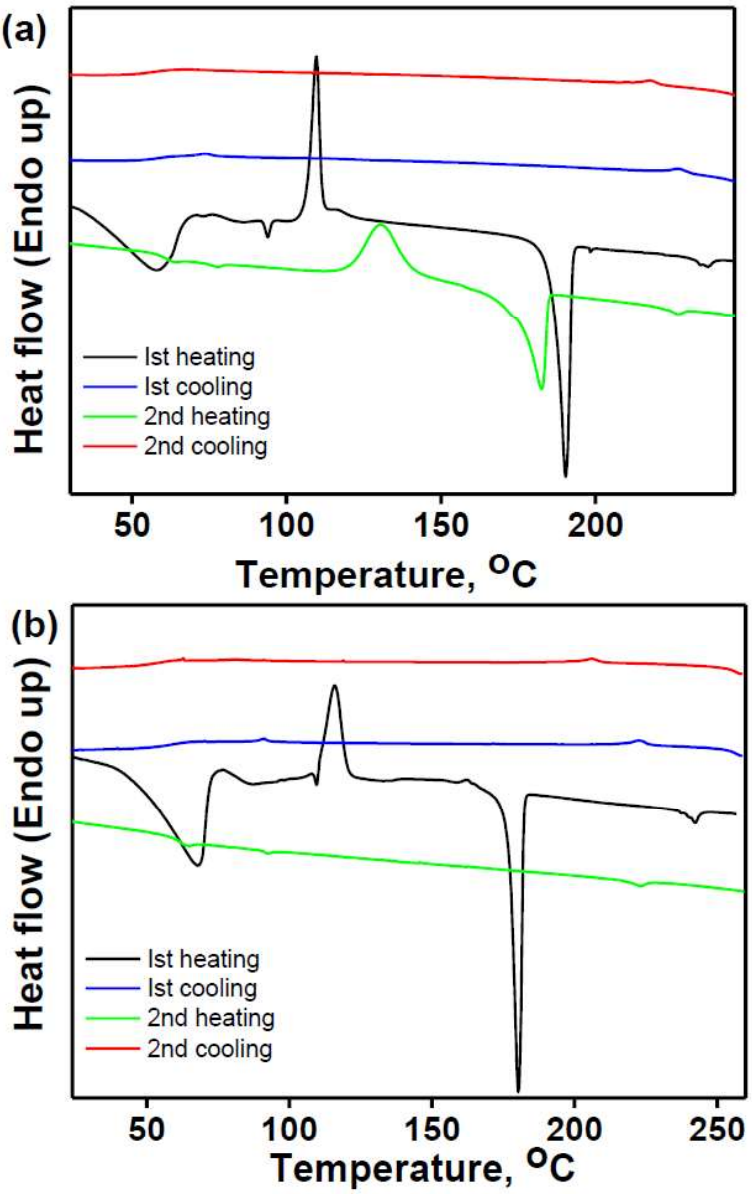

Figure5.18: DSC traces of **CS-1** (a) First heating and first cooling and (b) first cooling and second heating, and **CS-2** (c) First heating and first cooling and (d) first cooling and second heating recorded at a scan rate of 5 °C/minutes.

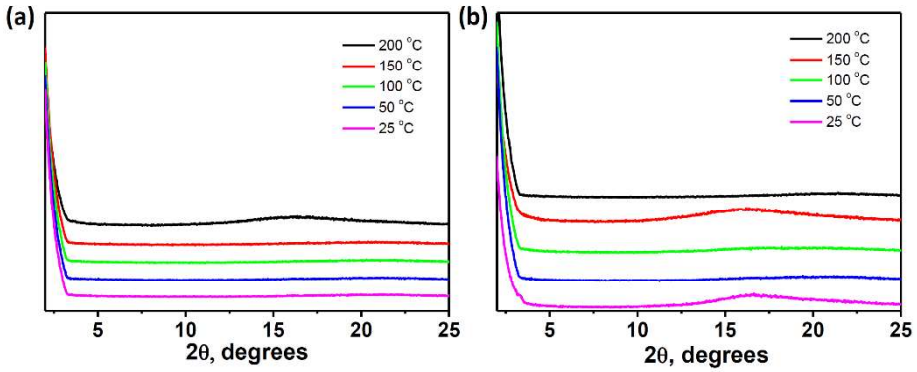

Figure 5. 19 Small angle X-ray diffraction pattern of (a) **CS-1** and (b) **CS-2** at different temperatures

these compounds in the first heating and cooling and second heating and cooling are presented in Figure 5.18. The DSC thermograms of both compounds exhibited crystal-to-crystal transitions before melting

Table.5.3: Phase sequence and transition temperatures (°C) obtained from DSC thermograms during the first heating and cooling cycles at 5 °C min^{-1}.

Compound	Phase sequence transition temperature in °C and the corresponding enthalpies in KJ/ mol [in brackets]; **Cr** = Crystal; **N*** = Chiral Nematic; **Iso** = isotropic
CS-1	Heating: **Cr** 189.5 [21. 59] **N*** 235.9 [0.69] **Iso** Cooling**: Iso** 226.7 [0. 45] **N*** 73.6 glassy **N***
CS-2	Heating: **Cr** 180.6[23 .1] **N*** 242.6 [0.53] **Iso** Cooling**: Iso** 223.0 [0. 45] **N*** 91.2 glassy **N***

to a mesophase. Compound **CS-1** on heating melt to **N*** phase at 184.2 ℃. On further heating, a chiral nematic to isotropic transition occurred at 230.8 ℃. On cooling from the isotropic phase, the **N*** phase appeared at 226.7 ℃ confirming the mesophase to be enantiotropic. Interestingly, the compound did not undergo crystallization on cooling to room temperature. On cooling to room temperature, no change in the oily streak texture of the **N*** phase was observed. However, the fluidity of the **N*** phase was arrested at 75.6 ℃ indicating the formation of glassy cholesteric phase. A shear test at a temperature below the glass transition confirmed the glassy nature of the cholesteric phase. A corresponding broad peak in the DSC further confirmed this transition. To confirm the phase to be a glassy chiral nematic even at room temperature, X-ray diffraction measurements were carried out in the liquid crystalline phase at various temperatures including room temperature (Figure5.19). The intensity versus diffraction angle (2θ) profile obtained from the diffractogram in the mesophase of **CS-1** at various temperatures displayed no lower-angle peaks indicating the absence of any other LC or crystalline phases.Irrespective of the rate of cooling, the formation of the glassy phase was observed here. However, leaving the sample at room temperature over time led to crystallization as indicated by the PXRD pattern of the melt-cooled sample of **CS-1M** (Figure 5.15a, red curve). Thus, stabilizing the helical supramolecular order of the N* phase at room temperature. Subsequent heating of the sample from the glassy N* phase led to heat induced crystallization at about 125 ℃. All these phase transitions observed under POM were also confirmed by DSC scansof the sample (Figure 5.18). Similar to **CS-1**, its positional isomer **CS-2** also exhibited an enantiotropic cholesteric phase with glass

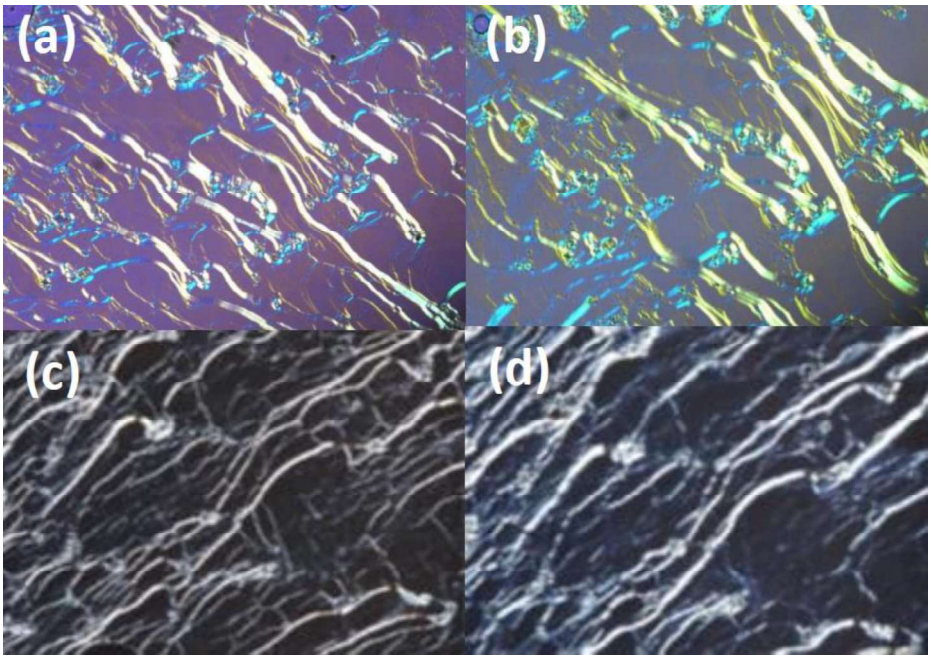

Figure 5.20: Polarizing optical photomicrograph of of (a) **CS-1** showing (a) characteristic oily streak texture of the N* phase at 188 ℃ and (b) **CS-1** showing glassy N* phase obtained at room temperature(c) **CS-2** showing characteristic oily streak texture of the N* phase at 207 ℃ and (d) **CS-2** glassy N* phase at room temperature forming property in room temperature. On the first heating cycle, compound **CS-2** melts to N* phase at 179.3 ℃ (Figure. 5.20a) and then from **N*** to isotropic transition at 244.0 ℃. Compared to **CS-1**, a wider range of **N*** phase was stabilized for its positional isomeric compound **CS-2**. Cooling from the isotropic phase resulted in a transition to **N*** phase that later transformed into a glassy **N*** phase at 94.8 ℃. Compound **CS-2** was also found to stabilize cholesteric mesomorphic order in the glassy state at room temperature (Figure 5.20b). One notable change in the mesomorphic

property of **CS-2** to that of **CS-1** was that the former compound did not exhibit any heat induced crystallization of the sample on subsequent heating cooling cycles. The positional isomerism obtained by the difference in connectivity of cholesterol appended cyanostyryl unit to thiophene moiety gives rise to unmatched photophysical properties in the solid state of **CS-1** and **CS-2**. The dissimilar stimuli responsive emission properties of **CS-2** in comparison to **CS-1** can be attributed to difference in molecular structure and packing.The poor susceptibility of **CS-1** to multiple stimuli can be attributed to the stronger intermolecular interaction present in **CS-1** as evident from single crystal structure analysis. As indicated by the POM and DSC, both molecules on cooling result in a cholesteric (N*) glass phase at room temperature. However, the crystalline nature of the melt cooled sample of **CS-1M** can be attributed to slow reorganization of molecules from cholesteric (N*) glass phase to crystalline phase upon standing at room temperature over time.

5.6 Conclusions

In summary, in this work, two cholesterol-appended cyanostyryl thiophene positional isomers **CS-1** and **CS-2** were synthesized**,** and their stimuli-responsive solid-state emission and liquid crystalline properties were investigated. The compounds **CS-1** and **CS-2** were strongly emissive in solid states compared to their respective THF solutions due to aggregation induced emission enhancement. Both **CS-1** and **CS-2** showed thermal-induced changes in solid-state emissions. In addition, **CS-2** showed mechanofluorochromism with reversible switching on exposure to methanol vapours. The dual

state emission in the pristine and ground samples of **CS-2** is attributed to the formation of two different crystalline forms as evident from powder X-ray diffractograms. The single crystal X-ray diffraction data obtained for crystals of **CS-1** showed various hydrogen bonding interactions. The powder X-ray diffractogram simulated from the single crystal X-ray diffraction data for **CS-1** resembled the diffractogram obtained for melt-processed **CS-1**, indicating both samples adopt a similar molecular packing. The observed stimuli responsive emission switching in **CS-2** under thermal and shear stress can be attributed to their crystalline to amorphous transitions. Reversibility in emission of the grounded sample of **CS-2** on exposure to methanol vapours is due to the transition from amorphous to a crystalline phase akin to pristine **CS-2**. The compound **CS-1** showed decreased quantum efficiency under thermal stimulus, while an increase in quantum yield was observed with **CS-2** under thermal and mechanical stimuli. Both **CS-1** and **CS-2** exhibited an enantiotropic liquid crystalline phase that stabilized as a glassy cholesteric (N*) phase at room temperature. The present study demonstrated how a simple change in the molecular design by bringing in positional isomers can lead to subtle control over multistimuli responsive emission in solution, solid state, and liquid crystalline properties.

5.7. References

1. D. Devadiga and T. N. Ahipa, *Soft Matter*, 2022, **18**, 8008–8016.
2. R. Kaneko, Y. Sagara, S. Katao, N. Tamaoki, C. Weder and H. Nakano, *Chem. Eur. J.*, 2019, **25**, 61626169.
3. S. Lin, K. G. Gutierrez-Cuevas, X. Zhang, J. Guo and Q. Li, *Adv. Funct. Mater.*, 2021, **31**, 2007957.
4. M. Martínez-Abadía, R. Giménez and M. B. Ros, *Adv. Mater.*, 2018, 30, 1704161.
5. B. K. An, S. K. Kwon, S. D. Jung and S. Y. Park, *J. Am. Chem. Soc.*, 2002, **124**, 14410–14415.
6. S.- J. Yoon and S. Park, *J. Mater. Chem.*, 2011, **21**, 8338-8346.
7. G. Fan and D. Yan, *Sci.Rep.*, 2014, **4**, 4933.
8. C. V. Yelamaggad, G. Shanker, U. S. Hiremath and S. K. Prasada *J. Mater. Chem.*, 2008, **18**, 2927-2949.
9. N. Tamaoki, Y. Aoki, M. Moriyama and M. Kidowaki, *Chem. Mater.*, 2003, **15**, 719–726.
10. Y. Wang, J. Shi, J. Chen, W. Zhu and E. Baranoff, *J. Mater. Chem. C*, 2015, **3**, 7993–8005.
11. D. Zhao,W. Bi and B. Z. Tang, *Adv. Opt. Mater.*, 2021, **9**, 2100489.
12. H. K. Bisoyi and Q. Li, *Chem. Rev.*, 2022, **122**, 5, 4887–4926.
13. M. - J. Gim, S. Turlapati, S. Debnath, N. V. S Rao, D. K. Yoon, *ACS Appl. Mater. Interfaces*, 2016, **8**, 3143–3149.
14. J. Sha, H. Lu, M. Zhou, G. Xia, Y. Fang, G. Zhang, L. Qiu, J. Yang, Y. Ding, *Org. Electron.*, 2017, **50**, 177–183.
15. M. T. Sims, *Liq. Cryst.*, 2016, **43**, 2363–2374.

16. W. Zhang, S. Suzuki, S. Cho, G. Watanabe, H. Yoshida, T. Sakurai, M. Aotani, Y. Tsutsui, M. Ozaki, S. Seki, *Langmuir*, 2019, **35**, 14031–14041.
17. M. Kinami, B. R. Crenshaw and C. Weder, *Chem. Mater.*, 2006, **18**, 4, 946–955.
18. L. Wen, J. Sun, C. Li, C. Zhu, X. Zhang, Z. Wang, Q. Song, C. Lv and Y. Zhang, *New J. Chem*., 2021, **45**, 11530-11535.
19. Y. Ooyama and Y. Harima, *J. Mater. Chem.*, 2011, **21**, 83728380.
20. I. Dierking. *Textures of liquid crystals*. John Wiley & Sons, 2003.

General Conclusion

The chapters of the thesis discuss the design, synthesis and photophysical properties of cyanostyrene-based photoluminescent molecules in the solution and solid states. The cyanostyrene moiety is functionalized with various groups and flexible alkyl chains to explore the aggregation induced emission and stimuli responsive emission in the solid state. The role of positional isomerism in determining the solid state photoluminescence properties of dicyanodistyrylbenzene derivatives is explored in Chapter 3. The positional isomers of dicyanodistyrylbenzene derives were obtained by varying the position of the octyloxy group on terminal phenyl ring. A Knoevengel condensation of ortho, meta or para octyloxy benzaldehyde with 2,2'-(1,4-phenylene)diacetonitrile resulted in corresponding positional isomers **CSO**, **CSM** and **CSP**. All three isomers showed AIEE behaviour in the solid state with red shifted emission compared to the spectra recorded from the corresponding THF solution of optical density 0.1. The *ortho* isomer which is less emissive in the solid state showed a blue shifted emission with enhanced quantum yield under applied mechanical stress. The *meta* isomer, which has the highest number of intramolecular interactions, is insensitive to any stimuli. The *para* showed tricolour emission switching under stimuli such as heat, shear stress and dichloromethane vapour. The multistimuli response in compound CSP is attributed crystal to crystal or crystal to amorphous transitions under various stimuli. The study investigated the contribution of various structural factors such as planarity of the π-system and molecular packing in the solid state using the structural information obtained from single crystal and powder X-ray diffraction.

In summary, single component tricolour emission switching and mechanochromic blueshift in octyloxy substituted dicyanodistyrylbenzene positional isomers by subtle tuning of multiple stimuli such as pressure, temperature and solvents.

The synthesis, structure and luminescence properties of a series of *ortho* alkyloxy substituted dicyanodistyrylbenzenes **OCS-1** to **OCS-6** are reported in Chapter 4. All the molecules were weakly emissive in 2-MeTHFsolutions at room temperature with structured bands. The emission spectra recorded for all the compounds in 2-MeTHF at 77 K with a delay of 0.5 ms showed redshifted emission spectra in each case with lifetime in milli seconds indicating the phosphorescence emission in these molecules. The importance of restriction of intramolecular motion in achieving the stable triplet state is substantiated in this work. The work in Chapter 4 also studied the structural factors that affect the quantum yield of the molecules **OCS-1** to **OCS-6** in a solid state. The alkyloxy substitution in the *ortho* position of dicyanodistyrylbenzene introduces molecular twist and rigid packing in the solid state which plays a pivotal role in achieving dicyanodistyrylbenzene systems with high quantum yields. The present report demonstrates the importance of restriction of intermolecular motions in achieving the stable triplet state and points out the interplay between the molecular twist, and the structural rigidity in determining the enhanced emission quantum yield.

Aggregation induced emission and stimuli responsive emission properties of two cholesterol appended cyanostyryl thiophene positional

isomers were explored in Chapter 5. Both the compounds were highly emissive in solid states due the aggregation induced emission enhancement. The compound **CS-2** showed sensitivity to stimuli such as heat, shear stress and methanol vapours, while **CS-1** is sensitive only to thermal stimuli. As evident from the powder X-ray diffraction data, the formation of a different crystalline phase is responsible for the thermochromic emission behaviour in **CS-1**. The single crystal X-ray diffraction data obtained for crystals of **CS-1** showed various hydrogen bonding interactions in the crystals. The powder X-ray diffractogram simulated from the single crystal X-ray diffraction data for **CS-1** resembled the diffractogram obtained for melt-processed **CS-1**, indicating both samples adopt a similar molecular packing. The observed stimuli responsive emission switching in **CS-2** under thermal and shear stress can be attributed to the crystalline to amorphous transitions. Reversibility in the emission of the grounded sample of **CS-2** on exposure to methanol vapours is due to the transition from amorphous to a crystalline phase akin to pristine **CS-2**. The compound **CS-1** showed decreased quantum efficiency under thermal stimulus, while an increase in quantum yield was observed with **CS-2** under thermal and mechanical stimuli. Both **CS-1** and **CS-2** exhibited an enantiotropic liquid crystalline phase that stabilized as a glassy cholesteric (N*) phase at room temperature.

In summary, the works in the thesis investigate the role of molecular packing in the sold state emission properties of the cyanostyryl systems functionalized with flexible alkyl moieties. The molecules discussed in the thesis are designed to demonstrate the role of the

structural features of the molecules on solid state emission and its stimuli responsive switching. The study also probes how positional isomerism brings about incomparable photophysical properties in the cyanostyrene class of molecules. The study explores fine structural features that contribute to aggregation induced emission and stimuli responsive emission in π-conjugated systems. This investigation can contribute to the design and synthesis of novel π-conjugated molecular systems with aggregation induced emission and stimuli responsive emission proper

Recommendations

Cyanostyrene based systems are known for their prominent solid state luminescence properties and stimuli responsive behaviour in the solid state.[1-5] A fine tuning of the emission properties in the solid state can be achieved by controlling the functional moieties on cyanostyrene core or molecular packing. The photoluminescence properties of most of the cyanostyrenes derivatives are highly sensitive towards various stimuli where a small disturbance in the structure gives rise to visible change in the emission properties.[3,6-9] To account for the stimuli responsive emission properties a detailed analysis of photophysical properties in conjunction with structural variation under stimuli applied condition is relevant.

The crystals of compound **CSP** discussed in **Chapter 3** showed temperature-dependent dynamic emission switching where these types of systems are rare in literature.[10] It is expected that the observed dynamic emission switching in crystals **CSP** originates from the switching of planarity under the influence of temperature as indicated by the temperature-dependent X-ray diffractograms. In this regard, an investigation of temperature dependent emission study on the crystals of **CSP** is proposed. Since the molecule is highly sensitive to thermal stimuli a detailed study regarding the structure-property correlation at higher temperatures is quite promising. The temperature dependent emission and related structural contribution can be probed using various methods such as temperature dependent photoluminescence spectroscopy, temperature dependent Raman spectroscopy and variable

temperature powder X-ray diffraction. The temperature dependent dynamic emission switching can be explored in temperature sensors.

Since the compound **CSP** is sensitive to mechanical stress and detailed study on structural origin of pressure dependent emission can be carried out using the pressure dependent Raman and photoluminescence spectroscopy. The pristine and ground forms of the *para* derivatives showed relatively good quantum efficiency, hence the stress and strain sensing applications of **CSP** can be envisaged. Detailed analysis of phase relation requires further exploration involving spectroscopic and microscopic studies can be carried out.

The *ortho* alkyloxydicyanodistyrylbenzene derivatives discussed in **Chapter 4** showed a dependence on the molecular packing in the crystalline state. A theoretical exploration to understand the energy levels in the single molecules and in the crystalline state is also recommended to obtain further insights into the observed properties. The compounds **CS-1** and **CS-2** discussed in **Chapter 5** showed the formation of glassy chiral nematic phase along photoluminescence properties hence the presence of circular polarized luminescence properties can be envisaged. Since the molecule with inherently chiral cholesterol group in the structure, a detailed investigation of CPL in both solid state solution state is recommended.

References

1. W. Fang, W. Zhao, P. Pei, R. Liu, Y. Zhang, L. Kong and J. Yang*, J. Mater. Chem. C,* 2018, **6**, 92699276.
2. Q. Jiang, H. Ruan, T. Wang, Y. Zhang, Y. Qiu, H. Wang, Y. Liao, and X. Xie, *Langmuir*, 2023, **39**, 10904–10912.
3. L. Zhu and Y. Zhao*, J. Mater. Chem. C*, 2013, **1**, 10591065.
4. H. J. Kim, J. Gierschner, S. Y. Park, *J. Mater. Chem. C*, 2020, **8**, 74177421.
5. S. J. Yoon, J. W. Chung, J. Gierschner, K. S. Kim, M. G. Choi, D. Kim and S. Y. Park, *J. Am. Chem. Soc.*, 2010, **132**, 1367513683.
6. B.-Kwan An, J. Gierschner and S. Y. Park*, Acc. Chem. Res.*, 2012, **45**, 544–554.
7. A. K. Vasu, M. Radhakrishna and S. Kanvah, *J. Phys. Chem. C*, 2017, **121**, 22478–22486.
8. P. Gayathri, S. Karthikeyan, M. Pannipara, A. G. A.-Sehemi, D. Moon and S. P. Anthony, *Cryst. Growth Des.*, 2022, **22**, 5432–5440.
9. C. Arivazhagan, P. Malakar, R. Jagan, E. Prasad and S. Ghosh, *CrystEngComm*, 2018, **20**, 31623166.
10. T. Mutai, H. Satou and K. Araki, *Nature Mater.,* 2005, **4**, 685–687.

LIST OF PUBLICATIONS

Based on the Thesis work:

1. **N. K. Ramya**, C. Femina, S. Suresh, D.S. Mohanakumari, R. Krishnan and R, Thomas, Dicyanodistyrylbenzene based positional isomers: a comparative study of AIEE and stimuli responsive multicolour fluorescence switching, *New J. Chem.*, 2022,46, 13391346., https://doi.org/10.1039/D1NJ04489C

2. **N. K. Ramya**, P.Athira, M. Mathews and R. Thomas, Cholesterol appended cyanostyryl thiophene positional isomers with multistimuli responsive emission switching and liquid crystalline properties, *New J. Chem.*, 2024, **48**, 59115918., https://doi.org/10.1039/D3NJ04310J
3. **N. K. Ramya**, D. S. Mohanakumari, H. Balasubramanian, R. Krishnan and R. Thomas, Aggregation induced photophysical behaviour of *o*-alkyloxy substituted cyanostyrylbenzene derivatives (Manuscript submitted to *Chemistry A European Journal*).

Other works

4. P. Athira, **N. K. Ramya**, A. R. Sachin, M. Yoosuf, G. Gopakumar and R. Thomas, Intramolecular Charge Transfer and Stimuli Responsive Emission in Cholesterol Appended Phenothiazine-Cyanostyryl based Donor-Acceptor Systems (Accepted in *Journal of Physical Chemistry A*)